

Sequential Statistical Signal Processing with Applications to Distributed Systems

Yasin Yılmaz

Submitted in partial fulfillment of the
requirements for the degree
of Doctor of Philosophy
in the Graduate School of Arts and Sciences

COLUMBIA UNIVERSITY

2014

©2014

Yasin Yılmaz

All Rights Reserved

ABSTRACT

Sequential Statistical Signal Processing with Applications to Distributed Systems

Yasin Yılmaz

Detection and estimation, two classical statistical signal processing problems with well-established theories, are traditionally studied under the fixed-sample-size and centralized setups, e.g., Neyman-Pearson target detection, and Bayesian parameter estimation. Recently, they appear in more challenging setups with stringent constraints on critical resources, e.g., time, energy, and bandwidth, in emerging technologies, such as wireless sensor networks, cognitive radio, smart grid, cyber-physical systems (CPS), internet of things (IoT), and networked control systems. These emerging systems have applications in a wide range of areas, such as communications, energy, the military, transportation, health care, and infrastructure.

Sequential (i.e., online) methods suit much better to the ever-increasing demand on time-efficiency, and latency constraints than the conventional fixed-sample-size (i.e., offline) methods. Furthermore, as a result of decreasing device sizes and tendency to connect more and more devices, there are stringent energy and bandwidth constraints on devices (i.e., nodes) in a distributed system (i.e., network), requiring *decentralized* operation with low transmission rates. Hence, for statistical inference (e.g., detection and/or estimation) problems in distributed systems, today's challenge is achieving high performance (e.g., time efficiency) while satisfying resource (e.g., energy and bandwidth) constraints.

In this thesis, we address this challenge by (i) first finding optimum (centralized) sequential schemes for detection, estimation, and *joint* detection and estimation if not available in the literature, (ii) and then developing their asymptotically optimal decentralized versions through an *adaptive* non-uniform sampling technique called *level-triggered sampling*. We propose and rigorously analyze decentralized detection, estimation, and joint detection and

estimation schemes based on level-triggered sampling, resulting in a systematic theory of *event-based statistical signal processing*. We also show both analytically and numerically that the proposed schemes significantly outperform their counterparts based on conventional uniform sampling in terms of time efficiency. Moreover, they are compatible with the existing hardware as they work with discrete-time observations produced by conventional A/D converters.

We apply the developed schemes to several problems, namely spectrum sensing and dynamic spectrum access in cognitive radio, state estimation and outage detection in smart grid, and target detection in multi-input multi-output (MIMO) wireless sensor networks.

Table of Contents

List of Figures	v
Acknowledgements	viii
1 Introduction	1
1.1 Contributions	4
1.2 Outline	5
I Detection	6
2 Sequential Distributed Detection	7
2.1 Introduction	7
2.2 System Descriptions	9
2.3 Channel-aware Fusion Rules	12
2.3.1 Binary Erasure Channels (BEC)	13
2.3.2 Binary Symmetric Channels (BSC)	13
2.3.3 Additive White Gaussian Noise (AWGN) Channels	14
2.3.4 Rayleigh Fading Channels	14
2.3.5 Rician Fading Channels	15
2.4 Performance Analysis	15
2.4.1 Information Entities	15
2.4.2 Ideal Channels	17
2.4.3 Noisy Channels	20

2.4.4	Discussions	25
2.5	Spectrum Sensing in Cognitive Radio Networks	28
2.5.1	Problem Formulation and Background	29
2.5.2	Decentralized Spectrum Sensing via Level-triggered Sampling	35
2.5.3	Performance Analysis	43
2.5.4	Simulation Results	48
2.6	Conclusion	52
II	Estimation	54
3	Sequential Estimation for Linear Models	55
3.1	Introduction	55
3.1.1	Literature Review	56
3.1.2	Outline	58
3.2	Problem Formulation and Background	59
3.3	Optimum Sequential Estimators	60
3.3.1	The Optimum Conditional Sequential Estimator	61
3.3.2	The Optimum Unconditional Sequential Estimator	63
3.4	Distributed Sequential Estimator	71
3.4.1	Key Approximations in Distributed Approach	72
3.4.2	Proposed Estimator Based on Level-triggered Sampling	74
3.4.3	Discussions	79
3.4.4	Simulation Results	81
3.5	Conclusion	84
III	Joint Detection and Estimation	86
4	Sequential Joint Detection and Estimation	87
4.1	Introduction	87
4.2	Optimum Sequential Joint Detection and Estimation	90
4.2.1	Problem Formulation	90

4.2.2	Optimum Solution	92
4.2.3	Separated Detection and Estimation Costs	96
4.2.4	Linear Quadratic Gaussian (LQG) Model	98
4.2.5	Independent LQG Model	99
4.3	Dynamic Spectrum Access in Cognitive Radio Networks	102
4.3.1	Background	102
4.3.2	Problem Formulation	103
4.3.3	Optimum Solution	104
4.3.4	Discussions	106
4.4	State Estimation in Smart Grid with Topological Uncertainty	109
4.4.1	Background and Problem Formulation	109
4.4.2	Optimum Solution	110
4.4.3	Discussions	111
4.5	Conclusion	114
IV	Conclusions	115
5	Conclusions	116
V	Bibliography	117
	Bibliography	118
VI	Appendices	130
A	Proofs in Part I	131
A.1	Theorem 2	131
A.2	Proposition 2	132
A.3	Lemma 1	132

B Proofs in Part II	133
B.1 Lemma 3	133
B.2 Lemma 4	134
B.3 Theorem 5	137
B.4 Proposition 3	137

List of Figures

1.1	The level-triggered sampling procedure.	3
2.1	A wireless sensor network with K sensors S_1, \dots, S_K , and a fusion center (FC). Sensors process their observations $\{y_t^k\}$, and transmits information bits $\{b_n^k\}$. Then, the FC, receiving $\{z_n^k\}$ through wireless channels, makes a detection decision $\delta_{\bar{\tau}}$. $I_i^k(t)$, $\hat{I}_i^k(t)$, $\tilde{I}_i^k(t)$ are the observed, transmitted and received information entities respectively, which will be defined in Section 2.4.1.	10
2.2	The KL information, $\tilde{I}_1^k(t_1^k)$, under BEC and BSC, as a function of the local error probabilities $\alpha_k = \beta_k$ and the channel error probability ϵ_k	22
2.3	The penalty term \mathcal{C}_i^k for Rayleigh fading channels as a function of ρ , where $\alpha_k = \beta_k = 0.1$, $\sigma_h^2 = \sigma^2 = 1$, $P^2 = 10$, $Q^2 = 1$	24
2.4	$\mathcal{C}_{1, a \neq b }^k - \mathcal{C}_{1, a = b }^k$ in Rician fading channels as a function of $ \mu ^2$ and σ_h^2 , where $P^2 = 10$, $Q^2 = 1$	25
2.5	Realizations of the LLRs $\tilde{\lambda}_n^k$ and $\tilde{\lambda}_t^k$ computed at the FC under reliable and unreliable detection of the sampling times, respectively.	27
2.6	Average decision delay vs error probabilities (α, β) for optimum centralized and Q-SPRT, RLT-SPRT with 1,2,3, ∞ number of bits.	49
2.7	Average decision delay normalized by the optimum centralized performance vs. error probabilities (α, β) for Q-SPRT and RLT-SPRT with 2 bits and communication period either $T = 4$ or $T = \Theta(\sqrt{ \log \alpha })$	51
2.8	Average decision delay vs SNR for optimum centralized and Q-SPRT, RLT-SPRT with 1, ∞ number of bits.	52

2.9	Average decision delay vs number of SUs (K) for optimum centralized and Q-SPRT, RLT-SPRT with $1, \infty$ number of bits.	53
3.1	The surface that defines the stopping rule for $\lambda = 1$, $\sigma^2 = 1$ and $h_{1,1}, h_{1,2} \sim \mathcal{N}(0, 1)$ in the two-dimensional case.	69
3.2	The stopping regions for $\rho_t = 0$, $\sigma^2 = 1$ and $h_{t,1}, h_{t,2} \sim \mathcal{N}(0, 1), \forall t$ in the unconditional problem with (a) $\lambda = 0.01$, (b) $\lambda = 1$, (c) $\lambda = 100$. That of the conditional problem is also shown in (c).	70
3.3	Illustration of sampling time s_m , transmission time t_m , transmission delay δ_m and overshoot q_m . We encode $q_m = (d_{s_m} - d_{s_{m-1}}) - \Delta < \theta_d$ in $\delta_m = t_m - s_m < 1$ using the slope $\phi_d > \theta_d$	76
3.4	Average stopping time performances of the optimal centralized scheme and the distributed schemes based on level-triggered sampling with quadratic and linear complexity vs. normalized MSE values when scaling coefficients are uncorrelated, i.e., $r_{ij} = 0, \forall i, j$	81
3.5	Average stopping time performances of the optimal centralized scheme and the distributed schemes based on level-triggered sampling with quadratic and linear complexity vs. normalized MSE values when scaling coefficients are correlated with $r_{ij} = 0.5, \forall i, j$	82
3.6	Average stopping time performances of the optimal centralized scheme and the distributed schemes based on level-triggered sampling with quadratic and linear complexity vs. correlation coefficient for normalized MSE fixed to 10^{-2}	83
4.1	Average stopping time vs. target accuracy level for SJDE in Corollary 1, the conventional SPRT detector & MMSE estimator, and the sequential LRT detector & MMSE estimator equipped with the stopping rule of SJDE.	108
4.2	Illustration for the IEEE-4bus system and the power injection (square) and power flow (circle) measurements.	112
4.3	Average stopping time vs. target accuracy level for SJDE and the combination of sequential LRT detector & MMSE estimator equipped with the stopping rule of SJDE.	114

B.1	The function $\mathcal{V}_1(z)$ is non-decreasing and concave.	135
B.2	The structures of the optimal cost function $\mathcal{V}(z)$ and the cost functions $F(z)$ and $G(z)$	137

Bismillah ir-Rahman ir-Rahim
Al-hamdu lillahi Rabbil alameen

Acknowledgments

First of all, I would like to express my deepest gratitudes to my advisors Prof. Xiaodong Wang and Prof. George Moustakides, who made this thesis possible. Prof. Wang, from the first moment he accepted me as a Ph.D. student until this final stage, has always guided me with patience and wisdom. With his prolific research career, professional attitude and tolerance, he greatly helped me manage this intense learning journey.

Prof. George Moustakides generously taught me sequential analysis along with other theoretical subjects which constitute the core of this thesis. Our collaboration in just two semesters we spent together paved the way for the rest of my Ph.D. work, and more importantly for my future research career. His truly immense experience in and dedication to mathematical sciences together with his friendly manner continue to inspire me.

I also would like to extend my thanks to the thesis committee members Prof. Ta-Hsin Li, Prof. John Wright, Prof. John Paisley, and Prof. Arian Maleki for taking time to read and evaluate this dissertation.

I am grateful to my friends at Columbia, especially Shang Li and Ziyu Guo, with whom I had fruitful discussions and collaborations.

My most special thanks are reserved for my parents İsmail and Hava Yılmaz, my uncle Ramazan Yılmaz, and my sisters Elif and Gülsüm, who always believed in and supported me with love.

Last but not least, my dear wife Filiz, and our beloved son Eren, the most valuable outcome of our Ph.D. period, are the invisible collaborators of this thesis. I cannot express well enough her devotion, understanding, and significant help in organizing my life in all aspects.

To my family

Canım aileme

Chapter 1

Introduction

In statistical signal processing, efficiency in terms of critical resources, such as time/number of observations, energy, and bandwidth, becomes increasingly important. In particular, minimizing the average decision making time/delay is crucial due to the ever-increasing need for speed in today's technology. This fact strongly underpins the significance of *sequential* (i.e., online) methodologies. A sequential method, unlike the traditional fixed-sample-size methods, is equipped with a stopping rule which *adapts* the number of observations used to make a decision, i.e., the time to stop taking new observations and make a decision, to the observation history. With such a *stopping* capability, a sequential method, for each realization of the random observation signal, can tailor the sample size (i.e., number of observations) to the constraints on specific performance measures in a problem [e.g., type I (false alarm) and type II (misdetection) error probabilities in detection; mean squared error (MSE) in estimation]. On the other hand, a fixed-sample-size (i.e., offline) method, regardless of the observation history, waits until a specific amount of observation is collected, and then at this deterministic time makes its decision (e.g., detection and/or estimation).

For example, it is known [1, Page 109] that the sequential probability ratio test (SPRT), which is the optimum sequential detector for i.i.d. observations, requires for Gaussian signals, on average, four times less samples than the best fixed-sample-size detector to reach a decision with the same level of confidence. This significant time efficiency comes with the costs of sophisticated analysis and some practical challenges. Particularly, a sequential method, in a distributed (i.e., networked) system, needs online information transmission,

posing a serious challenge for energy- and bandwidth-constrained systems. Considering that energy and bandwidth constraints are typical of many emerging technologies (e.g., wireless sensor networks, cyber-physical systems, internet of things) sequential methods that satisfy such resource constraints are of great interest recently.

In this thesis, we address the challenge briefly explained above. Specifically, we design optimum sequential detectors, estimators, and *joint* detectors and estimators; and then develop their *decentralized* versions that rely on low-rate information transmission in a distributed system. With the term decentralized, we denote distributed systems with low-rate information transmission from nodes to a fusion center (which may be one of the nodes), as opposed to centralized systems with high information transmission rates. Hence, it should not be confused with the term *ad hoc*, which denotes the lack of a fusion center. Here, we also sometimes use the terms distributed and decentralized interchangeably.

The main contributions of this thesis are twofolds: (i) the development of optimum sequential schemes, (ii) the design and analysis of decentralized sequential schemes based on an *event-based* non-uniform sampling technique called the *level-triggered* sampling. This *adaptive* sampling technique is key to achieving high efficiency in minimizing the average sample size through low-rate information transmission. The sampling times in level-triggered sampling are dynamically (i.e., adaptively) determined by the signal that is sampled, hence random. This is in contrast with the time-based sampling, in which sampling times are deterministic, e.g., the classical uniform-in-time sampling with periodic sampling times. More specifically, in level-triggered sampling, a new sample is taken when the signal changes at least by a constant Δ since the last sampling time, as shown in Fig. 1.1. The sampling times t_1, t_2, t_3, t_4 in Fig. 1.1 are dictated by the random signal X_t , whereas those of uniform sampling are given by a preselected period T , regardless of X_t .

Using uniform sampling in a distributed system we know the sampling times throughout the system, but sample magnitudes need to be quantized with a few bits to report to the fusion center, incurring considerable quantization errors at the fusion center. On the other hand, since the level-triggered sampling procedure is uniform in magnitude change, at each sampling time a node, transmitting only a single bit, can easily report to the fusion center whether the magnitude change since the last sampling time is above Δ or below

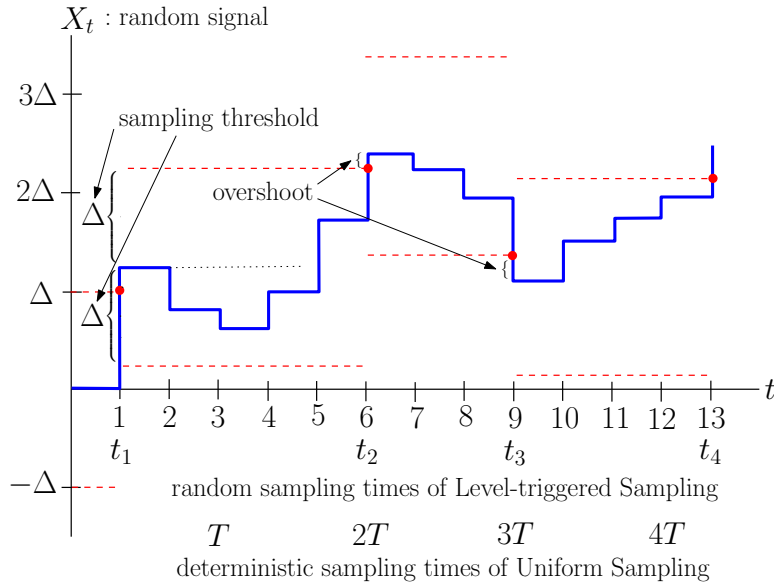


Figure 1.1: The level-triggered sampling procedure.

$-\Delta$. Moreover, the fusion center can infer the sampling times from the bit arrival times, although for the ultimate statistical task (e.g., detection and/or estimation) sampling times do not need to be precisely recovered, as opposed to data compression [2].

Some variants of level-triggered sampling are used in the literature under the names of level-crossing sampling, time-encoding machine, send-on-delta sampling, and Lebesgue sampling for , control systems [3; 4; 5], data compression [2], analog-to-digital (A/D) conversion [6; 7; 8], continuous-time data transmission [9; 10; 11], continuous-time detection [12; 13] and estimation [14], imaging applications [15; 16; 17]. It also naturally appears in biological sensing systems. Interestingly, the all-or-none principle, according to which neurons fire, i.e., transmit electrical signals, in many multicellular organisms, including plants, insects, reptiles and mammals, is closely related to level-triggered sampling [18]. Event-based techniques, as alternative to time-driven techniques, are first [3] and most commonly used in the context of control systems. Their appearance in the context of signal processing is much later [2].

1.1 Contributions

It was shown in [12; 14] that with continuous-time observations, level-triggered sampling is an ideal fit for information transmission in decentralized detection and estimation as it achieves a strong type of asymptotic optimality called *order-2* asymptotic optimality by transmitting a single bit per sample. In other words, it attains a very high performance standard while being extremely resource-efficient. This is possible due to the well-behaved (i.e., continuous-path) continuous-time observations since at each sampling time the magnitude change in such a continuous-time signal is exactly either Δ or $-\Delta$, without any overshoot (cf. Fig. 1.1), and thus the change information is fully represented by a single bit. However, these impressive theoretical results have practical limitations as they rely on applying level-triggered sampling to analog signals without A/D conversion. Although there are significant works (e.g., [8; 7; 19]) towards building a new digital signal processing (DSP) theory based on event-based sampling, such a theory is still not mature, and thus uniform sampling dominates today's DSP technology.

A vast majority of the existing devices work, and will continue to work in the near future, with discrete-time observations produced by conventional A/D converters based on uniform sampling and quantization. Hence, a comprehensive theory for discrete-time observations is needed to use level-triggered sampling for statistical signal processing tasks on the existing hardware. To that end, in this dissertation, we rigorously analyze the use of level-triggered sampling with discrete-time observations for the statistical signal processing tasks.

We should emphasize here that we are interested in level-triggered sampling as a means of transmitting local statistics/information to a remote center, not for A/D conversion. The real challenge in using level-triggered sampling with discrete-time observations is the overshoot problem due to the excess signal level above/below the sampling threshold, as shown in Fig. 1.1. Such an overshoot value is not represented by the single bit which can only encode the threshold (upper/lower) that triggered sampling. If this problem is not treated, the overshoot values cannot be recovered at the fusion center, and even worse accumulate in time. We propose and rigorously analyze several ways to overcome the overshoot problem.

Specifically, in [20], for the spectrum sensing problem in cognitive radio networks, we

use a few additional bits to quantize the overshoot value in each sample, and show that this scheme can achieve order-2 asymptotic optimality. In [21], for decentralized detection, assuming some local statistics are known we compute an average value for the overshoot, and use a single bit to represent each sample. Moreover, in [21] we consider non-ideal reporting channels between the fusion center and nodes. In [22], we encode each overshoot value in time, and transmit a single pulse for each sample in the context of target detection in wireless sensor networks. In [23], we propose asymptotically optimal decentralized estimators based on multi-bit level-triggered sampling, in which overshoot values are quantized as in [20]. For a restricted class of stopping times we find, in [24], the optimum (centralized) sequential vector parameter estimators under two different formulations, and develop a computationally efficient decentralized version of the more tractable one. Similarly, we find an optimum sequential joint detector and estimator in [25] for a set of problems in which both detection and estimation are equally important. Then, in [26], we extend this optimum sequential joint detection and estimation scheme to a cooperative multi-node setup, and apply this extended optimum solution to the dynamic spectrum access problem in cognitive radio networks.

1.2 Outline

The dissertation is organized into three parts for *detection, estimation, and joint detection and estimation*. Firstly, in Chapter 2, we consider sequential distributed detection, and spectrum sensing in cognitive radio networks as an application. Then, in Chapter 3, we treat the sequential estimation problem for linear models, and its application to a wireless sensor network. Finally, in Chapter 4, sequential joint detection and estimation is handled with two applications: dynamic spectrum access in cognitive radio networks, and state estimation in smart grid. We conclude the dissertation in Chapter 5.

We represent vectors and matrices with lower-case and upper-case bold letters, respectively.

Part I

Detection

Chapter 2

Sequential Distributed Detection

2.1 Introduction

We consider the problem of binary decentralized detection, i.e., hypothesis testing, where a number of distributed sensors, under bandwidth constraints, communicate with a fusion center (FC) which is responsible for making the final decision. In [27] it was shown that under a fixed fusion rule, with two sensors each transmitting one bit information to the FC, the optimum local decision rule is a likelihood ratio test (LRT) under the Bayesian criterion. Later, in [28] and [29] it was shown that the optimum fusion rule at the FC is also an LRT under the Bayesian and the Neyman-Pearson criteria, respectively. It was further shown in [30] that as the number of sensors tends to infinity it is asymptotically optimal to have all sensors perform an identical LRT. The case where sensors observe correlated signals was also considered, e.g., [31; 32].

Most works on decentralized detection, including the above mentioned, treat the fixed-sample-size approach where each sensor collects a fixed number of samples and the FC makes its final decision at a fixed time. There is also a significant volume of literature that considers the sequential detection approach, e.g., [33; 34; 35; 36; 12; 20; 21; 22]. In [36; 12; 20; 21; 22], the sequential probability ratio test (SPRT) is used both locally and globally. SPRT is optimal for i.i.d. observations in terms of minimizing the average sample number (i.e., decision delay) among all sequential tests satisfying the same error probability constraints [37]. It is also known that SPRT asymptotically requires, on average, four

times less samples (for Gaussian signals) to reach a decision than the best fixed-sample-size test, for the same level of confidence [1, Page 109]. Relaxing the one-bit messaging constraint, the optimality of the likelihood ratio quantization is established in [38]. Data fusion (multi-bit messaging) is known to be much more powerful than decision fusion (one-bit messaging) [39], albeit it consumes higher bandwidth. Moreover, the recently proposed sequential detection schemes based on level-triggered sampling, e.g., [12; 20], are as powerful as data-fusion techniques, and at the same time they are as simple and bandwidth-efficient as decision-fusion techniques.

Besides having noisy observations at sensors, in practice the channels between sensors and the FC are noisy. The conventional approach to decentralized detection ignores the latter, i.e., assumes ideal transmission channels, and addresses only the first source of uncertainty, e.g., [27; 12]. Adopting the conventional approach to the noisy channel case yields a two-step solution. First, a communication block is employed at the FC to recover the transmitted information bits from sensors, and then a signal processing block applies a fusion rule to the recovered bits to make a final decision. Such an independent block structure causes performance loss due to the data processing inequality [40]. To obtain the optimum performance the FC should process the received signal in a channel-aware manner [41], [42]. Most works assume parallel channels between sensors and the FC, e.g., [43; 44]. Other topologies such as serial [45] and multiple-access channels (MAC) [46] have also been considered. In [47] a scheme is proposed that adaptively switches between serial and parallel topologies.

In this chapter, we design and analyze channel-aware sequential decentralized detection schemes based on level-triggered sampling, under different types of discrete and continuous noisy channels. In Section 2.2, we describe the general structure of the decentralized detection approach based on level-triggered sampling with noisy channels between sensors and the FC. We derive channel-aware sequential detection schemes based on level-triggered sampling in Section 2.3. We then present, in Section 2.4, an information theoretic framework to analyze the decision delay performance of the proposed schemes based on which we provide an asymptotic analysis on the decision delays under various types of channels. The asymptotic analysis on decision delays facilitates finding appropriate signaling schemes

under different continuous channels. In Section 2.5, as an application, we deal with the cooperative spectrum sensing problem in cognitive radio networks. Finally, Section 2.6 concludes the chapter.

2.2 System Descriptions

Consider a wireless sensor network consisting of K sensors each of which observes a discrete-time signal $\{y_t^k, t \in \mathbb{N}\}, k = 1, \dots, K$. Each sensor k computes the log-likelihood ratio (LLR) $\{L_t^k, t \in \mathbb{N}\}$ of the signal it observes, samples the LLR sequence using the *level-triggered sampling*, and then sends the LLR samples to the fusion center (FC). The FC then combines the local LLR information from all sensors, and decides between two hypotheses, H_0 and H_1 , in a sequential manner.

Observations collected at the same sensor, $\{y_t^k\}_t$, are assumed to be i.i.d., and in addition observations collected at different sensors, $\{y_t^k\}_k$, are assumed to be independent. Hence, the local LLR at the k -th sensor, L_t^k , and the global LLR, L_t , are computed as

$$L_t^k \triangleq \log \frac{f_1^k(y_1^k, \dots, y_t^k)}{f_0^k(y_1^k, \dots, y_t^k)} = L_{t-1}^k + l_t^k = \sum_{n=1}^t l_n^k, \quad \text{and} \quad L_t = \sum_{k=1}^K L_t^k, \quad (2.1)$$

respectively, where $l_t^k \triangleq \log \frac{f_1^k(y_t^k)}{f_0^k(y_t^k)}$ is the LLR of the sample y_t^k received at the k -th sensor at time t ; $f_i^k, i = 0, 1$, is the probability density function (pdf) of the received signal by the k -th sensor under H_i . The k -th sensor samples L_t^k via the level-triggered sampling at a sequence of random sampling times $\{t_n^k\}_n$ that are dictated by L_t^k itself. Specifically, the n -th sample is taken from L_t^k whenever the accumulated LLR $L_t^k - L_{t_{n-1}^k}^k$, since the last sampling time t_{n-1}^k exceeds a constant Δ in absolute value, i.e.,

$$t_n^k \triangleq \inf \left\{ t > t_{n-1}^k : L_t^k - L_{t_{n-1}^k}^k \notin (-\Delta, \Delta) \right\}, \quad t_0^k = 0, \quad L_0^k = 0. \quad (2.2)$$

Let λ_n^k denote the accumulated LLR during the n -th inter-sampling interval, $(t_{n-1}^k, t_n^k]$, i.e.,

$$\lambda_n^k \triangleq \sum_{t=t_{n-1}^k+1}^{t_n^k} l_t^k = L_{t_n^k}^k - L_{t_{n-1}^k}^k. \quad (2.3)$$

Immediately after sampling at t_n^k , as shown in Fig. 2.1, an information bit b_n^k indicating

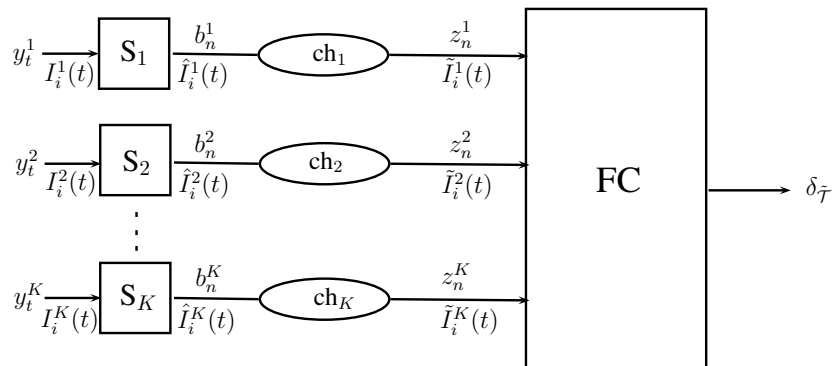


Figure 2.1: A wireless sensor network with K sensors S_1, \dots, S_K , and a fusion center (FC). Sensors process their observations $\{y_t^k\}$, and transmits information bits $\{b_n^k\}$. Then, the FC, receiving $\{z_n^k\}$ through wireless channels, makes a detection decision $\delta_{\bar{\tau}}$. $I_i^k(t)$, $\hat{I}_i^k(t)$, $\tilde{I}_i^k(t)$ are the observed, transmitted and received information entities respectively, which will be defined in Section 2.4.1.

the threshold crossed by λ_n^k is transmitted to the FC, i.e.,

$$b_n^k \triangleq \text{sign}(\lambda_n^k). \quad (2.4)$$

Let us now analyze the signals at the FC. Denote the received signal at the FC corresponding to b_n^k as z_n^k , as shown in Fig. 2.1. The FC then computes the LLR $\tilde{\lambda}_n^k$ of each received signal and approximates the global LLR L_t as

$$\tilde{L}_t \triangleq \sum_{k=1}^K \sum_{n=1}^{N_t^k} \tilde{\lambda}_n^k \quad \text{with} \quad \tilde{\lambda}_n^k \triangleq \log \frac{p_1^k(z_n^k)}{p_0^k(z_n^k)}, \quad (2.5)$$

where N_t^k is the total number of LLR messages the k -th sensor has transmitted up to time t , and $p_i^k(\cdot)$, $i = 0, 1$, is the pdf of z_n^k under H_i . In fact, the FC recursively updates \tilde{L}_t whenever it receives an LLR message from any sensor. In particular, suppose that the m -th LLR message $\tilde{\lambda}_m$ from any sensor is received at time t_m . Then at t_m , the FC first updates the global LLR as

$$\tilde{L}_{t_m} = \tilde{L}_{t_{m-1}} + \tilde{\lambda}_m. \quad (2.6)$$

It then performs an SPRT step by comparing \tilde{L}_{t_m} with two thresholds \tilde{A} and $-\tilde{B}$, and

applying the following decision rule

$$\delta_{t_m} \triangleq \begin{cases} \text{H}_1, & \text{if } \tilde{L}_{t_m} \geq \tilde{A}, \\ \text{H}_0, & \text{if } \tilde{L}_{t_m} \leq -\tilde{B}, \\ \text{continue to receive LLR messages,} & \text{if } \tilde{L}_{t_m} \in (-\tilde{B}, \tilde{A}). \end{cases} \quad (2.7)$$

The thresholds $(\tilde{A}, \tilde{B} > 0)$ are selected to satisfy the error probability constraints $\text{P}_0(\delta_{\tilde{\mathcal{T}}} = \text{H}_1) \leq \alpha$ and $\text{P}_1(\delta_{\tilde{\mathcal{T}}} = \text{H}_0) \leq \beta$ with equalities, where α, β are target error probability bounds, and

$$\tilde{\mathcal{T}} \triangleq \inf\{t > 0 : \tilde{L}_t \notin (-\tilde{B}, \tilde{A})\} \quad (2.8)$$

is the decision delay.

Note that each sensor, in fact, implements a local SPRT [cf. (2.7), (2.8)], with thresholds Δ and $-\Delta$ within each sampling interval. At sensor k the n -th local SPRT starts at time t_{n-1}^k and ends at time t_n^k when the local test statistic λ_n^k exceeds either Δ or $-\Delta$. This local hypothesis testing produces a local decision represented by the information bit b_n^k , and induces local error probabilities α_k and β_k which are given by

$$\alpha_k \triangleq \text{P}_0(b_n^k = 1), \quad \text{and} \quad \beta_k \triangleq \text{P}_1(b_n^k = -1) \quad (2.9)$$

respectively, where $\text{P}_i(\cdot)$, $i = 0, 1$, denotes the probability under H_i .

With ideal channels between sensors and the FC, we have $z_n^k = b_n^k$, so from (2.9) we can write the local LLR $\tilde{\lambda}_n^k = \hat{\lambda}_n^k$, where

$$\hat{\lambda}_n^k \triangleq \begin{cases} \log \frac{\text{P}_1(b_n^k=1)}{\text{P}_0(b_n^k=1)} = \log \frac{1-\beta_k}{\alpha_k} \geq \Delta, & \text{if } b_n^k = 1, \\ \log \frac{\text{P}_1(b_n^k=-1)}{\text{P}_0(b_n^k=-1)} = \log \frac{\beta_k}{1-\alpha_k} \leq -\Delta, & \text{if } b_n^k = -1 \end{cases} \quad (2.10)$$

is the LLR of the transmitted bit b_n^k . The inequalities above can be obtained by applying a change of measure. For example, to show the first one, we have $\alpha_k = \text{P}_0(\lambda_n^k \geq \Delta) = \text{E}_0[\mathbb{1}_{\{\lambda_n^k \geq \Delta\}}]$ where $\text{E}_i[\cdot]$ is the expectation under H_i , $i = 0, 1$ and $\mathbb{1}_{\{\cdot\}}$ is the indicator function. Noting that $e^{-\lambda_n^k} = \frac{f_0^k(y_{t_{n-1}^k+1}^k, \dots, y_{t_n^k}^k)}{f_1^k(y_{t_{n-1}^k+1}^k, \dots, y_{t_n^k}^k)}$, we can write

$$\alpha_k = \text{E}_1[e^{-\lambda_n^k} \mathbb{1}_{\{\lambda_n^k \geq \Delta\}}] \leq e^{-\Delta} \text{E}_1[\mathbb{1}_{\{\lambda_n^k \geq \Delta\}}] = e^{-\Delta} \text{P}_1(\lambda_n^k \geq \Delta) = e^{-\Delta}(1 - \beta_k).$$

Note that for the case of continuous-time and continuous-path observations at sensors, the inequalities in (2.10) become equalities as the local LLR sampled at a sensor [cf. (2.1)]

is now a continuous-time and continuous-path process. This suggests that the accumulated LLR during any inter-sampling interval [cf. (2.3)] due to continuity of its paths will hit exactly the local thresholds $\pm\Delta$. Therefore, from Wald's analysis for SPRT, $\alpha_k = \beta_k = \frac{1}{e^{\Delta+1}}$ [?]; hence a transmitted bit fully represents the LLR accumulated in the corresponding inter-sampling interval. Accordingly, the FC at sampling times exactly recovers the values of LLR processes observed by sensors [12].

On the other hand, when sensors observe discrete-time signals, due to randomly over/under shooting the local thresholds, the observed LLR λ_n^k in (2.3) is a random variable, which is in absolute value greater than Δ . However, the transmitted LLR $\hat{\lambda}_n^k$ in (2.10) is a fixed value, that is also greater than Δ in absolute value. While in continuous-time the FC fully recovers the LLR accumulated in an inter-sampling interval by using only the received bit, in discrete-time this is not possible. In order to ameliorate this problem, in [12; 21] it is assumed that the local error probabilities $\{\alpha_k, \beta_k\}$ are available to the FC; and therefore the LLR of z_n^k , that is, $\tilde{\lambda}_n^k = \hat{\lambda}_n^k$, can be obtained; while in [20] the overshoot is quantized by using extra bits in addition to b_n^k . Nevertheless, neither method enables the FC to fully recover λ_n^k unless an infinite number of bits is used.

In this chapter, we will initially assume in Sections 2.3 and 2.4 that the local error probabilities α_k, β_k , $k = 1, \dots, K$ are available at the FC in order to compute the LLR $\tilde{\lambda}_n^k$ of the received signals, as in [12; 21]. Then, in Section 2.5, following [20], we consider quantizing overshoot using additional bits. For the case of ideal channels, we denote the thresholds in (2.7) with A and $-B$, and the decision delay in (2.8) with \mathcal{T} . In the case of noisy channels, the received signal z_n^k is not always identical to the transmitted bit b_n^k , and thus the LLR $\tilde{\lambda}_n^k$ of z_n^k can be different from $\hat{\lambda}_n^k$ of b_n^k , given in (2.10). In the next section, we consider some popular channel models and give the corresponding expressions for $\tilde{\lambda}_n^k$.

2.3 Channel-aware Fusion Rules

In computing the LLR $\tilde{\lambda}_n^k$ of the received signal z_n^k , we will make use of the local sensor error probabilities α_k, β_k , and the channel parameters that characterize the statistical property of the channel. One subtle issue is that since the sensors asynchronously sample and transmit

the local LLR, in the presence of noisy channels, the FC needs to first reliably detect the sampling time in order to update the global LLR. In this section we assume that the sampling time is reliably detected and focus on deriving the fusion rule at the FC. In Section 2.4.4, we will discuss the issue of sampling time detection.

2.3.1 Binary Erasure Channels (BEC)

Consider binary erasure channels between sensors and the FC with erasure probabilities ϵ_k , $k = 1, \dots, K$. Under BEC, a transmitted bit b_n^k is lost with probability ϵ_k , and correctly received at the FC, i.e., $z_n^k = b_n^k$, with probability $1 - \epsilon_k$. Then the LLR of z_n^k is given by

$$\tilde{\lambda}_n^k = \begin{cases} \log \frac{P_1(z_n^k=1)}{P_0(z_n^k=1)} = \log \frac{1-\beta_k}{\alpha_k}, & \text{if } z_n^k = 1, \\ \log \frac{P_1(z_n^k=-1)}{P_0(z_n^k=-1)} = \log \frac{\beta_k}{1-\alpha_k}, & \text{if } z_n^k = -1. \end{cases} \quad (2.11)$$

Note that under BEC the channel parameter ϵ_k is not needed when computing the LLR $\tilde{\lambda}_n^k$. Note also that in this case, a received bit bears the same amount of LLR information as in the ideal channel case [cf. (2.10)], although a transmitted bit is not always received. Hence, the channel-aware approach coincides with the conventional approach which relies solely on the received signal. Although the LLR updates in (2.10) and (2.11) are identical, the fusion rules under BEC and ideal channels are not. This is because the thresholds \tilde{A} and $-\tilde{B}$ of BEC, due to the information loss, are in general different from the thresholds A and $-B$ of the ideal channel case.

2.3.2 Binary Symmetric Channels (BSC)

Next, we consider binary symmetric channels with crossover probabilities ϵ_k between sensors and the FC. Under BSC, the transmitted bit b_n^k is flipped, i.e., $z_n^k = -b_n^k$, with probability ϵ_k , and it is correctly received, i.e., $z_n^k = b_n^k$, with probability $1 - \epsilon_k$. The LLR of z_n^k can be computed as

$$\begin{aligned} \tilde{\lambda}_n^k(z_n^k = 1) &= \log \frac{P_1(z_n^k = 1|b_n^k = 1)P_1(b_n^k = 1) + P_1(z_n^k = 1|b_n^k = -1)P_1(b_n^k = -1)}{P_0(z_n^k = 1|b_n^k = 1)P_0(b_n^k = 1) + P_0(z_n^k = 1|b_n^k = -1)P_0(b_n^k = -1)} \\ &= \log \frac{(1 - \epsilon_k)(1 - \beta_k) + \epsilon_k\beta_k}{(1 - \epsilon_k)\alpha_k + \epsilon_k(1 - \alpha_k)} = \log \frac{1 - \overbrace{[(1 - 2\epsilon_k)\beta_k + \epsilon_k]}^{\hat{\beta}_k}}{\underbrace{(1 - 2\epsilon_k)\alpha_k + \epsilon_k}_{\hat{\alpha}_k}} \end{aligned} \quad (2.12)$$

where $\hat{\alpha}_k$ and $\hat{\beta}_k$ are the effective local error probabilities at the FC under BSC. Similarly we can write

$$\tilde{\lambda}_n^k(z_n^k = -1) = \log \frac{\hat{\beta}_k}{1 - \hat{\alpha}_k}. \quad (2.13)$$

Note that $\hat{\alpha}_k > \alpha_k$, $\hat{\beta}_k > \beta_k$ if $\alpha_k < 0.5$, $\beta_k < 0.5$, $\forall k$, which we assume true for $\Delta > 0$. Thus, we have $|\tilde{\lambda}_{n,BSC}^k| < |\tilde{\lambda}_{n,BEC}^k|$ from which we expect the performance loss under BSC to be higher than the one under BEC. The numerical results provided in Fig. 2.2 will illustrate this claim. Finally, note also that, unlike the BEC case, under BSC the FC needs to know the channel parameters $\{\epsilon_k\}$ to operate in a channel-aware manner.

2.3.3 Additive White Gaussian Noise (AWGN) Channels

Now, assume that the channel between each sensor and the FC is an AWGN channel. The received signal at the FC is given by

$$z_n^k = h_n^k x_n^k + w_n^k \quad (2.14)$$

where $h_n^k = h_k, \forall k, n$, is a known constant complex channel gain; $w_n^k \sim \mathcal{N}_c(0, \sigma_k^2)$; x_n^k is the transmitted signal at sampling time t_n^k , given by

$$x_n^k = \begin{cases} a, & \text{if } \lambda_n^k \geq \Delta, \\ b, & \text{if } \lambda_n^k \leq -\Delta, \end{cases} \quad (2.15)$$

where the transmission levels a and b are complex in general.

The distribution of the received signal given x_n^k is then $z_n^k \sim \mathcal{N}_c(h_k x_n^k, \sigma_k^2)$. The LLR of z_n^k is given by

$$\begin{aligned} \tilde{\lambda}_n^k &= \log \frac{p_k(z_n^k | x_n^k = a) \mathbb{P}_1(x_n^k = a) + p_k(z_n^k | x_n^k = b) \mathbb{P}_1(x_n^k = b)}{p_k(z_n^k | x_n^k = a) \mathbb{P}_0(x_n^k = a) + p_k(z_n^k | x_n^k = b) \mathbb{P}_0(x_n^k = b)} \\ &= \log \frac{(1 - \beta_k) \exp(-c_n^k) + \beta_k \exp(-d_n^k)}{\alpha_k \exp(-c_n^k) + (1 - \alpha_k) \exp(-d_n^k)}, \end{aligned} \quad (2.16)$$

where $c_n^k \triangleq \frac{|z_n^k - h_k a|^2}{\sigma_k^2}$ and $d_n^k \triangleq \frac{|z_n^k - h_k b|^2}{\sigma_k^2}$.

2.3.4 Rayleigh Fading Channels

If a Rayleigh fading channel is assumed between each sensor and the FC, the received signal model is also given by (2.14)-(2.15), but with $h_n^k \sim \mathcal{N}_c(0, \sigma_{h,k}^2)$. We then have

$z_n^k \sim \mathcal{N}_c(0, |x_n^k|^2 \sigma_{h,k}^2 + \sigma_k^2)$ given x_n^k ; and accordingly, similar to (2.16), $\tilde{\lambda}_n^k$ is written as

$$\tilde{\lambda}_n^k = \log \frac{\frac{1-\beta_k}{\sigma_{a,k}^2} \exp(-c_n^k) + \frac{\beta_k}{\sigma_{b,k}^2} \exp(-d_n^k)}{\frac{\alpha_k}{\sigma_{a,k}^2} \exp(-c_n^k) + \frac{1-\alpha_k}{\sigma_{b,k}^2} \exp(-d_n^k)} \quad (2.17)$$

where $\sigma_{a,k}^2 \triangleq |a|^2 \sigma_{h,k}^2 + \sigma_k^2$, $\sigma_{b,k}^2 \triangleq |b|^2 \sigma_{h,k}^2 + \sigma_k^2$, $c_n^k \triangleq \frac{|z_n^k|^2}{\sigma_{a,k}^2}$ and $d_n^k \triangleq \frac{|z_n^k|^2}{\sigma_{b,k}^2}$.

2.3.5 Rician Fading Channels

For Rician fading channels, we have $h_n^k \sim \mathcal{N}_c(\mu_k, \sigma_{h,k}^2)$ in (2.14), and hence $z_n^k \sim \mathcal{N}_c(\mu_k x_n^k, |x_n^k|^2 \sigma_{h,k}^2 + \sigma_k^2)$ given x_n^k . Using $\sigma_{a,k}^2$ and $\sigma_{b,k}^2$ as defined in the Rayleigh fading case, and defining $c_n^k \triangleq \frac{|z_n^k - \mu_k a|^2}{\sigma_{a,k}^2}$, $d_n^k \triangleq \frac{|z_n^k - \mu_k b|^2}{\sigma_{b,k}^2}$ we can write $\tilde{\lambda}_n^k$ as in (2.17).

2.4 Performance Analysis

In this section, we first define some information entities which will be used throughout the section; then find the non-asymptotic expression for the average decision delay $\mathbb{E}_i[\mathcal{T}]$, and provide an asymptotic analysis on it as the error probability bounds $\alpha, \beta \rightarrow 0$ for ideal and noisy channels.

2.4.1 Information Entities

Note that the expectation of an LLR corresponds to a *Kullback-Leibler (KL) information* entity. For instance,

$$I_1^k(t) \triangleq \mathbb{E}_1 \left[\log \frac{f_1^k(y_1^k, \dots, y_t^k)}{f_0^k(y_1^k, \dots, y_t^k)} \right] = \mathbb{E}_1[L_t^k], \quad \text{and} \quad I_0^k(t) \triangleq \mathbb{E}_0 \left[\log \frac{f_0^k(y_1^k, \dots, y_t^k)}{f_1^k(y_1^k, \dots, y_t^k)} \right] = -\mathbb{E}_0[L_t^k] \quad (2.18)$$

are the KL divergences of the local LLR sequence $\{L_t^k\}_t$ under \mathbf{H}_1 and \mathbf{H}_0 , respectively.

Similarly

$$\begin{aligned} \hat{I}_1^k(t) &\triangleq \mathbb{E}_1 \left[\log \frac{p_1^k(b_1^k, \dots, b_{N_t^k}^k)}{p_0^k(b_1^k, \dots, b_{N_t^k}^k)} \right] = \mathbb{E}_1[\hat{L}_t^k], \quad \hat{I}_0^k(t) \triangleq -\mathbb{E}_0[\hat{L}_t^k] \\ \tilde{I}_1^k(t) &\triangleq \mathbb{E}_1 \left[\log \frac{p_1^k(z_1^k, \dots, z_{N_t^k}^k)}{p_0^k(z_1^k, \dots, z_{N_t^k}^k)} \right] = \mathbb{E}_1[\tilde{L}_t^k], \quad \tilde{I}_0^k(t) \triangleq -\mathbb{E}_0[\tilde{L}_t^k] \end{aligned} \quad (2.19)$$

are the KL divergences of the local LLR sequences $\{\hat{L}_t^k\}_t$ and $\{\tilde{L}_t^k\}_t$ respectively. Define also $I_i(t) \triangleq \sum_{k=1}^K I_i^k(t)$, $\hat{I}_i(t) \triangleq \sum_{k=1}^K \hat{I}_i^k(t)$, and $\tilde{I}_i(t) \triangleq \sum_{k=1}^K \tilde{I}_i^k(t)$ as the KL divergences of the global LLR sequences $\{L_t\}$, $\{\hat{L}_t\}$, and $\{\tilde{L}_t\}$ respectively.

In particular, we have

$$I_1^k(1) = \mathbb{E}_1 \left[\log \frac{f_1^k(y_1^k)}{f_0^k(y_1^k)} \right] = \mathbb{E}_1[l_1^k], \text{ and } I_0^k(1) = \mathbb{E}_0 \left[\log \frac{f_0^k(y_1^k)}{f_1^k(y_1^k)} \right] = -\mathbb{E}_0[l_1^k] \quad (2.20)$$

as the KL information numbers of the LLR sequence $\{l_t^k\}$; and $I_i(1) \triangleq \sum_{k=1}^K I_i^k(1)$, $i = 0, 1$ are those of the global LLR sequence $\{l_t\}$. Moreover,

$$\begin{aligned} I_1^k(t_1^k) &= \mathbb{E}_1 \left[\log \frac{f_1^k(y_1^k, \dots, y_{t_1^k}^k)}{f_0^k(y_1^k, \dots, y_{t_1^k}^k)} \right] = \mathbb{E}_1[\lambda_1^k], \quad \hat{I}_1^k(t_1^k) = \mathbb{E}_1 \left[\log \frac{p_1^k(b_1^k)}{p_0^k(b_1^k)} \right] = \mathbb{E}_1[\hat{\lambda}_1^k], \\ &\text{and } \tilde{I}_1^k(t_1^k) = \mathbb{E}_1 \left[\log \frac{p_1^k(z_1^k)}{p_0^k(z_1^k)} \right] = \mathbb{E}_1[\tilde{\lambda}_1^k] \end{aligned} \quad (2.21)$$

are the KL information numbers of the local LLR sequences $\{\lambda_n^k\}$, $\{\hat{\lambda}_n^k\}$, and $\{\tilde{\lambda}_n^k\}$, respectively, under H_1 . Likewise, we have $I_0^k(t_1^k) = -\mathbb{E}_0[\lambda_n^k]$, $\hat{I}_0^k(t_1^k) = -\mathbb{E}_0[\hat{\lambda}_n^k]$, and $\tilde{I}_0^k(t_1^k) = -\mathbb{E}_0[\tilde{\lambda}_n^k]$ under H_0 . To summarize, $I_i^k(t)$, $\hat{I}_i^k(t)$, and $\tilde{I}_i^k(t)$ are respectively the observed (at sensor k), transmitted (by sensor k), and received (by the FC) KL information entities as illustrated in Fig. 2.1.

Next we define the following information ratios,

$$\hat{\eta}_i^k \triangleq \frac{\hat{I}_i^k(t_1^k)}{I_i^k(t_1^k)}, \text{ and } \tilde{\eta}_i^k \triangleq \frac{\tilde{I}_i^k(t_1^k)}{I_i^k(t_1^k)}, \quad (2.22)$$

which represent how efficiently information is transmitted from sensor k and received by the FC, respectively. Due to the data processing inequality, we have $0 \leq \hat{\eta}_i^k, \tilde{\eta}_i^k \leq 1$, for $i = 0, 1$ and $k = 1, \dots, K$. We further define

$$\hat{I}_i(1) \triangleq \sum_{k=1}^K \hat{\eta}_i^k I_i^k(1) = \sum_{k=1}^K \hat{I}_i^k(1), \text{ and } \tilde{I}_i(1) \triangleq \sum_{k=1}^K \tilde{\eta}_i^k I_i^k(1) = \sum_{k=1}^K \tilde{I}_i^k(1) \quad (2.23)$$

as the effective transmitted and received values corresponding to the KL information $I_i(1)$, respectively. Note that $\hat{I}_i(1)$ and $\tilde{I}_i(1)$ are not real KL information numbers, but projections of $I_i(1)$ onto the filtrations generated by the transmitted, (i.e., $\{b_n^k\}$), and received, (i.e., $\{z_n^k\}$), signal sequences, respectively. This is because sensors do not transmit and the FC does not receive the LLR of a single observation, but instead they transmit and it receives the

LLR messages of several observations. Hence, we cannot have the KL information for single observations at the two ends of the communication channel, but we can define hypothetical KL information to serve analysis purposes. In fact, the hypothetical information numbers $\hat{I}_i(1)$ and $\tilde{I}_i(1)$, defined using the information ratios $\hat{\eta}_i^k$ and $\tilde{\eta}_i^k$, are crucial for our analysis as will be seen in the this section.

The KL information $I_i^k(1)$ of a sensor whose information ratio, $\tilde{\eta}_i^k$, is high and close to 1 is well projected to the FC. Conversely, $I_i^k(1)$ of a sensor which undergoes high information loss is poorly projected to the FC. Note that there are two sources of information loss for sensors, namely, the overshoot effect due to having discrete-time observations and noisy transmission channels. The latter appears only in $\tilde{\eta}_i^k$, whereas the former appears in both $\hat{\eta}_i^k$ and $\tilde{\eta}_i^k$. In general with discrete-time observations at sensors we have $\hat{I}_i(1) \neq I_i(1)$ and $\tilde{I}_i(1) \neq I_i(1)$. Lastly, note that under ideal channels, since $z_n^k = b_n^k, \forall k, n$, we have $\tilde{I}_i(1) = \hat{I}_i(1)$.

2.4.2 Ideal Channels

Let $\{\tau_n^k : \tau_n^k = t_n^k - t_{n-1}^k\}$ denote the inter-arrival times of the LLR messages transmitted from the k -th sensor. Note that τ_n^k depends on the observations $y_{t_{n-1}^k+1}^k, \dots, y_{t_n^k}^k$, and since $\{y_t^k\}$ are i.i.d., $\{\tau_n^k\}$ are also i.i.d. random variables. Hence, the counting process $\{N_t^k\}$ is a renewal process. Similarly the LLRs $\{\hat{\lambda}_n^k\}$ of the received signals at the FC are also i.i.d. random variables, and form a renewal-reward process. Note from (2.8) that the SPRT can stop in between two arrival times of sensor k , e.g., $t_n^k \leq \mathcal{T} < t_{n+1}^k$. The event $N_{\mathcal{T}}^k = n$ occurs if and only if $t_n^k = \tau_1^k + \dots + \tau_n^k \leq \mathcal{T}$ and $t_{n+1}^k = \tau_1^k + \dots + \tau_{n+1}^k > \mathcal{T}$, so it depends on the first $(n+1)$ LLR messages. From the definition of *stopping time* [48, pp. 104] we conclude that $N_{\mathcal{T}}^k$ is not a stopping time for the processes $\{\tau_n^k\}$ and $\{\hat{\lambda}_n^k\}$ since it depends on the $(n+1)$ -th message. However, $N_{\mathcal{T}}^k + 1$ is a stopping time for $\{\tau_n^k\}$ and $\{\hat{\lambda}_n^k\}$ since we have $N_{\mathcal{T}}^k + 1 = n \iff N_{\mathcal{T}}^k = n - 1$ which depends only on the first n LLR messages.

Hence, from Wald's identity [48, pp. 105] we can directly write the following equalities

$$\mathbb{E}_i \left[\sum_{n=1}^{N_{\mathcal{T}}^k+1} \tau_n^k \right] = \mathbb{E}_i[\tau_1^k](\mathbb{E}_i[N_{\mathcal{T}}^k] + 1), \quad (2.24)$$

$$\text{and } \mathbb{E}_i \left[\sum_{n=1}^{N_{\mathcal{T}}^k+1} \hat{\lambda}_n^k \right] = \mathbb{E}_i[\hat{\lambda}_1^k](\mathbb{E}_i[N_{\mathcal{T}}^k] + 1). \quad (2.25)$$

We have the following theorem on the average decision delay under ideal channels.

Theorem 1. *Consider the decentralized detection scheme given in Section 2.2, with ideal channels between sensors and the FC. Its average decision delay under \mathbf{H}_i is given by*

$$\mathbb{E}_i[\mathcal{T}] = \frac{\hat{I}_i(\mathcal{T})}{\hat{I}_i(1)} + \frac{\sum_{k=1}^K \hat{I}_i^k(t_{N_{\mathcal{T}}^k+1}^k) - \mathbb{E}_i[\mathcal{Y}_k] \hat{I}_i^k(1)}{\hat{I}_i(1)} \quad (2.26)$$

where \mathcal{Y}_k is a random variable representing the time interval between the stopping time and the arrival of the first bit from the k -th sensor after the stopping time, i.e., $\mathcal{Y}_k \triangleq t_{N_{\mathcal{T}}^k+1}^k - \mathcal{T}$.

Proof. From (2.24) and (2.25) we obtain

$$\mathbb{E}_i \left[\sum_{n=1}^{N_{\mathcal{T}}^k+1} \tau_n^k \right] = \mathbb{E}_i[\tau_1^k] \frac{\mathbb{E}_i \left[\sum_{n=1}^{N_{\mathcal{T}}^k+1} \hat{\lambda}_n^k \right]}{\mathbb{E}_i[\hat{\lambda}_1^k]}$$

where the left-hand side equals to $\mathbb{E}_i[\mathcal{T}] + \mathbb{E}_i[\mathcal{Y}_k]$. Note that $\mathbb{E}_i[\tau_1^k]$ is the expected stopping time of the local SPRT at the k -th sensor and by Wald's identity it is given by $\mathbb{E}_i[\tau_1^k] = \frac{\mathbb{E}_i[\lambda_1^k]}{\mathbb{E}_i[l_1^k]}$, provided that $\mathbb{E}_i[l_1^k] \neq 0$. Hence, we have

$$\mathbb{E}_i[\mathcal{T}] = \frac{\mathbb{E}_i[\lambda_1^k]}{\mathbb{E}_i[\hat{\lambda}_1^k]} \frac{\mathbb{E}_i \left[\sum_{n=1}^{N_{\mathcal{T}}^k+1} \hat{\lambda}_n^k \right]}{\mathbb{E}_i[l_1^k]} - \mathbb{E}_i[\mathcal{Y}_k] = \frac{I_i^k(t_1^k)}{\hat{I}_i^k(t_1^k)} \frac{\hat{I}_i^k(\mathcal{T}) + \hat{I}_i^k(t_{N_{\mathcal{T}}^k+1}^k)}{I_i^k(1)} - \mathbb{E}_i[\mathcal{Y}_k]$$

where we used the fact that $\mathbb{E}_1 \left[\sum_{n=1}^{N_{\mathcal{T}}^k+1} \hat{\lambda}_n^k \right] = \mathbb{E}_1[\hat{L}_{\mathcal{T}}^k] + \tilde{\mathbb{E}}_1[\hat{\lambda}_{N_{\mathcal{T}}^k+1}^k] = \hat{I}_1^k(\mathcal{T}) + \hat{I}_1^k(t_{N_{\mathcal{T}}^k+1}^k)$ and similarly $\mathbb{E}_0 \left[\sum_{n=1}^{N_{\mathcal{T}}^k+1} \hat{\lambda}_n^k \right] = -\hat{I}_0^k(\mathcal{T}) - \hat{I}_0^k(t_{N_{\mathcal{T}}^k+1}^k)$. Note that $\tilde{\mathbb{E}}_i[\cdot]$ is the expectation with respect to $\hat{\lambda}_{N_{\mathcal{T}}^k+1}^k$ and $N_{\mathcal{T}}^k$ under \mathbf{H}_i . By rearranging the terms and then summing over k on both sides, we obtain

$$\mathbb{E}_i[\mathcal{T}] \underbrace{\sum_{k=1}^K I_i^k(1) \frac{\hat{I}_i^k(t_1^k)}{I_i^k(t_1^k)}}_{\hat{I}_i(1)} = \hat{I}_i(\mathcal{T}) + \sum_{k=1}^K \left\{ \hat{I}_i^k(t_{N_{\mathcal{T}}^k+1}^k) - \mathbb{E}_i[\mathcal{Y}_k] \underbrace{I_i^k(1) \frac{\hat{I}_i^k(t_1^k)}{I_i^k(t_1^k)}}_{\hat{I}_i^k(1)} \right\}$$

which is equivalent to (2.26). \square

The result in (2.26) is in fact very intuitive. Recall that $\hat{I}_i(\mathcal{T})$ is the KL information at the detection time at the FC. It naturally lacks some local information that has been accumulated at sensors, but has not been transmitted to the FC, i.e., the information gathered at sensors after their last sampling times. The numerator of the second term on the right hand side of (2.26) replaces such missing information by using the hypothetical KL information. Note that in (2.26) $\hat{I}_i^k(t_{N_{\mathcal{T}}^k+1}^k) \neq \hat{I}_i^k(t_1^k)$, i.e., $\tilde{\mathbf{E}}_i[\hat{\lambda}_{N_{\mathcal{T}}^k+1}^k] \neq \mathbf{E}_i[\hat{\lambda}_1^k]$, since $N_{\mathcal{T}}^k$ and $\hat{\lambda}_{N_{\mathcal{T}}^k+1}^k$ are not independent.

The next result gives the asymptotic decision delay performance under ideal channels.

Theorem 2. *As the error probability bounds tend to zero, i.e., $\alpha, \beta \rightarrow 0$, the average decision delay under ideal channels given by (2.26) satisfies*

$$\mathbf{E}_1[\mathcal{T}] = \frac{|\log \alpha|}{\hat{I}_1(1)} + O(1), \quad \text{and} \quad \mathbf{E}_0[\mathcal{T}] = \frac{|\log \beta|}{\hat{I}_0(1)} + O(1), \quad (2.27)$$

where $O(1)$ represents a constant term.

Proof. See Appendix A. □

It is seen from (2.27) that the hypothetical KL information number, $\hat{I}_i(1)$, plays a key role in the asymptotic decision delay expression. In particular, we need to maximize $\hat{I}_i(1)$ to asymptotically minimize $\mathbf{E}_i[\mathcal{T}]$. Recalling its definition

$$\hat{I}_i(1) = \sum_{k=1}^K \frac{\hat{I}_i^k(t_1^k)}{I_i^k(t_1^k)} I_i^k(1)$$

we see that three information numbers are required to compute it. Note that $I_i^k(1) = \mathbf{E}_i[l_1^k]$ and $I_i^k(t_1^k) = \mathbf{E}_i[\lambda_1^k]$, which is given in (2.28) below, are computed based on local observations at sensors, thus do not depend on the channels between sensors and the FC. Specifically, we have

$$\begin{aligned} I_1^k(t_1^k) &= (1 - \beta_k)(\Delta + \mathbf{E}_1[\bar{\theta}_n^k]) - \beta_k(\Delta + \mathbf{E}_1[\underline{\theta}_n^k]), \\ \text{and} \quad I_0^k(t_1^k) &= \alpha_k(\Delta + \mathbf{E}_0[\bar{\theta}_n^k]) - (1 - \alpha_k)(\Delta + \mathbf{E}_0[\underline{\theta}_n^k]) \end{aligned} \quad (2.28)$$

where $\bar{\theta}_n^k$ and $\underline{\theta}_n^k$ are local over(under)shoots given by $\bar{\theta}_n^k \triangleq \lambda_n^k - \Delta$ if $\lambda_n^k \geq \Delta$ and $\underline{\theta}_n^k \triangleq -\lambda_n^k - \Delta$ if $\lambda_n^k \leq -\Delta$. Due to $|l_t^k| < \infty, \forall k, t$ we have $\bar{\theta}_n^k, \underline{\theta}_n^k < \infty, \forall k, n$.

On the other hand, $\hat{I}_i^k(t_1^k)$ represents the information received in an LLR message by the FC, so it heavily depends on the channel type. In the ideal channel case, from (2.10) it is given by

$$\begin{aligned} \hat{I}_1^k(t_1^k) &= (1 - \beta_k) \log \frac{1 - \beta_k}{\alpha_k} + \beta_k \log \frac{\beta_k}{1 - \alpha_k}, \\ \text{and } \hat{I}_0^k(t_1^k) &= \alpha_k \log \frac{1 - \beta_k}{\alpha_k} + (1 - \alpha_k) \log \frac{\beta_k}{1 - \alpha_k}. \end{aligned} \quad (2.29)$$

Since $\hat{I}_i^k(t_1^k)$ is the only channel-dependent term in the asymptotic decision delay expression, we will next obtain its expression for each noisy channel type considered in Section 2.3.

2.4.3 Noisy Channels

In all noisy channel types that we consider in this chapter, we assume that channel parameters are either constants or i.i.d. random variables across time. In other words, ϵ_k, h_k are constant for all k (see Sections 2.3.1, 2.3.2, 2.3.3), and $\{h_n^k\}_n, \{w_n^k\}_n$ are i.i.d. for all k (see Sections 2.3.3, 2.3.4, 2.3.5). Thus, in all noisy channel cases discussed in Section 2.3 the inter-arrival times $\{\tilde{\tau}_n^k\}$ of the LLR messages, and the LLRs $\{\tilde{\lambda}_n^k\}$ of the received signals are i.i.d. across time as in the ideal channel case. Accordingly the average decision delay in these noisy channels has the same expression as (2.26), as given by the following proposition. The proof is similar to that of Theorem 1.

Proposition 1. *Under each type of noisy channel discussed in Section 2.3, the average decision delay is given by*

$$\mathbf{E}_i[\tilde{\mathcal{T}}] = \frac{\tilde{I}_i(\tilde{\mathcal{T}})}{\tilde{I}_i(1)} + \frac{\sum_{k=1}^K \tilde{I}_i^k(t_{N_{\tilde{\mathcal{T}}}^k+1}^k) - \mathbf{E}_i[\tilde{\mathcal{Y}}_k] \tilde{I}_i^k(1)}{\tilde{I}_i(1)} \quad (2.30)$$

where $\tilde{\mathcal{Y}}_k \triangleq t_{N_{\tilde{\mathcal{T}}}^k+1}^k - \tilde{\mathcal{T}}$.

The asymptotic performances under noisy channels can also be analyzed analogously to the ideal channel case.

Proposition 2. *As $\alpha, \beta \rightarrow 0$, the average decision delay under noisy channels given by (2.30) satisfies*

$$\mathbf{E}_1[\tilde{\mathcal{T}}] = \frac{|\log \alpha|}{\tilde{I}_1(1)} + O(1), \quad \text{and} \quad \mathbf{E}_0[\tilde{\mathcal{T}}] = \frac{|\log \beta|}{\tilde{I}_0(1)} + O(1). \quad (2.31)$$

Proof. See Appendix A. \square

Recall that $\tilde{I}_i(1) = \sum_{k=1}^K \frac{\tilde{I}_i^k(t_1^k)}{I_i^k(t_1^k)} I_i^k(1)$ in (2.31) where $I_i^k(1)$ and $I_i^k(t_1^k)$ are independent of the channel type, i.e., they are same as in the ideal channel case. We will next compute $\tilde{I}_i^k(t_1^k)$ for each noisy channel type, and consider the choices of the signaling levels a, b in (2.15) that maximize $\tilde{I}_i^k(t_1^k)$.

BEC:

Under BEC, from (2.11) we can write the LLR of the received bits at the FC as

$$\tilde{\lambda}_n^k = \begin{cases} \hat{\lambda}_n^k, & \text{with probability } 1 - \epsilon_k, \\ 0, & \text{with probability } \epsilon_k. \end{cases} \quad (2.32)$$

Hence, we have

$$\tilde{I}_i^k(t_1^k) = \mathbb{E}_i[\tilde{\lambda}_1^k] = (1 - \epsilon_k) \hat{I}_i^k(t_1^k) \quad (2.33)$$

where $\hat{I}_i^k(t_1^k)$ is given in (2.29). As can be seen in (2.33) the performance degradation under BEC is only determined by the channel parameter ϵ_k . In general, from (2.27), (2.31) and (2.33) this asymptotic performance loss can be quantified as $\frac{1}{1 - \min_k \epsilon_k} \leq \frac{\mathbb{E}_i[\tilde{\mathcal{T}}]}{\mathbb{E}_i[\mathcal{T}]} \leq \frac{1}{1 - \max_k \epsilon_k}$. Specifically, if $\epsilon_k = \epsilon, \forall k$, then we have $\frac{\mathbb{E}_i[\tilde{\mathcal{T}}]}{\mathbb{E}_i[\mathcal{T}]} = \frac{1}{1 - \epsilon}$ as $\alpha, \beta \rightarrow 0$.

BSC:

Recall from (2.12) and (2.13) that under BSC local error probabilities α_k, β_k undergo a linear transformation to yield the effective local error probabilities $\hat{\alpha}_k, \hat{\beta}_k$ at the FC. Therefore, using (2.12) and (2.13), similar to (2.29), $\tilde{I}_i^k(t_1^k)$ is written as follows

$$\begin{aligned} \tilde{I}_1^k(t_1^k) &= (1 - \hat{\beta}_k) \log \frac{1 - \hat{\beta}_k}{\hat{\alpha}_k} + \hat{\beta}_k \log \frac{\hat{\beta}_k}{1 - \hat{\alpha}_k}, \\ \text{and } \tilde{I}_0^k(t_1^k) &= \hat{\alpha}_k \log \frac{1 - \hat{\beta}_k}{\hat{\alpha}_k} + (1 - \hat{\alpha}_k) \log \frac{\hat{\beta}_k}{1 - \hat{\alpha}_k} \end{aligned} \quad (2.34)$$

where $\hat{\alpha}_k = (1 - 2\epsilon_k)\alpha_k + \epsilon_k$ and $\hat{\beta}_k = (1 - 2\epsilon_k)\beta_k + \epsilon_k$. Notice that the performance loss in this case also depends only on the channel parameter ϵ_k .

In Fig. 2.2 we plot $\tilde{I}_1^k(t_1^k)$ as a function of $\alpha_k = \beta_k$ and ϵ_k , for both BEC and BSC. It is seen that the KL information of BEC is higher than that of BSC, implying that the asymptotic average decision delay is lower for BEC, as anticipated in Section 2.3.2.

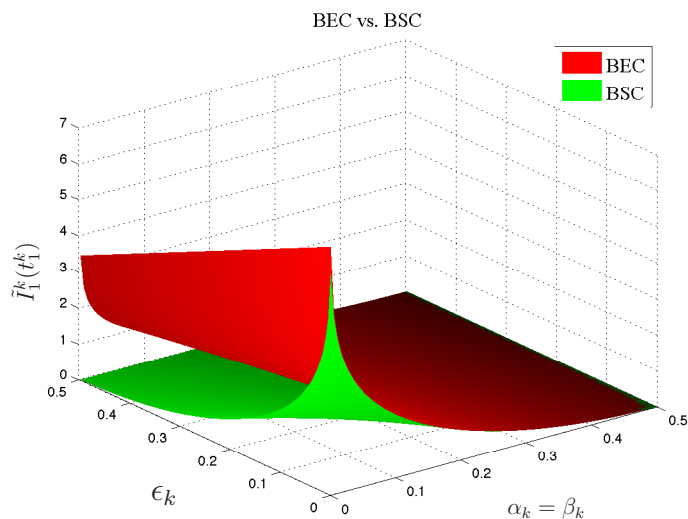


Figure 2.2: The KL information, $\tilde{I}_1^k(t_1^k)$, under BEC and BSC, as a function of the local error probabilities $\alpha_k = \beta_k$ and the channel error probability ϵ_k .

AWGN:

In the remainder of the section, we will drop the sensor index k of $\sigma_{h,k}^2$ and σ_k^2 for simplicity. In the AWGN case, it follows from Section 2.3.3 that if the transmitted signal is a , i.e., $x_n^k = a$, then $c_n^k = u, d_n^k = v_a$; and if $x_n^k = b$, then $c_n^k = v_b, d_n^k = u$ where $u \triangleq \frac{|w_n^k|^2}{\sigma^2}, v_a \triangleq \frac{|w_n^k + (a-b)h_k|^2}{\sigma^2}, v_b \triangleq \frac{|w_n^k + (b-a)h_k|^2}{\sigma^2}$. Accordingly, from (2.16) we write the KL information as

$$\begin{aligned}
 \tilde{I}_1^k(t_1^k) &= \bar{E}_1[\tilde{\lambda}_1^k] = (1 - \beta_k) \mathbb{E} \left[\log \frac{(1 - \beta_k)e^{-u} + \beta_k e^{-v_a}}{\alpha_k e^{-u} + (1 - \alpha_k)e^{-v_a}} \right] + \beta_k \mathbb{E} \left[\log \frac{(1 - \beta_k)e^{-v_b} + \beta_k e^{-u}}{\alpha_k e^{-v_b} + (1 - \alpha_k)e^{-u}} \right] \\
 &= \underbrace{(1 - \beta_k) \log \frac{1 - \beta_k}{\alpha_k} + \beta_k \log \frac{\beta_k}{1 - \alpha_k}}_{\hat{I}_1^k(t_1^k)} + \\
 &\quad \beta_k \underbrace{\left(\frac{1 - \beta_k}{\beta_k} \mathbb{E} \left[\log \frac{1 + \frac{\beta_k}{1 - \beta_k} e^{u - v_a}}{1 + \frac{1 - \alpha_k}{\alpha_k} e^{u - v_a}} \right] + \mathbb{E} \left[\log \frac{1 + \frac{1 - \beta_k}{\beta_k} e^{u - v_b}}{1 + \frac{\alpha_k}{1 - \alpha_k} e^{u - v_b}} \right] \right)}_{C_1^k}, \tag{2.35}
 \end{aligned}$$

where $\mathbb{E}[\cdot]$ denotes the expectation with respect to the channel noise w_n^k only, and $\bar{E}_1[\cdot]$ denotes the expectation with respect to both x_n^k and w_n^k under H_1 . Since w_n^k is independent of x_n^k under both H_0 and H_1 , we used the identity $\bar{E}_1[\cdot] = \mathbb{E}[\bar{E}_1[\cdot]]$ in (2.35).

Note from (2.35) that we have $\tilde{I}_1^k(t_1^k) = \hat{I}_1^k(t_1^k) + \beta_k \mathcal{C}_1^k$ and $\tilde{I}_0^k(t_1^k) = \hat{I}_0^k(t_1^k) + \alpha_k \mathcal{C}_0^k$. Similar to \mathcal{C}_1^k we have $\mathcal{C}_0^k \triangleq -\mathcal{E}_1 - \frac{1-\alpha_k}{\alpha_k} \mathcal{E}_2$. Since we know $\tilde{I}_i^k(t_1^k) \leq \hat{I}_i^k(t_1^k)$, the extra terms, $\mathcal{C}_1^k, \mathcal{C}_0^k \leq 0$ are penalty terms that correspond to the information loss due to the channel noise. Our focus will be on these terms as we want to optimize the performance under AWGN channels by choosing the transmission signal levels a and b that maximize \mathcal{C}_i^k .

From (2.14), we see that the received signal z_n^k will have the same variance, but different means, ah_k and bh_k , if $x_n^k = a$ and $x_n^k = b$ are transmitted respectively. Hence, we expect that the detection performance under AWGN channels will improve if the difference $|a - b|$ between the transmission levels increases. In [21, Lemma 2], we show that this is in fact true, i.e., maximizing \mathcal{C}_i^k is equivalent to maximizing $|a - b|$. If we consider a constraint on the maximum allowed transmission power at sensors, i.e., $\max(|a|^2, |b|^2) \leq P^2$, then the antipodal signaling is optimum, i.e., $|a| = |b| = P$ and $a = -b$.

Rayleigh Fading:

It follows from Section 2.3.4 that $c_n^k = u_a$, $d_n^k = \frac{\sigma_a^2}{\sigma_b^2} u_a$ when $x_n^k = a$; and $c_n^k = \frac{\sigma_b^2}{\sigma_a^2} u_b$, $d_n^k = u_b$ when $x_n^k = b$ where $u_a \triangleq \frac{|ah_n^k + w_n^k|^2}{\sigma_a^2}$, $u_b \triangleq \frac{|bh_n^k + w_n^k|^2}{\sigma_b^2}$, and $\sigma_a^2 = |a|^2 \sigma_h^2 + \sigma^2$, $\sigma_b^2 = |b|^2 \sigma_h^2 + \sigma^2$ as defined in Section 2.3.4. Define further $\rho \triangleq \frac{\sigma_a^2}{\sigma_b^2}$. Hence, using (2.17) we write the KL information as

$$\begin{aligned} \tilde{I}_1^k(t_1^k) &= (1 - \beta_k) \mathbb{E} \left[\log \frac{\frac{1-\beta_k}{\sigma_a^2} e^{-u_a} + \frac{\beta_k}{\sigma_b^2} e^{-\rho u_a}}{\frac{\alpha_k}{\sigma_a^2} e^{-u_a} + \frac{1-\alpha_k}{\sigma_b^2} e^{-\rho u_a}} \right] + \beta_k \mathbb{E} \left[\log \frac{\frac{1-\beta_k}{\sigma_a^2} e^{-\rho^{-1} u_b} + \frac{\beta_k}{\sigma_b^2} e^{-u_b}}{\frac{\alpha_k}{\sigma_a^2} e^{-\rho^{-1} u_b} + \frac{1-\alpha_k}{\sigma_b^2} e^{-u_b}} \right] \\ &= (1 - \beta_k) \underbrace{\log \frac{1 - \beta_k}{\alpha_k}}_{\hat{I}_1^k(t_1^k)} + \beta_k \underbrace{\log \frac{\beta_k}{1 - \alpha_k}}_{\hat{I}_1^k(t_1^k)} + \\ &\quad \underbrace{\beta_k \left(\mathbb{E} \left[\log \frac{1 + \frac{1-\beta_k}{\beta_k} \rho^{-1} e^{\zeta_b}}{1 + \frac{\alpha_k}{1-\alpha_k} \rho^{-1} e^{\zeta_b}} \right] + \frac{1 - \beta_k}{\beta_k} \mathbb{E} \left[\log \frac{1 + \frac{\beta_k}{1-\beta_k} \rho e^{\zeta_a}}{1 + \frac{1-\alpha_k}{\alpha_k} \rho e^{\zeta_a}} \right] \right)}_{\mathcal{C}_1^k} \end{aligned} \quad (2.36)$$

where $\zeta_a \triangleq u_a(1 - \rho)$ and $\zeta_b \triangleq u_b(1 - \rho^{-1})$.

Note that when $|a| = |b|$ which corresponds to the optimal signaling in the AWGN case, we have $\rho = 1$, $\zeta_a = \zeta_b = 0$ and therefore $\tilde{I}_1^k(t_1^k) = 0$ in (2.36). This result is quite intuitive since in the Rayleigh fading case the received signals differ only in their variances. Specifically, from Section 2.3.4, the received signals at the FC will have zero mean and the

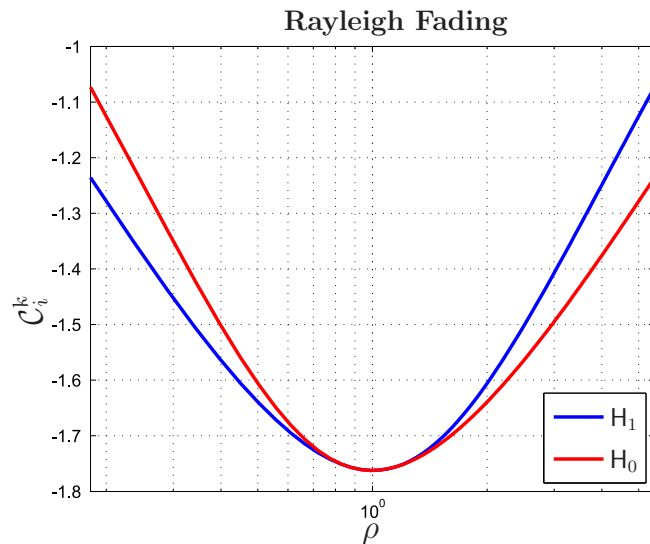


Figure 2.3: The penalty term C_i^k for Rayleigh fading channels as a function of ρ , where $\alpha_k = \beta_k = 0.1$, $\sigma_h^2 = \sigma^2 = 1$, $P^2 = 10$, $Q^2 = 1$.

variances σ_a^2 and σ_b^2 when $x_n^k = a$ and $x_n^k = b$, respectively. Therefore, in this case intuitively we should increase the difference between the two variances, i.e., $||a|^2 - |b|^2|$. Consider the following constraints: $\max(|a|^2, |b|^2) \leq P^2$ and $\min(|a|^2, |b|^2) \geq Q^2$, where the first one is the peak power constraint as before, and the second is to ensure reliable detection of an incoming signal by the FC. In Fig. 2.3, we numerically show that the optimum signaling scheme, that maximizes C_i^k , corresponds to $|a| = P, |b| = Q$ (ρ maximum) or $|a| = Q, |b| = P$ (ρ minimum).

Rician Fading:

In the Rician fading case, upon defining $\tilde{h}_n^k \triangleq h_n^k - \mu_k$ from Section 2.3.5 we have $c_n^k = \frac{|a\tilde{h}_n^k + w_n^k|^2}{\sigma_a^2}$, $d_n^k = \frac{|a\tilde{h}_n^k + w_n^k + (a-b)\mu_k|^2}{\sigma_b^2}$ when $x_n^k = a$; and $c_n^k = \frac{|b\tilde{h}_n^k + w_n^k + (b-a)\mu_k|^2}{\sigma_a^2}$, $d_n^k = \frac{|b\tilde{h}_n^k + w_n^k|^2}{\sigma_b^2}$ when $x_n^k = b$. We will drop the subscript k in μ_k for convenience. We further define $\tilde{z}_a \triangleq a\tilde{h}_n^k + w_n^k$ and $\tilde{z}_b \triangleq b\tilde{h}_n^k + w_n^k$ that are zero-mean Gaussian variables with variances σ_a^2 and σ_b^2 , respectively. Then from Section 2.3.5 similar to (2.36) we write the KL information

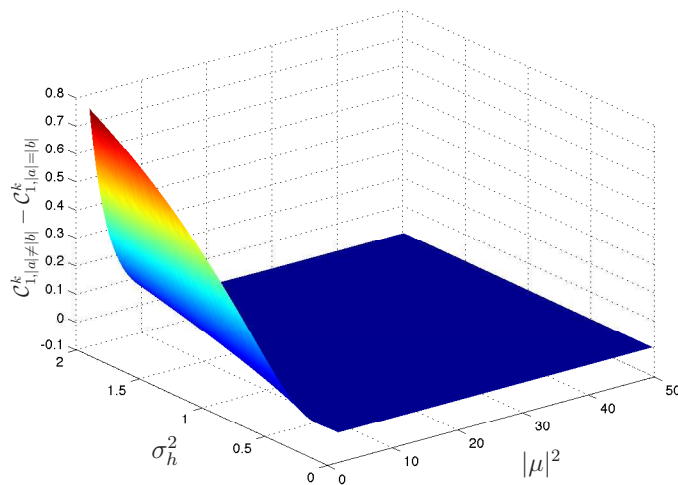


Figure 2.4: $C_{1,|a|≠|b|}^k - C_{1,|a|=|b|}^k$ in Rician fading channels as a function of $|\mu|^2$ and σ_h^2 , where $P^2 = 10, Q^2 = 1$.

as

$$\tilde{I}_1^k(t_1^k) = \hat{I}_1^k(t_1^k) + \beta_k \underbrace{\left(\mathbb{E} \left[\log \frac{1 + \frac{1-\beta_k}{\beta_k} \rho^{-1} e^{\zeta_b}}{1 + \frac{\alpha_k}{1-\alpha_k} \rho^{-1} e^{\zeta_b}} \right] + \frac{1-\beta_k}{\beta_k} \mathbb{E} \left[\log \frac{1 + \frac{\beta_k}{1-\beta_k} \rho e^{\zeta_a}}{1 + \frac{1-\alpha_k}{\alpha_k} \rho e^{\zeta_a}} \right] \right)}_{C_1^k} \quad (2.37)$$

where $\zeta_a \triangleq - \left(\frac{|\tilde{z}_a + (a-b)\mu|^2}{\sigma_b^2} - \frac{|\tilde{z}_a|^2}{\sigma_a^2} \right)$ and $\zeta_b \triangleq - \left(\frac{|\tilde{z}_b + (b-a)\mu|^2}{\sigma_a^2} - \frac{|\tilde{z}_b|^2}{\sigma_b^2} \right)$.

Since AWGN and Rayleigh fading are specific cases of Rician fading when $\sigma_h = 0$ and $|\mu| = 0$, respectively, the optimum signaling scheme in this case is a function of $|\mu|$ and σ_h . In Fig. 2.4, we show that the non-symmetric constellation, which is optimum under Rayleigh fading, is much better than the symmetric one, which is optimum under AWGN, for small $|\mu|$. On the other hand, for large $|\mu|$, the symmetric constellation is only slightly better than the non-symmetric one. Hence, a non-symmetric constellation should be used if μ and σ_h are unavailable.

2.4.4 Discussions

Considering the unreliable detection of the sampling times under continuous channels, we should ideally integrate this uncertainty into the fusion rule of the FC. In other words, at

the FC the LLR $\tilde{\lambda}_t^k$ of the received signal z_t^k should be computed at each time instant t if the sampling time of the k -th sensor cannot be reliably detected. In the LLR computations in (2.16) and (2.17) the prior probabilities $\mathbf{P}_i(x_n^k = a)$ and $\mathbf{P}_i(x_n^k = b)$ are used. These probabilities are conditioned on the sampling time t_n^k . Here, we need the unconditioned prior probabilities of the signal x_t^k which at each time t takes a value of a or b or 0 , i.e.,

$$x_t^k = \begin{cases} a & \text{if } L_t^k - L_{t_{n-1}^k}^k \geq \Delta \\ b & \text{if } L_t^k - L_{t_{n-1}^k}^k \leq -\Delta \\ 0 & \text{if } L_t^k - L_{t_{n-1}^k}^k \in (-\Delta, \Delta). \end{cases} \quad (2.38)$$

As before, the received signal at time t is $z_t^k = h_t^k x_t^k + w_t^k$. Then, the LLR $\tilde{\lambda}_t^k$ of z_t^k is given by

$$\tilde{\lambda}_t^k = \log \frac{(1 - \beta_k) \mathbf{P}_{s,1}^k p(z_t^k | x_t^k = a) + \beta_k \mathbf{P}_{s,1}^k p(z_t^k | x_t^k = b) + (1 - \mathbf{P}_{s,1}^k) p(z_t^k | x_t^k = 0)}{\alpha_k \mathbf{P}_{s,0}^k p(z_t^k | x_t^k = a) + (1 - \alpha_k) \mathbf{P}_{s,0}^k p(z_t^k | x_t^k = b) + (1 - \mathbf{P}_{s,0}^k) p(z_t^k | x_t^k = 0)} \quad (2.39)$$

where $\mathbf{P}_{s,i}^k$ is the probability that the FC receives a signal from sensor k under H_i . Since the FC has no prior information on the sampling times of the sensors, this probability can be shown to be $\frac{1}{\mathbf{E}_i[\tau_1^k]}$, where $\mathbf{E}_i[\tau_1^k]$ is the average intersampling (communication) interval for sensor k under H_i , $i = 0, 1$. For instance, under AWGN channels [cf. (2.16)] by defining $c_t^k \triangleq \frac{|z_t^k - h_k a|^2}{\sigma_k^2}$, $d_t^k \triangleq \frac{|z_t^k - h_k b|^2}{\sigma_k^2}$, and $g_t^k \triangleq \frac{|z_t^k|^2}{\sigma_k^2}$ we have

$$\tilde{\lambda}_t^k = \log \frac{(1 - \beta_k) \mathbf{P}_{s,1}^k e^{-c_t^k} + \beta_k \mathbf{P}_{s,1}^k e^{-d_t^k} + (1 - \mathbf{P}_{s,1}^k) e^{-g_t^k}}{\alpha_k \mathbf{P}_{s,0}^k e^{-c_t^k} + (1 - \alpha_k) \mathbf{P}_{s,0}^k e^{-d_t^k} + (1 - \mathbf{P}_{s,0}^k) e^{-g_t^k}}. \quad (2.40)$$

Under fading channels $\tilde{\lambda}_t^k$ is computed similarly. Realizations of $\tilde{\lambda}_t^k$ of (2.40) and $\tilde{\lambda}_n^k$ of (2.16) are shown in Fig. 2.5 where $P = 10$ is used.

Note that in this case, $\{\tilde{\lambda}_t^k\}$ are i.i.d. across time, and so are $\{\tilde{\lambda}_t\}$ where $\tilde{\lambda}_t \triangleq \sum_{k=1}^K \tilde{\lambda}_t^k$ is the global LLR at time t . Hence, from Wald's identity, similar to Theorem 2 we can write $\mathbf{E}_1[\mathcal{T}] = \frac{\mathbf{E}_1[\sum_{t=1}^{\mathcal{T}} \tilde{\lambda}_t]}{\mathbf{E}_1[\tilde{\lambda}_t]} = \frac{|\log \alpha|}{\mathbf{E}_1[\tilde{\lambda}_t]} + O(1)$. Therefore, we again need to maximize the KL information $\mathbf{E}_1[\tilde{\lambda}_t^k]$ (resp. $-\mathbf{E}_0[\tilde{\lambda}_t^k]$) in order to minimize the average delay $\mathbf{E}_1[\mathcal{T}]$ (resp. $\mathbf{E}_0[\mathcal{T}]$). However, analyzing this expectation is now much more involved than analyzing (2.35). On the other hand, in practice we need to ensure reliable detection of the sampling times by using high enough signaling levels P and Q . Then, the average delay performance

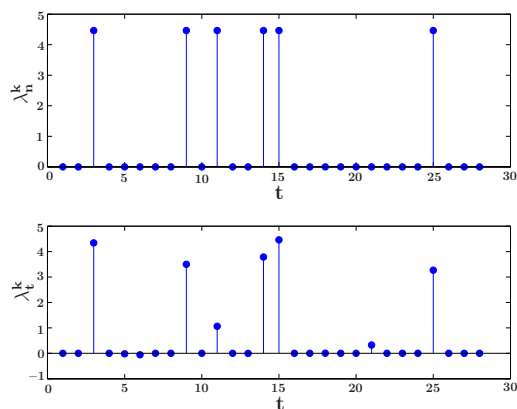


Figure 2.5: Realizations of the LLRs $\tilde{\lambda}_n^k$ and $\tilde{\lambda}_t^k$ computed at the FC under reliable and unreliable detection of the sampling times, respectively.

of this unreliable detection scheme becomes identical to that of the reliable detection scheme analyzed in Section 2.4.3.

As an alternative approach, in the unreliable detection case one can follow a two-step procedure to mimic the reliable detection case. Since it is known that most of the computed LLRs $\{\tilde{\lambda}_t^k\}$ are uninformative that correspond to the no message case, a simple thresholding operation can be applied to update the LLR only when it is informative. The thresholding step is in fact a Neyman-Pearson test between the presence and absence of a message signal. The threshold can be adjusted to control the false alarm and misdetection probabilities. Setting the threshold appropriately we can obtain a negligible false alarm probability, leaving us with the misdetection probability. Note that such a test would turn a continuous channel into a BEC with erasure probability, $\tilde{\epsilon}_k$, equal to the misdetection probability. Recall from Section 2.3.1 that under BEC $\tilde{\lambda}_n^k$ is the same as in the ideal channel case which corresponds to the reliable detection case here. Thus, if an LLR survives after thresholding, in the second step it is recomputed as in the channel-aware fusion rules obtained in Sections 2.3.3, 2.3.4 and 2.3.5. Moreover, the KL information in (2.35), (2.36) and (2.37) will only be scaled by $(1 - \tilde{\epsilon}_k)$ as shown in (2.33). Consequently, the results obtained in Section 2.4.3 are also valid in this approach to the unreliable detection case.

2.5 Spectrum Sensing in Cognitive Radio Networks

Spectrum sensing is one of the most important functionalities in a cognitive radio system [49], by which the secondary users (SU) decide whether or not the spectrum is being used by the primary users. Various spectrum sensing methods have been developed based on exploiting different features of the primary user's signal [50]. On the other hand, cooperative sensing, where multiple secondary users monitor the spectrum band of interest simultaneously and cooperate to make a sensing decision, is an effective way to achieve fast and reliable spectrum sensing [51; 52; 53; 54; 55].

In cooperative sensing, each secondary user collects its own local channel statistic, and sends it to a fusion center (FC), which then combines all local statistics received from the secondary users to make a final sensing decision. The decision mechanism at the FC can be either sequential or fixed sample size. In other words, the FC can either try to make a decision every time it receives new information or it can wait to collect a specific number of samples and then make a final decision using them. It is known that sequential methods are much more effective in minimizing the decision delay than their fixed sample size counterparts. In particular, the sequential probability ratio test (SPRT) is the dual of the fixed sample size Neyman-Pearson test, and it is optimal among all sequential tests in terms of minimizing the average sample number (decision delay) for i.i.d. observations [56; 37]. Sequential approaches to spectrum sensing have been proposed in a number of recent works [57; 58; 59; 60; 61; 62].

The majority of existing works on cooperative and sequential sensing assume that the SUs synchronously communicate to the FC. This implies the existence of a global clock according to which SUs sample their local test statistics using conventional uniform sampling. There are a few works allowing for asynchrony among SUs (e.g., [60; 61]), but none of them provides an analytical discussion on the optimality or the efficiency of the proposed schemes. In this section, we develop a new framework for cooperative sensing based on a class of non-uniform samplers called the *event-triggered samplers*, in which the sampling times are determined in a dynamic way by the signal to be sampled. Such a sampling scheme naturally outputs low-rate information (e.g., 1 bit per sample) without performing any quantization, and permits asynchronous communication between the SUs

and the FC [12]. Both features are ideally suited for cooperative sensing in cognitive radio systems since the control channel for transmitting local statistics has a low bandwidth and it is difficult to maintain synchrony among the SUs. Moreover, we will show that by properly designing the operations at the SUs and FC, the cooperative sensing scheme based on event-triggered sampling can significantly outperform the one based on the conventional uniform sampling.

2.5.1 Problem Formulation and Background

2.5.1.1 Spectrum Sensing via SPRT

Consider a cognitive radio network where there are K secondary users performing spectrum sensing and dynamic spectrum access. Let $\{y_t^k\}$, $t \in \mathbb{N}$, be the discrete-time signal observed by the k -th SU, which processes it and transmits some form of local information to a fusion center. Using the information received at the fusion center from the K SUs, we are interested in deciding between two hypotheses, H_0 and H_1 , for the SU signals: i.e., whether the primary user (PU) is present (H_1) or not (H_0). Specifically, every time the fusion center receives new information, it performs a test and either 1) stops accepting more data and decides between the two hypotheses; or 2) postpones its decision until a new data sample arrives from the SUs. When the fusion center stops and selects between the two hypotheses, the whole process is terminated.

Note that the decision mechanism utilizes the received data sequentially as they arrive at the fusion center. This type of test is called sequential as opposed to the conventional fixed sample size test in which one waits until a specific number of samples has been accumulated and then uses them to make the final hypothesis selection. Since the pioneering work of Wald [56], it has been observed that sequential methods require, on average, approximately four times [1, Page 109] less samples (for Gaussian signals) to reach a decision than their fixed sample size counterparts, for the same level of confidence. Consequently, whenever possible, it is always preferable to use sequential over fixed sample size approaches.

Assuming independence across the signals observed by different SUs, we can cast our

problem of interest as the following *binary* hypothesis testing problem

$$\begin{aligned} \mathbf{H}_0 : \quad & \{y_1^1, \dots, y_t^1\} \sim f_0^1; \{y_1^2, \dots, y_t^2\} \sim f_0^2; \dots; \{y_1^K, \dots, y_t^K\} \sim f_0^K \\ \mathbf{H}_1 : \quad & \{y_1^1, \dots, y_t^1\} \sim f_1^1; \{y_1^2, \dots, y_t^2\} \sim f_1^2; \dots; \{y_1^K, \dots, y_t^K\} \sim f_1^K, \end{aligned} \quad (2.41)$$

where \sim denotes “distributed according to” and f_0^k and f_1^k are the joint probability density functions of the received signal by the k -th SU, under \mathbf{H}_0 and \mathbf{H}_1 respectively. Since we assume independence across different SUs the log-likelihood ratio (LLR) L_t of all the signals received up to time t , which is a sufficient statistic for our problem, can be split as

$$L_t = \sum_{k=1}^K L_t^k \quad (2.42)$$

where L_t^k represents the *local* LLR of the signal received by the k -th SU, namely

$$L_t^k \triangleq \log \frac{f_1^k(y_1^k, \dots, y_t^k)}{f_0^k(y_1^k, \dots, y_t^k)}. \quad (2.43)$$

Hence, each SU can compute its own LLR based on its corresponding observed signal, and send it to the fusion center which collects them and computes the global cumulative LLR L_t using (2.42). Note that the local LLRs can be obtained recursively. That is, at each time t , the new observation y_t^k gives rise to an LLR increment l_t^k , and the local cumulative LLR can then be updated as

$$L_t^k = L_{t-1}^k + l_t^k = \sum_{n=1}^t l_n^k, \quad (2.44)$$

where

$$l_t^k \triangleq \log \frac{f_1^k(y_t^k | y_1^k, \dots, y_{t-1}^k)}{f_0^k(y_t^k | y_1^k, \dots, y_{t-1}^k)}, \quad (2.45)$$

and $f_i^k(y_t^k | y_1^k, \dots, y_{t-1}^k)$ denotes the conditional pdf of y_t^k given the past (local) signal samples under hypothesis \mathbf{H}_i . Of course when the samples of the received signal in each SU are also i.i.d., that is, we have independence across time, then the previous expression simplifies considerably and we can write $l_t^k = \log \frac{f_1^k(y_t^k)}{f_0^k(y_t^k)}$ where now f_i^k represents the pdf of a single sample in the k -th SU under hypothesis \mathbf{H}_i .

As we mentioned, the fusion center collects the local LLRs and at each time instant t is faced with a decision, namely to wait for more data to come, or to stop receiving more data and select one of the two hypotheses $\mathbf{H}_0, \mathbf{H}_1$. In other words the sequential test consists of

a pair $(\mathcal{T}, \delta_{\mathcal{T}})$ where \mathcal{T} is a *stopping time* that decides when to stop (receiving more data) and $\delta_{\mathcal{T}}$ a selection rule that selects one of the two hypotheses based on the information available up to the time of stopping \mathcal{T} .

Of course the goal is to make a decision as soon as possible which means that we would like to minimize the delay \mathcal{T} , on average, that is,

$$\min_{\mathcal{T}, \delta_{\mathcal{T}}} \mathbf{E}_0[\mathcal{T}], \quad \text{and/or} \quad \min_{\mathcal{T}, \delta_{\mathcal{T}}} \mathbf{E}_1[\mathcal{T}]. \quad (2.46)$$

At the same time we would also like to assure the satisfactory performance of the decision mechanism through suitable constraints on the Type-I and Type-II error probabilities, namely

$$\mathbf{P}_0(\delta_{\mathcal{T}} = 1) \leq \alpha \quad \text{and} \quad \mathbf{P}_1(\delta_{\mathcal{T}} = 0) \leq \beta, \quad (2.47)$$

where $\mathbf{P}_i(\cdot), \mathbf{E}_i[\cdot]$, $i = 0, 1$ denote probability and the corresponding expectation under hypothesis i . Levels $\alpha, \beta \in (0, 1)$ are parameters specified by the designer.

Actually, minimizing in (2.46) each $\mathbf{E}_i[\mathcal{T}]$, $i = 0, 1$ over the pairs $(\mathcal{T}, \delta_{\mathcal{T}})$ that satisfy the two constraints in (2.47), defines *two* separate constrained optimization problems. However, Wald first suggested [56] and then proved [37] that the Sequential Probability Ratio Test (SPRT) *solves both problems simultaneously*. SPRT consists of the pair $(\mathcal{S}, \delta_{\mathcal{S}})$ which is defined as follows

$$\mathcal{S} = \inf \{t > 0 : L_t \notin (-B, A)\}, \quad \delta_{\mathcal{S}} = \begin{cases} 1, & \text{if } L_{\mathcal{S}} \geq A, \\ 0, & \text{if } L_{\mathcal{S}} \leq -B. \end{cases} \quad (2.48)$$

In other words, at every time instant t , we compare the running LLR L_t with two thresholds $-B, A$ where $A, B > 0$. As long as L_t stays within the interval $(-B, A)$ we continue taking more data and update L_t ; the first time L_t exits $(-B, A)$ we stop (accepting more data) and we use the already accumulated information to decide between the two hypotheses $\mathbf{H}_0, \mathbf{H}_1$. If we call \mathcal{S} the time of stopping (which is clearly random, since it depends on the received data), then when $L_{\mathcal{S}} \geq A$ we decide in favor of \mathbf{H}_1 , whereas if $L_{\mathcal{S}} \leq -B$ in favor of \mathbf{H}_0 . The two thresholds A, B are selected through simulations so that SPRT satisfies the two constraints in (2.47) with equality. This is always possible provided that $\alpha + \beta < 1$. In the opposite case there is a trivial randomized test that can meet the two constraints without

taking any samples (delay equal to 0). Note that these simulations to find proper values for A, B are performed once offline, i.e. before the scheme starts, for each sensing environment.

The popularity of SPRT is due to its simplicity, but primarily to its very unique optimality properties. Regarding the latter we must say that optimality in the sense of (2.46), (2.47) is assured only in the case of i.i.d. observations. For more complex data models, SPRT is known to be only asymptotically optimum.

SPRT, when employed in our problem of interest, exhibits two serious practical weaknesses. First the SUs need to send their local LLRs to the fusion center at the Nyquist-rate of the signal; and secondly, the local LLR is a real number which needs infinite (practically large) number of bits to be represented. These two problems imply that a substantial communication overhead between the SUs and the fusion center is incurred. In this work, we are interested in *decentralized* schemes by which we mean that the SUs transmit *low-rate* information to the fusion center.

2.5.1.2 Decentralized Q-SPRT Scheme

A straightforward way to achieve low-rate transmission is to let each SU transmit its local cumulative LLR at a lower rate, say at time instants $T, 2T, \dots, mT, \dots$, where the period $T \in \mathbb{N}$; and to quantize the local cumulative LLRs using a finite number of quantization levels. Specifically, during time instants $(m-1)T+1, \dots, mT$, each SU computes its incremental LLR $L_{mT}^k - L_{(m-1)T}^k$ of the observations $y_{(m-1)T+1}^k, \dots, y_{mT}^k$, to obtain

$$\lambda_{mT}^k \triangleq L_{mT}^k - L_{(m-1)T}^k = \sum_{t=(m-1)T+1}^{mT} l_t^k, \quad (2.49)$$

where l_t^k is the LLR of observation y_t^k , defined in (2.45). It then quantizes λ_{mT}^k into $\tilde{\lambda}_{mT}^k$ using a finite number \tilde{r} of quantization levels. Although there are several ways to perform quantization, here we are going to analyze the simplest strategy, namely uniform quantization. We will also make the following assumption

$$\max_{k,t} |l_t^k| < \phi < \infty, \quad (2.50)$$

stating that the LLRs of all observations are uniformly bounded by a finite constant ϕ across time and across SUs.

From (2.49) and (2.50) we can immediately conclude that $|\lambda_{mT}^k| < T\phi$. For our quantization scheme we can now divide the interval $(-T\phi, T\phi)$ uniformly into \tilde{r} subintervals and assign the mid-value of each subinterval as the corresponding quantized value. Specifically we define

$$\tilde{\lambda}_{mT}^k = -T\phi + \frac{T\phi}{\tilde{r}} + \left\lfloor \frac{\tilde{r}(\lambda_{mT}^k + T\phi)}{2T\phi} \right\rfloor \frac{2T\phi}{\tilde{r}}. \quad (2.51)$$

These quantized values are then transmitted to the FC. Of course the SU does not need to send the actual value but only its index which can be encoded with $\log_2 \tilde{r}$ bits.

The FC receives the quantized information from all SUs, *synchronously*, and updates the approximation of the global running LLR based on the information received, i.e.

$$\tilde{L}_{mT} = \tilde{L}_{(m-1)T} + \sum_{k=1}^K \tilde{\lambda}_{mT}^k. \quad (2.52)$$

Mimicking the SPRT introduced above, we can then define the following sequential scheme $(\tilde{\mathcal{S}}, \delta_{\tilde{\mathcal{S}}})$, where

$$\tilde{\mathcal{S}} = T\mathcal{M}; \quad \mathcal{M} = \inf \left\{ m > 0 : \tilde{L}_{mT} \notin (-\tilde{B}, \tilde{A}) \right\}; \quad \delta_{\tilde{\mathcal{S}}} = \begin{cases} 1, & \text{if } \tilde{L}_{\tilde{\mathcal{S}}} \geq \tilde{A}, \\ 0, & \text{if } \tilde{L}_{\tilde{\mathcal{S}}} \leq -\tilde{B}. \end{cases} \quad (2.53)$$

Again, the two thresholds \tilde{A}, \tilde{B} are selected to satisfy the two error probability constraints with equality. We call this scheme the *Quantized-SPRT* and denote it as Q-SPRT.

As we will see in our analysis, the performance of Q-SPRT is directly related to the quantization error of each SU. Since we considered the simple uniform quantization, it is clear that

$$|\lambda_{mT}^k - \tilde{\lambda}_{mT}^k| < \frac{T\phi}{\tilde{r}}. \quad (2.54)$$

We next consider three popular spectrum sensing methods and give the corresponding local LLR expressions.

2.5.1.3 Examples - Spectrum Sensing Methods

Energy Detector

The energy detector performs spectrum sensing by detecting the primary user's signal energy. We assume that when the primary user is present, the received signal at the k -th SU

is $y_t^k = x_t^k + w_t^k$, where x_t^k is the received primary user signal, and $w_t^k \sim \mathcal{N}_c(0, \sigma_w^2)$ is the additive white Gaussian noise. Denote $\theta_k \triangleq \frac{\mathbb{E}[|x_t^k|^2]}{\sigma_w^2/2}$ then the received signal-to-noise ratio (SNR) at the k -th SU is $\frac{\mathbb{E}[|x_t^k|^2]}{\sigma_w^2} = \frac{\theta_k}{2}$. Also define $\gamma_t^k \triangleq \frac{|y_t^k|^2}{\sigma_w^2/2}$. The energy detector is based on the following hypothesis testing formulation [50]

$$\begin{aligned} \mathbf{H}_0 : \quad & \gamma_t^k \sim \chi_2^2, \\ \mathbf{H}_1 : \quad & \gamma_t^k \sim \chi_2^2(\theta_k), \end{aligned} \tag{2.55}$$

where χ_2^2 denotes a central chi-squared distribution with 2 degrees of freedom; and $\chi_2^2(\theta_k)$ denotes a non-central chi-squared distribution with 2 degrees of freedom and noncentrality parameter θ_k .

Using the pdfs of central and non-central chi-squared distributions, we write the local LLR, l_t^k , of the observations as follows

$$l_t^k = \log \frac{\frac{1}{2} \exp\left(-\frac{\gamma_t^k + \theta_k}{2}\right) I_0\left(\sqrt{\theta_k \gamma_t^k}\right)}{\frac{1}{2} \exp\left(-\frac{\gamma_t^k}{2}\right)} = \log I_0\left(\sqrt{\theta_k \gamma_t^k}\right) - \frac{\theta_k}{2}, \tag{2.56}$$

where $I_0(x)$ is the modified Bessel function of the first kind and 0-th order.

Spectral Shape Detector

A certain class of primary user signals, such as the television broadcasting signals, exhibit strong spectral correlation that can be exploited by the spectrum sensing algorithm [63]. The corresponding hypothesis testing then consists in discriminating between the channel's white Gaussian noise, and the correlated primary user signal. The spectral shape of the primary user signal is assumed known a priori, which can be approximated by a p -th order auto-regressive (AR) model. Hence the hypothesis testing problem can be written as

$$\begin{aligned} \mathbf{H}_0 : \quad & y_t^k = w_t^k, \\ \mathbf{H}_1 : \quad & y_t^k = \sum_{i=1}^p a_i y_{t-i}^k + v_t^k, \end{aligned} \tag{2.57}$$

where $\{w_t^k\}, \{v_t^k\}$ are i.i.d. sequences with $w_t^k \sim \mathcal{N}_c(0, \sigma_w^2)$ and $v_t^k \sim \mathcal{N}_c(0, \sigma_v^2)$, while a_1, \dots, a_p are the AR model coefficients.

Using the Gaussian pdf the likelihoods under \mathbf{H}_0 and \mathbf{H}_1 can be easily derived. Then,

accordingly the local LLR of the sample received at time t at the k -th SU can be written as

$$\begin{aligned} l_t^k &= \log \frac{f_1^k(y_t^k | y_{t-1}^k, \dots, y_{t-p}^k)}{f_0^k(y_t^k)} = \log \frac{\frac{1}{\pi \sigma_v^2} \exp \left[-\frac{1}{\sigma_v^2} |y_t^k - \sum_{i=1}^p a_i y_{t-i}^k|^2 \right]}{\frac{1}{\pi \sigma_w^2} \exp \left(-\frac{1}{\sigma_w^2} |y_t^k|^2 \right)} \\ &= \frac{1}{\sigma_w^2} |y_t^k|^2 - \frac{1}{\sigma_v^2} \left| y_t^k - \sum_{i=1}^p a_i y_{t-i}^k \right|^2 + \log \frac{\sigma_w^2}{\sigma_v^2}. \end{aligned} \quad (2.58)$$

Gaussian Detector

In general, when the primary user is present, the received signal by the k -th SU can be written as $y_t^k = h_t^k s_t + w_t^k$, where $h_t^k \sim \mathcal{N}_c(0, \rho_k^2)$ is the fading channel response between the primary user and the k -th secondary user; s_t is the digitally modulated signal of the primary user drawn from a certain modulation, with $\mathbb{E}[|s_t|^2] = 1$; and $w_t^k \sim \mathcal{N}_c(0, \sigma_w^2)$ is the additive white Gaussian noise. It is shown in [64] that under both fast fading and slow fading conditions, spectrum sensing can be performed based on the following hypothesis testing between two Gaussian signals:

$$\begin{aligned} \text{H}_0 : \quad & y_t^k \sim \mathcal{N}_c(0, \sigma_w^2), \\ \text{H}_1 : \quad & y_t^k \sim \mathcal{N}_c(0, \rho_k^2 + \sigma_w^2). \end{aligned} \quad (2.59)$$

Then, using the Gaussian pdf the local incremental LLR l_t^k is derived as

$$l_t^k = \log \frac{f_1^k(y_t^k)}{f_0^k(y_t^k)} = \log \frac{\frac{1}{\pi(\rho_k^2 + \sigma_w^2)} \exp \left(-\frac{|y_t^k|^2}{\rho_k^2 + \sigma_w^2} \right)}{\frac{1}{\pi \sigma_w^2} \exp \left(-\frac{|y_t^k|^2}{\sigma_w^2} \right)} = \frac{\rho_k^2}{\sigma_w^2 (\rho_k^2 + \sigma_w^2)} |y_t^k|^2 + \log \frac{\sigma_w^2}{\rho_k^2 + \sigma_w^2}. \quad (2.60)$$

2.5.2 Decentralized Spectrum Sensing via Level-triggered Sampling

Here, we achieve the low-rate transmission required by the decentralized SPRT by adopting event-triggered sampling, that is, a sampling strategy in which the sampling times are dictated by the actual signal to be sampled, in a dynamic way and as the signal evolves in time. One could suggest to find the optimum possible combination of event-triggered sampling and sequential detection scheme by directly solving the double optimization problem defined in (2.46), (2.47) over the triplet sampling, stopping time, and decision function. Unfortunately the resulting optimization turns out to be extremely difficult not accepting a simple solution. We therefore adopt an indirect path. In particular, we propose a decentralized spectrum sensing approach based on a simple form of event-triggered sampling,

namely, the level-triggered sampling. Then we show that the performance loss incurred by adopting this scheme as compared to the *centralized* optimum SPRT is insignificant. This clearly suggests that solving the more challenging optimization problem we mentioned before, produces only minor performance gains.

2.5.2.1 Level-triggered Sampling at each SU

Using level-triggered sampling, each SU samples its local cumulative LLR process $\{L_t^k\}$ at a sequence of *random times* $\{t_n^k\}$, which is particular to each SU. In other words we do not assume any type of synchronization in sampling and therefore communication. The corresponding sequence of samples is $\{L_{t_n^k}^k\}$ with the sequence of sampling times recursively defined as follows

$$t_n^k \triangleq \inf \left\{ t > t_{n-1}^k : L_t^k - L_{t_{n-1}^k}^k \notin (-\Delta, \Delta) \right\}, \quad t_0^k = 0, \quad L_0^k = 0. \quad (2.61)$$

where Δ is a constant. As we realize from (2.61) the sampling times depend on the actual *realization* of the observed LLR process and are therefore, as we pointed out, random. Parameter Δ can be selected to control the *average* sampling periods $\mathbf{E}_i[t_n^k - t_{n-1}^k]$, $i = 0, 1$. In Section 2.5.3.2, we propose a practically meaningful method to set this design parameter Δ in a way that assures a fair comparison of our method with the classical decentralized scheme, that is, Q-SPRT.

What is interesting with this sampling mechanism is that it is not necessary to know the exact sampled value but only whether the incremental LLR $L_t^k - L_{t_{n-1}^k}^k$ crossed the upper or the lower threshold. This information can be represented by using a *single* bit. Denote with $\{b_n^k\}$ the sequence of these bits, where $b_n^k = +1$ means that the LLR increment crossed the upper boundary while $b_n^k = -1$ the lower. In fact we can also define this bit as $b_n^k = \text{sign}(\lambda_n^k)$ where $\lambda_n^k \triangleq L_{t_n^k}^k - L_{t_{n-1}^k}^k$.

We can now approximate the local incremental LLR as $\hat{\lambda}_n^k = b_n^k \Delta$, and since $L_{t_n^k}^k = \sum_{j=1}^n \lambda_j^k$ we conclude that we can approximate the local LLR at the sampling times using the following equation

$$\hat{L}_{t_n^k}^k = \sum_{j=1}^n \hat{\lambda}_j^k = \sum_{j=1}^n b_j^k \Delta = \hat{L}_{t_{n-1}^k}^k + b_n^k \Delta. \quad (2.62)$$

Note that we have *exact recovery*, i.e., $\hat{L}_{t_n}^k = L_{t_n}^k$, if the difference $L_t^k - L_{t_{n-1}^k}^k$, at the times of sampling, hits exactly one of the two boundaries $\pm\Delta$. This is for example the case when $\{L_t^k\}$ is a continuous-time process with continuous paths.

The advantage of the level-triggered approach manifests itself if we desire to communicate the sampled information, as is the case of decentralized spectrum sensing. Indeed note that with classical sampling we need to transmit, every T units of time, the *real numbers* L_{mT}^k (or their digitized version with fixed number of bits). On the other hand, in the level-triggered case, transmission is performed at the random time instants $\{t_n^k\}$ and at each t_n^k we simply transmit the *1-bit* value b_n^k . This property of 1-bit communication induces significant savings in bandwidth and transmission power, which is especially valuable for the cognitive radio applications, where low-rate and low-power signaling among the secondary users is a key issue for maintaining normal operating conditions for the primary users.

We observe that by using (2.44), we have $L_t^k - L_{t_{n-1}^k}^k = \sum_{j=t_{n-1}^k+1}^t l_j^k$ where, we recall, l_t^k is the (conditional) LLR of the observation y_t^k at time t at the k -th SU defined in (2.45). Hence (2.61) can be rewritten as

$$t_n^k = \inf \left\{ t > t_{n-1}^k : \sum_{j=t_{n-1}^k+1}^t l_j^k \notin (-\Delta, \Delta) \right\}. \quad (2.63)$$

The level-triggered sampling procedure at each secondary user is summarized in Algorithm 1. Until the fusion center terminates it, the algorithm produces the bit stream $\{b_n^k\}$ based on the local cumulative LLR values L_t^k at time instants $\{t_n^k\}$, and sends these bits to the fusion center instantaneously as they are generated.

Remarks:

- Note that the level-triggered sampling naturally censors unreliable local information gathered at SUs, and allows only informative LLRs to be sent to the FC.
- Note also that each SU essentially performs a *local* SPRT with thresholds $\pm\Delta$. The stopping times of the local SPRT are the inter-sampling intervals and the corresponding decisions are the bits $\{b_n^k\}$ where $b_n^k = +1$ and $b_n^k = -1$ favor H_1 and H_0 respectively.

Algorithm 1 The level-triggered sampling procedure at the k -th SU

- 1: Initialization: $t \leftarrow 0$, $n \leftarrow 0$
 - 2: $\lambda \leftarrow 0$
 - 3: **while** $\lambda \in (-\Delta, \Delta)$ **do**
 - 4: $t \leftarrow t + 1$
 - 5: Compute l_t^k (cf. Sec. 2.5.1.3)
 - 6: $\lambda \leftarrow \lambda + l_t^k$
 - 7: **end while**
 - 8: $n \leftarrow n + 1$
 - 9: $t_n^k = t$
 - 10: Send $b_n^k = \text{sign}(\lambda)$ to the fusion center at time instant t_n^k
 - 11: Stop if the fusion center instructs so; otherwise go to line 2.
-

2.5.2.2 Proposed Decentralized Scheme

The bit streams $\{b_n^k\}_k$ from different SUs arrive at the FC asynchronously. Using (2.42) and (2.62), the global running LLR at any time t is approximated by

$$\hat{L}_t = \sum_{k=1}^K \hat{L}_t^k = \Delta \sum_{k=1}^K \sum_{n: t_n^k \leq t} b_n^k. \quad (2.64)$$

In other words the FC adds all the received bits transmitted by all SUs up to time t and then normalizes the result with Δ . Actually the update of \hat{L}_t is even simpler. If $\{t_n\}$ denotes the sequence of communication instants of the FC with any SU, and $\{b_n\}$ the corresponding sequence of received bits then $\hat{L}_{t_n} = \hat{L}_{t_{n-1}} + b_n \Delta$ while the global running LLR is kept constant between transmissions. In case the FC receives more than one bit simultaneously (possible in discrete time), it processes each bit separately, as we described, following any random or fixed ordering of the SUs.

Every time the global LLR process $\{\hat{L}_t\}$ is updated at the FC it will be used in an SPRT-like test to decide whether to stop or continue (receiving more information from the SUs) and in the case of stopping to choose between the two hypotheses. Specifically the corresponding sequential test $(\hat{S}, \hat{\delta}_{\hat{S}})$ is defined, similarly to the centralized SPRT and Q-SPRT, as

$$\hat{S} = t_{\mathcal{N}}; \quad \mathcal{N} = \inf \left\{ n > 0 : \hat{L}_{t_n} \notin (-\hat{B}, \hat{A}) \right\}; \quad \hat{\delta}_{\hat{S}} = \begin{cases} 1, & \text{if } \hat{L}_{\hat{S}} \geq \hat{A}, \\ 0, & \text{if } \hat{L}_{\hat{S}} \leq -\hat{B}. \end{cases} \quad (2.65)$$

$\hat{\mathcal{S}}$ counts in physical time units, whereas \mathcal{N} in number of messages transmitted from the SUs to the FC. Clearly (2.65) is the equivalent of (2.53) in the case of Q-SPRT and expresses the reduction in communication rate as compared to the rate by which observations are acquired. In Q-SPRT the reduction is deterministic since the SUs communicate once every T unit times, whereas here it is random and dictated by the local level triggered sampling mechanism at each SU. The thresholds \hat{A}, \hat{B} , as before, are selected so that $(\hat{\mathcal{S}}, \hat{\delta}_{\mathcal{S}})$ satisfies the two error probability constraints with equality. The operations performed at the FC are also summarized in Algorithm 2.

Algorithm 2 The SPRT-like procedure at the fusion center

- 1: Initialization: $\hat{L} \leftarrow 0, n \leftarrow 0$
 - 2: **while** $\hat{L} \in (-\hat{B}, \hat{A})$ **do**
 - 3: $n \leftarrow n + 1$
 - 4: Listen to the SUs and wait to receive the next bit b_n at time t_n from some SU
 - 5: $\hat{L} \leftarrow \hat{L} + b_n \Delta$
 - 6: **end while**
 - 7: Stop at time $\hat{\mathcal{S}} = t_n$
 - 8: **if** $\hat{L} \geq \hat{A}$ **then**
 - 9: $\hat{\delta}_{\mathcal{S}} = 1$ – the primary user is present
 - 10: **else**
 - 11: $\hat{\delta}_{\mathcal{S}} = 0$ – the primary user is not present
 - 12: **end if**
 - 13: Inform all SUs the spectrum sensing result
-

2.5.2.3 Enhancement

A very important source of performance degradation in our proposed scheme is the difference between the exact value of L_t^k and its approximation \hat{L}_t^k (see [12]). In fact the more accurately we approximate L_t^k the better the performance of the corresponding SPRT-like scheme is going to be. In what follows we discuss an enhancement to the decentralized spectrum sensing method described above at the SU and FC, respectively. Specifically, for the SU, we consider using more than one bit to quantize the local incremental LLR values, while at the FC, we are going to use this extra information in a specific reconstruction method that will improve the approximation \hat{L}_t^k and, consequently, the approximation of the global running LLR. We anticipate that this enhancement will induce a significant im-

provement in the overall performance of the proposed scheme by using only a small number of additional bits. Finally we should stress that there is no need for extra bits in the case of continuous-time and continuous-path signals since, as we mentioned, in this case \hat{L}_t^k and L_t^k coincide.

Overshoot Quantization at the SU

Recall that for the continuous-time case, at each sampling instant, either the upper or the lower boundary can be hit exactly by the local LLR, and therefore the information transmitted to the fusion center was simply a 1-bit sequence and this is sufficient to recover completely the sampled LLR using (2.62). In discrete-time case, at the time of sampling, the LLR is no longer necessarily equal to the boundary since, due to the discontinuity of the discrete-time signal, we can overshoot the upper boundary or undershoot the lower boundary. The over/under shoot phenomenon introduces a discrepancy in the whole system resulting in an additional information loss (besides the loss in time resolution due to sampling). Here we consider the simple idea of allowing the transmission of more than one bits, which could help approximate more accurately the local LLR and consequently reduce the performance loss due to the over/under shoot phenomenon.

Bit b_n^k informs whether the difference $\lambda_n^k \triangleq L_{t_n^k}^k - L_{t_{n-1}^k}^k$ overshoots the upper threshold Δ or undershoots the lower threshold $-\Delta$. Consequently the difference $q_n^k \triangleq |\lambda_n^k| - \Delta \geq 0$, corresponds to the absolute value of the over/under shoot. It is exactly this value we intend to further quantize at each SU. Note that q_n^k cannot exceed in absolute value the last observed LLR increment, namely $|l_{t_n^k}^k|$. To simplify our analysis we will assume that $|l_t^k| < \phi < \infty$ for all k, t as in (2.50). In other words the LLR of each observation is uniformly bounded across time and SUs.

Since for the amplitude q_n^k of the overshoot we have $q_n^k \leq |l_{t_n^k}^k|$ this means that $0 \leq q_n^k < \phi$. Let us now divide the interval $[0, \phi)$, uniformly, into the following \hat{r} subintervals $[(m-1)\frac{\phi}{\hat{r}}, m\frac{\phi}{\hat{r}})$, $m = 1, \dots, \hat{r}$. Whenever q_n^k falls into one such subintervals the corresponding SU must transmit a quantized value \hat{q}_n^k to the FC. Instead of adopting some deterministic strategy and always transmit the same value for each subinterval, we propose the following

simple *randomized* quantization rule

$$\hat{q}_n^k = \begin{cases} \lfloor \frac{q_n^k \hat{r}}{\phi} \rfloor \frac{\phi}{\hat{r}}, & \text{with probability } p = \frac{1 - \exp(q_n^k - (\lfloor \frac{q_n^k \hat{r}}{\phi} \rfloor + 1) \frac{\phi}{\hat{r}})}{1 - \exp(-\frac{\phi}{\hat{r}})} \\ (\lfloor \frac{q_n^k \hat{r}}{\phi} \rfloor + 1) \frac{\phi}{\hat{r}}, & \text{with probability } 1 - p = \frac{\exp(q_n^k - (\lfloor \frac{q_n^k \hat{r}}{\phi} \rfloor + 1) \frac{\phi}{\hat{r}}) - 1}{\exp(\frac{\phi}{\hat{r}}) - 1}. \end{cases} \quad (2.66)$$

Simply said, if $q_n^k \in [(m-1), m) \frac{\phi}{\hat{r}}$ then we quantize q_n^k either with the lower *or* the upper end of the subinterval by selecting randomly between the two values. The quantized value \hat{q}_n^k that needs to be transmitted to the FC clearly depends on the outcome of a random game and is not necessarily the same every time q_n^k falls into the same subinterval. Regarding the randomization probability p the reason it has the specific value depicted in (2.66) will become apparent in Lemma 1.

If we have \hat{r} subintervals then we transmit $\hat{r} + 1$ different messages corresponding to the values $m \frac{\phi}{\hat{r}}$, $m = 0, \dots, \hat{r}$. Combining them with the sign bit b_n^k that also needs to be communicated to the FC, yields a total of $2(\hat{r} + 1)$ possible messages requiring $\log_2 2(1 + \hat{r}) = 1 + \log_2(1 + \hat{r})$ bits for transmitting this information. It is clear that each SU needs to transmit only an index value since we assume that the FC knows the list of all $2(1 + \hat{r})$ quantized values.

Modified Update at the FC

Let us now turn to the FC and see how it is going to use this additional information. Note that the k -th SU, every time it samples, transmits the pair (b_n^k, \hat{q}_n^k) where, we recall, the sign bit b_n^k informs whether we overshoot the upper threshold Δ or undershoot the lower threshold $-\Delta$ and \hat{q}_n^k the quantized version of the absolute value of the overshoot. Consequently since we have $\lambda_n^k = b_n^k(\Delta + q_n^k)$ it is only natural to approximate the difference as follows

$$\hat{\lambda}_n^k = b_n^k (\Delta + \hat{q}_n^k), \quad (2.67)$$

which leads to the following update of the local running LLR

$$\hat{L}_{t_n^k}^k = \hat{L}_{t_{n-1}^k}^k + b_n^k (\Delta + \hat{q}_n^k). \quad (2.68)$$

This should be compared with the simplified version (2.62) where the term \hat{q}_n^k is missing. It is exactly this additional term that increases the accuracy of our approximation and

contributes to a significant performance improvement in our scheme. Of course the update of the global running LLR is much simpler. If the FC receives at time t_n information (b_n, \hat{q}_n) from some SU, then it will update its approximation of the global running LLR as follows

$$\hat{L}_{t_n} = \hat{L}_{t_{n-1}} + b_n (\Delta + \hat{q}_n). \quad (2.69)$$

The updated value will be held constant until the next arrival of information from some SU.

For the SU operations given in Algorithm 1, only line 10 should be modified when multiple bits are used at each sampling instant, as follows

10: Quantize q_n^k as in (2.66) and send (b_n^k, \hat{q}_n^k) to the fusion center at time t_n^k .

On the other hand, for the FC operations given in Algorithm 2, lines 4 and 5 should be modified as follows

4: Listen to the SUs and wait to receive the next message (b_n, \hat{q}_n) from some SU.
 5: $\hat{L} \leftarrow \hat{L} + b_n (\Delta + \hat{q}_n)$.

With the proposed modification at each SU and at the FC we have in fact altered the communication protocol between the SUs and the FC and also the way the FC approximates the global running LLR. The final sequential test $(\hat{S}, \hat{\delta}_S)$ however, is exactly the same as in (2.65). We are going to call our decentralized test *Randomized Level Triggered SPRT* and denote it as RLT-SPRT¹. As we will demonstrate theoretically and also through simulations, the employment of extra bits in the communication between SUs and FC will improve, considerably, the performance of our test, practically matching that of the optimum.

Let us now state a lemma that presents an important property of the proposed quantization scheme. Its proof is given in Appendix A.

Lemma 1. *Let \hat{q}_n^k be the $(\hat{r}+1)$ -level quantization scheme defined in (2.66) for the overshoot q_n^k , then*

$$\mathbb{E}[e^{\pm b_n^k (\Delta + \hat{q}_n^k)} | b_n^k, q_n^k] \leq e^{\pm b_n^k (\Delta + q_n^k)} = e^{\pm (L_{t_n^k}^k - L_{t_{n-1}^k}^k)}, \quad (2.70)$$

where $\mathbb{E}[\cdot]$ denotes expectation with respect to the randomization probabilities.

¹In [12] the corresponding decentralized D-SPRT test that uses level triggered sampling at the sensors (that play the role of the SUs) is based only on 1-bit communication.

Note that the approximation in the incremental LLR $L_{t_n^k}^k - L_{t_{n-1}^k}^k$ induces an equivalent approximation for the incremental LR $\exp(L_{t_n^k}^k - L_{t_{n-1}^k}^k)$. The randomization is selected so that the latter, in average (over the randomization), does not exceed the exact incremental LR. One could instead select p so that the average of the approximation of the incremental LLR matches the exact LLR value. Even though this seems as the most sensible selection, unfortunately, it leads to severe analytical complications which are impossible to overcome. The proposed definition of p , as we will see in the next section, does not have such problems.

2.5.3 Performance Analysis

In this section, we provide an asymptotic analysis on the stopping time of the decentralized spectrum sensing method based on the level-triggered sampling scheme proposed in Section 2.5.2, and compare it with the centralized SPRT procedure given by (2.48). A similar comparison is performed for the conventional decentralized approach that uses uniform sampling and quantization [cf. (2.49),(2.52)]. For our comparisons we will be concerned with the notion of asymptotic optimality for which we distinguish different levels [12; 65].

Definition 1. Consider any sequential scheme $(\mathcal{T}, \delta_{\mathcal{T}})$ with stopping time \mathcal{T} and decision function $\delta_{\mathcal{T}}$ satisfying the two error probability constraints $P_0(\delta_{\mathcal{T}} = 1) \leq \alpha$ and $P_1(\delta_{\mathcal{T}} = 0) \leq \beta$. If \mathcal{S} denotes the optimum SPRT that satisfies the two error probability constraints with equality then, as the Type-I and Type-II error probabilities $\alpha, \beta \rightarrow 0$, the sequential scheme $(\mathcal{T}, \delta_{\mathcal{T}})$ is said to be order-1 asymptotically optimal if²

$$1 \leq \frac{E_i[\mathcal{T}]}{E_i[\mathcal{S}]} = 1 + o_{\alpha, \beta}(1); \quad (2.71)$$

order-2 asymptotically optimal if

$$0 \leq E_i[\mathcal{T}] - E_i[\mathcal{S}] = O(1); \quad (2.72)$$

²A quick reminder for the definitions of the notations $o(\cdot)$, $O(\cdot)$ and $\Theta(\cdot)$: $f(x) = o(g(x))$ if $f(x)$ grows with a lower rate than $g(x)$; $f(x) = O(g(x))$ if $f(x)$ grows with a rate that is no larger than the rate of $g(x)$; and $f(x) = \Theta(g(x))$ if $f(x)$ grows with exactly the same rate as $g(x)$. Thus $o(1)$ represents a term that tends to 0. Particularly for this case we will write $o_x(1)$ to indicate a quantity that becomes negligible with x and $o_{x,y}(1)$ to indicate a quantity that becomes negligible either with x or with y or with both.

and finally order-3, if

$$0 \leq \mathbb{E}_i[\mathcal{T}] - \mathbb{E}_i[\mathcal{S}] = o_{\alpha,\beta}(1), \quad (2.73)$$

where $\mathbb{P}_i(\cdot)$ and $\mathbb{E}_i[\cdot]$ denote probability and the corresponding expectation under hypothesis \mathbb{H}_i , $i = 0, 1$.

Remark: In our definitions the left-hand side inequalities are automatically satisfied because \mathcal{S} is the optimum test. Note that order-2 asymptotic optimality implies order-1 because $\mathbb{E}_i[\mathcal{S}], \mathbb{E}_i[\mathcal{T}] \rightarrow \infty$ as $\alpha, \beta \rightarrow 0$; the opposite is not necessarily true. Order-1 is the most frequent form of asymptotic optimality encountered in the literature but it is also the weakest. This is because it is possible for $\mathbb{E}_i[\mathcal{T}]$ to diverge from the optimum $\mathbb{E}_i[\mathcal{S}]$ without bound and still have a ratio that tends to 1. Order-2 optimality clearly limits the difference to bounded values, it is therefore stronger than order-1. Finally the best would be the difference to become arbitrarily small, as the two error probabilities tend to 0, which is the order-3 asymptotic optimality. This latter form of asymptotic optimality is extremely rare in the Sequential Analysis literature and corresponds to schemes which, for all practical purposes, are considered as optimum per se.

Next we study the three sequential tests of interest, namely the optimum centralized SPRT, the Q-SPRT and the RLT-SPRT and compare the last two with the optimum in order to draw conclusions about their asymptotic optimality. We start by recalling from the literature the basic results concerning the tests of interest in continuous time. Then we continue with a detailed presentation of the discrete-time case where we analyze the performance of Q-SPRT and RLT-SPRT when the corresponding quantization schemes have a number of quantization levels that depends on the error probabilities.

2.5.3.1 Analysis of Centralized SPRT, Q-SPRT and RLT-SPRT

With continuous-time and continuous-path observations at the SUs, it is known that RLT-SPRT, using only 1-bit achieves *order-2* asymptotic optimality [12], whereas Q-SPRT cannot enjoy any type of optimality by using fixed number of bits [66].

In discrete time the corresponding analysis of the three sequential schemes of interest becomes more involved, basically due to the overshoot effect. This is particularly apparent in RLT-SPRT where because of the overshoots, 1-bit communication is no longer capable

of assuring order-2 asymptotic optimality as in the continuous-time and continuous-path case. In order to recover this important characteristic in discrete time, we are going to use the enhanced quantization/communication scheme proposed in Section 2.5.2.3. Let us now consider in detail each test of interest separately.

In discrete time, for the optimum centralized SPRT, we have the following lemma that provides the necessary information for the performance of the test.

Lemma 2. *Assuming that the two error probabilities $\alpha, \beta \rightarrow 0$ at the same rate, the centralized SPRT, \mathcal{S} , satisfies*

$$\mathbb{E}_0[\mathcal{S}] \geq \frac{1}{Kl_0} \mathcal{H}(\alpha, \beta) = \frac{|\log \beta|}{Kl_0} + o_\beta(1); \quad \mathbb{E}_1[\mathcal{S}] \geq \frac{1}{Kl_1} \mathcal{H}(\beta, \alpha) = \frac{|\log \alpha|}{Kl_1} + o_\alpha(1), \quad (2.74)$$

where $\mathcal{H}(x, y) = x \log \frac{x}{1-y} + (1-x) \log \frac{1-x}{y}$; and $l_i = \frac{1}{K} |\mathbb{E}_i[L_1]|$, $i = 0, 1$ are the average Kullback-Leibler information numbers of the process $\{L_t\}$ under the two hypotheses.

Proof. It should be noted that these inequalities become equalities in the continuous-time continuous-path case. The proof can be found in [67, Page 21]. \square

Let us now turn our attention to the two decentralized schemes, namely the classical Q-SPRT and the proposed RLT-SPRT. We have the following theorem that captures the performance of Q-SPRT.

Theorem 3. *Assuming that the two error probabilities $\alpha, \beta \rightarrow 0$ at the same rate, and that the number \tilde{r} of quantization levels increases with α, β , then the performance of Q-SPRT, $\tilde{\mathcal{S}}$, as compared to the optimum centralized SPRT, \mathcal{S} , satisfies*

$$\begin{aligned} 0 \leq \mathbb{E}_1[\tilde{\mathcal{S}}] - \mathbb{E}_1[\mathcal{S}] &\leq \frac{2|\log \alpha|}{Kl_1^2} \frac{\phi}{\tilde{r}} \{1 + o_{\tilde{r}}(1)\} + T \frac{\phi}{l_1} \{1 + o_{\tilde{r}}(1)\} + o_\alpha(1) \\ 0 \leq \mathbb{E}_0[\tilde{\mathcal{S}}] - \mathbb{E}_0[\mathcal{S}] &\leq \frac{2|\log \beta|}{Kl_0^2} \frac{\phi}{\tilde{r}} \{1 + o_{\tilde{r}}(1)\} + T \frac{\phi}{l_0} \{1 + o_{\tilde{r}}(1)\} + o_\beta(1). \end{aligned} \quad (2.75)$$

Proof. We provide the proof in [20, Appendix A]. \square

As with the classical scheme, let us now examine the behavior of the proposed test when the number of quantization levels increases as a function of the two error probabilities α, β . We have the next theorem that summarizes the behavior of RLT-SPRT.

Theorem 4. *Assuming that the two error probabilities $\alpha, \beta \rightarrow 0$ at the same rate, and that the number \hat{r} of quantization levels increases with α, β , then the performance of RLT-SPRT, $\hat{\mathcal{S}}$, as compared to the optimum centralized SPRT, \mathcal{S} , satisfies*

$$\begin{aligned} 0 \leq \mathbb{E}_1[\hat{\mathcal{S}}] - \mathbb{E}_1[\mathcal{S}] &\leq \frac{|\log \alpha|}{K l_1 \Delta \tanh(\frac{\Delta}{2})} \frac{\phi}{\max\{\hat{r}, 1\}} \{1 + o_{\Delta, \hat{r}}(1)\} + \frac{1}{l_1} (\Delta + \phi) + o_{\Delta, \hat{r}}(1) + o_\alpha(1), \\ 0 \leq \mathbb{E}_0[\hat{\mathcal{S}}] - \mathbb{E}_0[\mathcal{S}] &\leq \frac{|\log \beta|}{K l_0 \Delta \tanh(\frac{\Delta}{2})} \frac{\phi}{\max\{\hat{r}, 1\}} \{1 + o_{\Delta, \hat{r}}(1)\} + \frac{1}{l_0} (\Delta + \phi) + o_{\Delta, \hat{r}}(1) + o_\beta(1). \end{aligned} \quad (2.76)$$

Proof. The proof can be found in [20, Appendix B]. \square

2.5.3.2 Comparisons

In order to make fair comparisons, the two decentralized schemes need to satisfy the same communication constraints. First, each SU is allowed to use at most s bits per communication. This means that the number of quantization levels \tilde{r} in Q-SPRT must satisfy $\tilde{r} = 2^s$ while for RLT-SPRT we have $2(1 + \hat{r}) = 2^s$ suggesting that $\hat{r} = 2^{s-1} - 1$.

The second parameter that needs to be specified is the information flow from the SUs to the FC. Since receiving more messages per unit time increases the capability of the FC to make a faster decision, it makes sense to use the *average rate of received messages* by the FC as a measure of the information flow. In Q-SPRT, every T units of time the FC receives, synchronously, K messages (from all SUs), therefore the average message rate is $\frac{K}{T}$. Computing the corresponding quantity for RLT-SPRT is less straightforward. Consider the time interval $[0, t]$ and denote with \mathcal{N}_t the total number of messages received by the FC until t . We clearly have $\mathcal{N}_t = \sum_{k=1}^K \mathcal{N}_t^k$ where \mathcal{N}_t^k is the number of messages sent by the k -th SU. We are interested in computing the following limit

$$\lim_{t \rightarrow \infty} \frac{\mathcal{N}_t}{t} = \lim_{t \rightarrow \infty} \sum_{k=1}^K \frac{\mathcal{N}_t^k}{t} = \sum_{k=1}^K \lim_{t \rightarrow \infty} \frac{1}{\frac{1}{\mathcal{N}_t^k} (\sum_{n=1}^{\mathcal{N}_t^k} t_n^k - t_{n-1}^k) + \frac{1}{\mathcal{N}_t^k} (t - t_{\mathcal{N}_t^k}^k)} = \sum_{k=1}^K \frac{1}{\mathbb{E}_i[t_1^k]}, \quad (2.77)$$

where we recall that $\{t_n^k\}$ is the sequence of sampling times at the k -th SU and for the last equality we used the Law of Large Numbers since when $t \rightarrow \infty$ we also have $\mathcal{N}_t^k \rightarrow \infty$. Consequently we need to select Δ so that $\sum_{k=1}^K \frac{1}{\mathbb{E}_i[t_1^k]} = \frac{K}{T}$. To obtain a convenient formula we are going to become slightly unfair for RLT-SPRT. From [20, Lemma 7] we

have that $\frac{1}{\mathbb{E}_i[t_1^k]} \leq \frac{|\mathbb{E}_i[L_1^k]|}{\Delta \tanh(\frac{\Delta}{2})}$, which means that, $\sum_{k=1}^K \frac{1}{\mathbb{E}_i[t_1^k]} \leq \frac{Kl_i}{\Delta \tanh(\frac{\Delta}{2})}$. Therefore, if we set $\frac{Kl_i}{\Delta \tanh(\frac{\Delta}{2})} = \frac{K}{T}$ or, equivalently, $\Delta \tanh(\frac{\Delta}{2}) = Tl_i$, the average message rate of RLT-SPRT becomes slightly smaller than the corresponding of Q-SPRT. Note that the average Kullback-Leibler information numbers, $l_i, i = 0, 1$, can be once computed offline via simulations.

Under the previous parameter specifications, we have the following final form for the performance of the two schemes. For Q-SPRT

$$\begin{aligned} 0 &\leq \mathbb{E}_1[\tilde{\mathcal{S}}] - \mathbb{E}_1[\mathcal{S}] \leq \frac{\phi}{Kl_1^2} \frac{|\log \alpha|}{2^{s-1}} \{1 + o_s(1)\} + T \frac{\phi}{l_1} \{1 + o_s(1)\} + o_\alpha(1) \\ 0 &\leq \mathbb{E}_0[\tilde{\mathcal{S}}] - \mathbb{E}_0[\mathcal{S}] \leq \frac{\phi}{Kl_0^2} \frac{|\log \beta|}{2^{s-1}} \{1 + o_s(1)\} + T \frac{\phi}{l_0} \{1 + o_s(1)\} + o_\beta(1); \end{aligned} \quad (2.78)$$

while for RLT-SPRT

$$\begin{aligned} 0 &\leq \mathbb{E}_1[\hat{\mathcal{S}}] - \mathbb{E}_1[\mathcal{S}] \leq \frac{1}{T} \frac{\phi}{Kl_1^2} \frac{|\log \alpha|}{\max\{2^{s-1} - 1, 1\}} \{1 + o_{T,s}(1)\} + T + \frac{\phi}{l_1} + o_{T,s}(1) + o_\alpha(1), \\ 0 &\leq \mathbb{E}_0[\hat{\mathcal{S}}] - \mathbb{E}_0[\mathcal{S}] \leq \frac{1}{T} \frac{\phi}{Kl_0^2} \frac{|\log \beta|}{\max\{2^{s-1} - 1, 1\}} \{1 + o_{T,s}(1)\} + T + \frac{\phi}{l_0} + o_{T,s}(1) + o_\alpha(1). \end{aligned} \quad (2.79)$$

Comparing (2.78) with (2.79) there is a definite resemblance between the two cases. However in RLT-SPRT we observe the factor $\frac{1}{T}$ in the first term of the right hand side which, as we will immediately see, produces significant performance gains. Since T is the communication period, and we are in discrete time, we have $T \geq 1$. Actually, for the practical problem of interest we have $T \gg 1$ suggesting that the first term in RLT-SPRT is smaller by a factor T , which can be large.

For fixed T and s , none of the two schemes is asymptotically optimum even of order-1. However, in RLT-SPRT we can have order-1 asymptotic optimality when we fix the number of bits s and impose large communication periods. Indeed using (2.74) of Lemma 2 we obtain

$$1 \leq \frac{\mathbb{E}_1[\hat{\mathcal{S}}]}{\mathbb{E}_1[\mathcal{S}]} = 1 + \frac{\mathbb{E}_1[\hat{\mathcal{S}}] - \mathbb{E}_1[\mathcal{S}]}{\mathbb{E}_1[\mathcal{S}]} \leq 1 + \Theta\left(\frac{1}{T}\right) + \frac{TKl_1}{|\log \alpha|} + o_\alpha(1), \quad (2.80)$$

consequently selecting $T \rightarrow \infty$ but $\frac{T}{|\log \alpha|} \rightarrow 0$ we assure order-1 optimality. It is easy to verify that the best speed of convergence towards 1 of the previous right hand side expression is achieved when $T = \Theta(\sqrt{|\log \alpha|})$.

We should emphasize that similar order-1 optimality result, just by controlling the period T , cannot be obtained in Q-SPRT, and this is due to the missing factor $\frac{1}{T}$ in (2.78). Consequently this is an additional indication (besides the continuous-time case) that the proposed scheme is more efficient than the classical decentralized Q-SPRT.

Let us now examine how the asymptotic optimality properties of the two methods improve when we allow the number of bits s to grow with α, β , while keeping T constant. Note that in the case of Q-SPRT selecting $2^{s-1} = |\log \alpha|$ or, equivalently, $s = 1 + \log_2 |\log \alpha|$ assures order-2 asymptotic optimality. For RLT-SPRT, using for simplicity the approximation $2^{s-1} - 1 \approx 2^{s-1}$, the same computation yields $s = 1 + \log_2 |\log \alpha| - \log_2 T$. Of course the two expressions are of the same order of magnitude, however in RLT-SPRT the additional term $-\log_2 T$, for all practical purposes, can be quite important resulting in a need of significantly less bits than Q-SPRT to assure order-2 asymptotic optimality. The conclusions obtained through our analysis, as we will see in the next section, are also corroborated by our simulations.

2.5.4 Simulation Results

In this section, we provide simulation results to evaluate the performance of the proposed cooperative spectrum sensing technique based on level-triggered sampling and that based on conventional uniform sampling, and how the two tests compare with the optimum centralized scheme. In the simulations, the sampling period of the uniform sampling is set as $T = 4$. For the level triggered sampling, we adjust the local threshold Δ so that the average rate of received messages by the FC matches that of uniform sampling, i.e. $\sum_{k=1}^K \frac{1}{\mathbb{E}_i[t_1^k]} = \frac{K}{T}$ (see Section 2.5.3.2). The upper-bound ϕ for overshoot values is set as the 10^{-4} quantile of the LLR of a single observation which is computed once offline via simulations. We mainly consider a cognitive radio system with two SUs, i.e., $K = 2$, but the effect of increasing user diversity is also analyzed in the last subsection. All results are obtained by averaging 10^4 trials and using importance sampling to compute probabilities of rare events. We primarily focus on the energy detector since it is the most widely used spectrum sensing method. The results for the spectral shape detector and the Gaussian detector are quite similar. In the subsequent figures average sensing delay performances are plotted under H_1 .

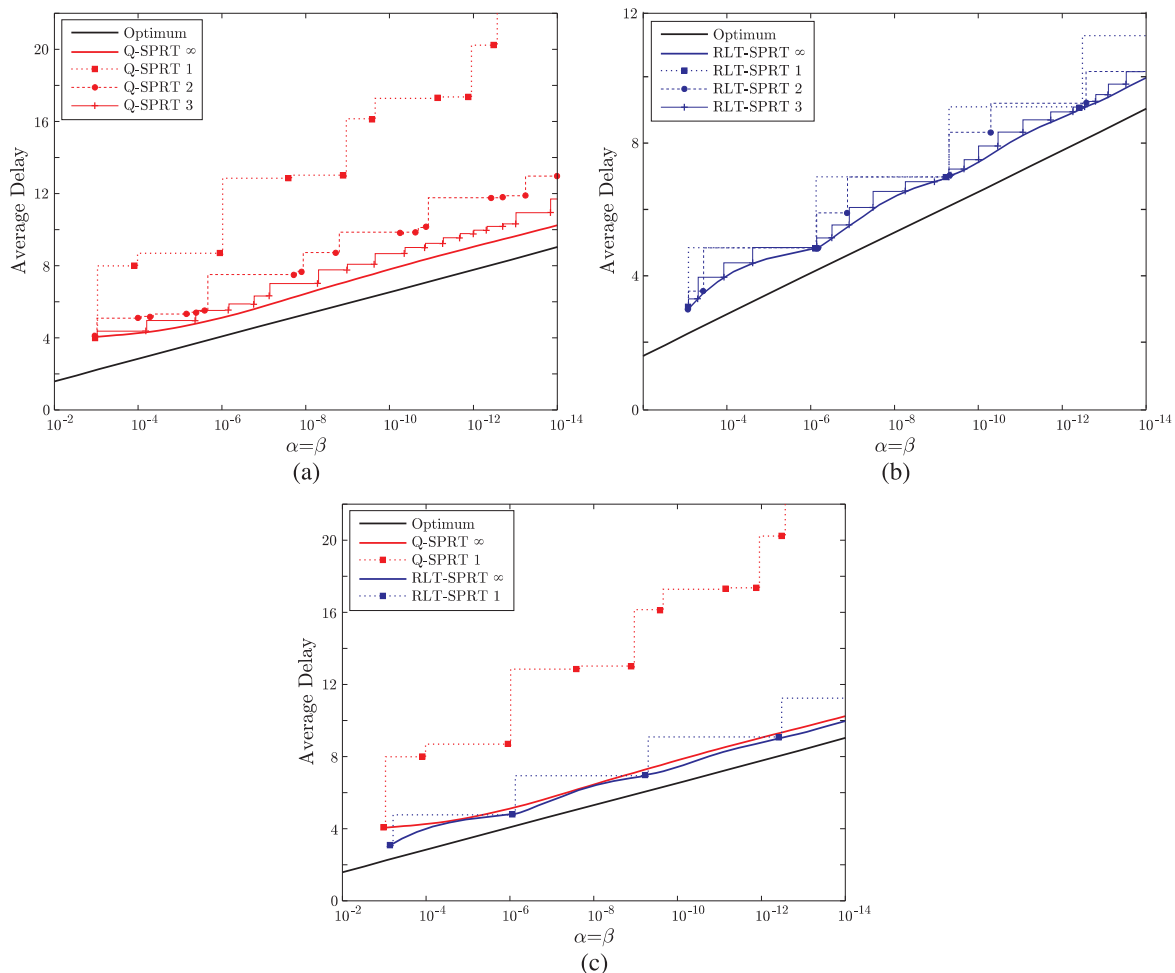


Figure 2.6: Average decision delay vs error probabilities (α, β) for optimum centralized and Q-SPRT, RLT-SPRT with 1,2,3, ∞ number of bits.

Fixed SNR and K , varying α, β : We first verify the theoretical findings presented in Section 2.5.3 on the asymptotic optimality properties of the decentralized schemes. We assume two SUs operate in the system, i.e. $K = 2$. For the energy detector, we set the receiver SNR for each SU to 5 dB and vary the error probabilities α and β together between 10^{-1} and 10^{-10} .

Fig. 2.6 illustrates asymptotic performances of the decentralized schemes using 1,2, 3 and ∞ number of bits. Our first interesting result is the fact that by using a finite number of bits we can only achieve a discrete number of error rates. Specifically, if a finite number of bits is used to represent local incremental LLR packages, then there is

a finite number of possible values to update the global running LLR (e.g. for one bit we have $\pm\Delta$). Hence, the global running LLR, which is our global test statistic, can assume only a discrete number of possible values. This suggests that any threshold between two consecutive LLR values will produce the same error probability. Consequently, only a discrete set of error probabilities (α, β) are achievable. Increasing the number of bits clearly increases the number of available error probabilities. With infinite number of bits any error probability can be achieved. The case of infinite number of bits corresponds to the best achievable performance for Q-SPRT and RLT-SPRT. Having their performance curves parallel to that of the optimum centralized scheme, the ∞ -bit case for both Q-SPRT and RLT-SPRT exhibits order-2 asymptotic optimality. Recall that both schemes can enjoy order-2 optimality if the number of bits tends to infinity with a rate of $\log |\log \alpha|$.

It is notable that the performance of RLT-SPRT with a small number of bits is very close to that of ∞ -bit RLT-SPRT at achievable error rates. For instance, the performance of 1-bit case coincides with that of ∞ -bit case, but only at a discrete set of points as can be seen in Fig. 2.6–b. However, we do not observe this feature for Q-SPRT. Q-SPRT with a small number of bits (especially one bit) performs significantly worse than ∞ -bit case Q-SPRT as well as its RLT-SPRT counterpart. In order to achieve a target error probability that is not in the achievable set of a specific finite bit case, one should use the thresholds corresponding to the closest smaller error probability. This incurs a delay penalty in addition to the delay of the ∞ -bit case for the target error probability, demonstrating the advantage of using more bits. Moreover, it is a striking result that 1-bit RLT-SPRT is superior to ∞ -bit Q-SPRT at its achievable error rates, which can be seen in Fig. 2.6–c.

Fig. 2.7 corroborates the theoretical result related to order-1 asymptotic optimality that is obtained in (2.80). Using a fixed a number of bits, $s = 2$, the performance of RLT-SPRT improves and achieves order-1 asymptotic optimality, i.e. $\frac{E_1[\hat{S}]}{E_1[S]} = 1 + o(1)$, as the communication period tends to infinity, $T = \Theta(\sqrt{|\log \alpha|})$. Conversely, the performance of Q-SPRT deteriorates under the same conditions. Although in both cases Q-SPRT converges to the same performance level, its convergence speed is significantly smaller in the increasing T case, which can be obtained theoretically by applying the derivation in (2.80) to (2.78). This important advantage of RLT-SPRT over Q-SPRT is due to the fact that the quanti-

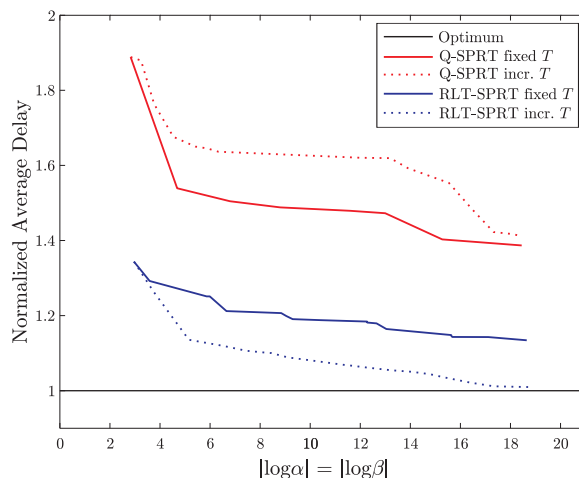


Figure 2.7: Average decision delay normalized by the optimum centralized performance vs. error probabilities (α, β) for Q-SPRT and RLT-SPRT with 2 bits and communication period either $T = 4$ or $T = \Theta(\sqrt{|\log \alpha|})$.

zation error (overshoot error) observed by SUs at each communication time in RLT-SPRT depends only on the LLR of a single observation, but not on the communication period, whereas that in Q-SPRT increases with increasing communication period. Consequently, quantization error accumulated at the FC becomes smaller in RLT-SPRT, but larger in Q-SPRT when $T = \Theta(\sqrt{|\log \alpha|})$ compared to the fixed T case. Note in Fig. 2.7 that, as noted before, only a discrete number of error rates are achievable since two bits are used. Here, we preferred to linearly combine the achievable points to emphasize the changes in the asymptotic performances of RLT-SPRT and Q-SPRT although the true performance curves of the 2-bit case should be stepwise as expressed in Fig. 2.6.

Fixed α, β and K , varying SNR: Next, we consider the sensing delay performances of Q-SPRT and RLT-SPRT under different SNR conditions with fixed $\alpha = \beta = 10^{-6}$ and $K = 2$. In Fig. 2.8, it is clearly seen that at low SNR values there is a huge difference between Q-SPRT and RLT-SPRT when we use one bit, which is the most important case in practice. This remarkable difference stems from the fact that the one bit RLT-SPRT transmits the most part of the sampled LLR information (except the overshoot), whereas Q-SPRT fails to transmit sufficient information by quantizing the LLR information. Moreover, as we can see the performance of the 1-bit RLT-SPRT is very close to that of the infinite bit case and

the optimum centralized scheme. At high SNR values depicted in Fig. 2.8–b, schemes all behave similarly, but again RLT-SPRT is superior to Q-SPRT. This is because the sensing delay of Q-SPRT cannot go below the sampling interval $T = 4$, whereas RLT-SPRT is not bounded by this limit due to the asynchronous communication it implements.

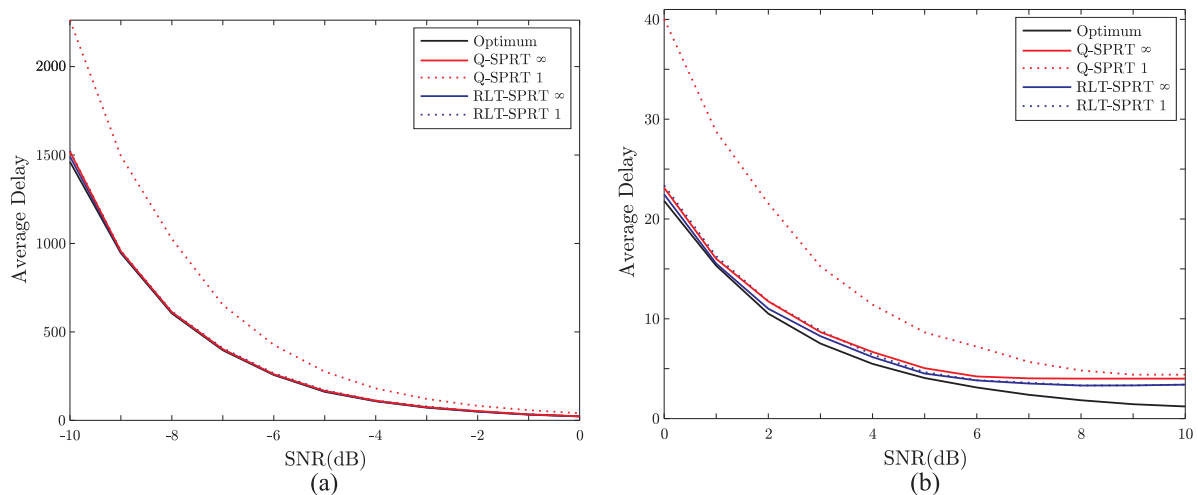


Figure 2.8: Average decision delay vs SNR for optimum centralized and Q-SPRT, RLT-SPRT with $1, \infty$ number of bits.

Fixed SNR, α and β , varying K : We, then, analyze the case where the user diversity increases. In Fig. 2.9, it is seen that with increasing number of SUs, the average sensing delays of all schemes decay with the same rate of $1/K$ as shown in Section 2.5.3 (cf. (2.74), (2.75) and (2.76)). The decay is more notable for the 1-bit case because the overshoot accumulation is more intense, but very quickly becomes less pronounced as we increase the number of SUs. It is again interesting to see that the 1-bit RLT-SPRT is superior to the ∞ -bit Q-SPRT for values of K greater than 3.

2.6 Conclusion

In this chapter, we considered detection in distributed systems with resource (e.g., time, energy, bandwidth) constraints. We have proposed sequential detectors that use level-triggered sampling for information transmission, as opposed to the classical fixed-sample-size detectors and conventional information transmission methods based on uniform sampling

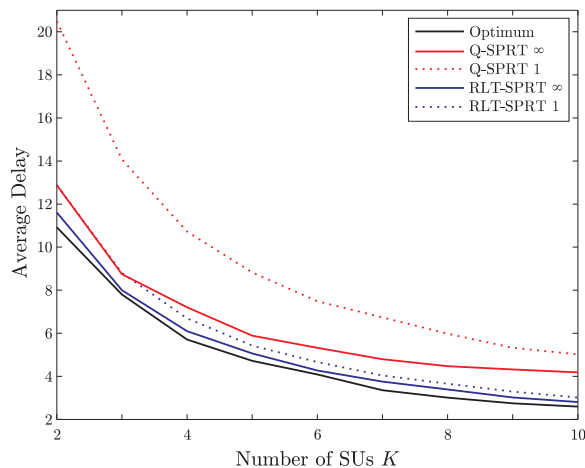


Figure 2.9: Average decision delay vs number of SUs (K) for optimum centralized and Q-SPRT, RLT-SPRT with $1, \infty$ number of bits.

and quantization. The proposed detectors are designed to satisfy timing (i.e., latency) constraints thanks to their sequential nature, which aims to minimize average decision delay; and also energy and bandwidth constraints by transmitting low rate information through level-triggered sampling. And they significantly outperform their classical counterparts.

We have first proposed a detector that transmits a single bit per sample, and assumes that the local error probabilities at nodes are available to the fusion center. We have further designed the proposed detector to operate in a channel-aware manner under different noisy channel models. The average decision delay performance of the proposed detector has also been analyzed (both non-asymptotically and asymptotically). And based on the asymptotic analysis the appropriate signaling constellations have been identified under different continuous channels.

We have then developed a similar sequential detector based on level-triggered sampling for cooperative spectrum sensing in cognitive radio networks. In this detector, without assuming the knowledge of local error probabilities, a few additional bits per sample are used as an alternative method to deal with the overshoot problem. We have shown both analytically and numerically that the proposed spectrum sensing scheme performs much better than its conventional counterpart based on uniform sampling in terms of average sensing delay.

Part II

Estimation

Chapter 3

Sequential Estimation for Linear Models

3.1 Introduction

In this chapter, we are interested in sequentially estimating a vector of parameters (i.e., regression coefficients) $\boldsymbol{x} \in \mathbb{R}^n$ at a random stopping time \mathcal{S} in the following linear (regression) model,

$$y_t = \boldsymbol{h}_t^T \boldsymbol{x} + w_t, \quad t \in \mathbb{N}, \quad (3.1)$$

where $y_t \in \mathbb{R}$ is the observed sample, $\boldsymbol{h}_t \in \mathbb{R}^n$ is the vector of regressors and $w_t \in \mathbb{R}$ is the additive noise. We consider the general case in which \boldsymbol{h}_t is random and observed at time t , which covers the deterministic \boldsymbol{h}_t case as a special case. This linear model is commonly used in many applications. For example, in system identification, \boldsymbol{x} is the unknown system coefficients, \boldsymbol{h}_t is the (random) input applied to the system, and y_t is the output at time t . Another popular example is the signal amplitude estimation in a communications channel, where \boldsymbol{x} is the transmitted signal, y_t is the received signal, \boldsymbol{h}_t is the (fading) channel gain (which is also estimated periodically using pilot signals), and w_t is the additive channel noise.

A sequential estimator $(\mathcal{S}, \hat{\boldsymbol{x}}_{\mathcal{S}})$, as opposed to a traditional fixed-sample-size estimator, is equipped with a stopping rule which determines an appropriate time \mathcal{S} to stop taking

samples based on the observed samples. Hence, the stopping time \mathcal{S} (i.e., the number of samples used in estimation) is a random variable. Endowed with a stopping mechanism, a sequential estimator is preferred to its fixed-sample-size counterpart especially when taking samples is costly, and thus we want to minimize the average sample number. Another advantage of sequential estimators is that they provide online estimates, whereas fixed-sample-size estimators produce offline estimates. More specifically, in sequential estimation, we keep refining our estimate as new samples arrive until no further refinement is needed (i.e., the accuracy of our estimator reaches a target level). On the other hand, in fixed-sample-size estimation, a single estimate is provided after observing a certain number of samples.

Distributed (e.g., cyber-physical) systems are currently a key area of research, with many emerging technologies such as wireless sensor networks, cognitive radio networks, smart grids, and networked control systems. Distributed estimation is a fundamental task that can be realized in such systems. Timing constraints are typical of distributed systems, which we can address with sequential estimators. However, the online nature of sequential estimation, in the ideal case, requires frequent high-rate data communications across the system, which becomes prohibitive for energy-constrained systems (e.g., a wireless sensor network with a large number of sensors). Thus, for such resource-constrained systems, designing resource-efficient distributed estimators is of utmost importance. On the other hand, fixed-sample-size estimators fail to satisfy both the timing and resource constraints in distributed systems since a considerable amount of data communications simultaneously takes place at the deterministic estimation time, which may also cause congestion in the system [23].

3.1.1 Literature Review

The stopping capability of sequential estimators comes with the cost of sophisticated analysis. In most cases, finding an optimum sequential estimator that attains the sequential Cramér-Rao lower bound (CRLB) is not a tractable problem if the stopping time \mathcal{S} is adapted to the complete observation history [68]. Alternatively, [69] and more recently in [14; 23] proposed to restrict \mathcal{S} to stopping times that are adapted to a specific subset of the

complete observation history, which leads to simple solutions with alternative optimality. This idea of using a restricted stopping time first appears in [69] without any optimality result. In the case of continuous-time observations, a sequential estimator with a restricted stopping time was shown to achieve the sequential version of the CRLB in [14]. In the discrete-time case, a similar sequential estimator was shown to achieve the conditional sequential CRLB in [23].

Here, with discrete-time observations and using a similar restricted stopping time we present the optimum sequential estimator for the more challenging *unconditional* problem. Moreover, we treat the *vector* parameter estimation problem, whereas only the scalar parameter estimation problem was considered in [69; 14; 23].

Distributed vector parameter estimation has been studied in a variety of papers, e.g., [70; 71; 72; 73; 74; 75; 76; 77; 78; 79]. Among those [70; 71; 73; 74; 75] consider a wireless sensor network with a fusion center (FC), which computes a global estimator using local information received from sensors, whereas [76; 77; 78; 79] consider ad hoc wireless sensor networks, where sensors in the absence of an FC compute their local estimators and communicate them through the network. Distributed estimation under both network topologies is reviewed in [72]. In [70; 72; 75; 76; 78; 79] a general nonlinear signal model is assumed.

The majority of pertinent works in the literature, e.g., [70; 71; 72; 73; 74; 75; 76; 77], studies fixed-sample-size estimation. There are a few works, such as [78; 79], that consider sequential distributed vector parameter estimation. Nevertheless, [78; 79] assume that sensors transmit real numbers, which obviously requires quantization in practice. In many applications quantization must be performed using a small number of bits due to strict energy constraints. Recently, in a series of papers [12; 20; 21; 14; 23] it was shown that level-triggered sampling, which is a non-uniform sampling method, meets such strict constraints by infrequently transmitting a single bit from sensors to the FC. Moreover, distributed schemes based on level-triggered sampling can significantly outperform their counterparts based on traditional uniform-in-time sampling [20].

Following the distributed schemes based on level-triggered sampling presented for scalar parameter estimation in [14] and [23] we propose in this chapter a computationally efficient distributed scheme for *vector* parameter estimation. In the level-triggered sampling proce-

ture, we propose to encode the random overshoot in each sample, which is due to discrete-time observations, *in time*, unlike [20; 23], which quantize the random overshoot, and [12; 21], which compute an average value for it. Instead of the direct implementation of level-triggered sampling for each dimension of the unknown parameter vector, which has a quadratic computational complexity in the number of dimensions, we develop a simplified distributed estimator based on level-triggered sampling with a *linear* computational complexity.

3.1.2 Outline

In the first part of the chapter, for a restricted class of stopping rules that depend solely on the regressors, $\{\mathbf{h}_t\}$ in (3.1), we formulate the problem in Section 3.2. We then derive, in Section 3.3, the optimum sequential estimators, that minimize the average sample number for a given target accuracy level, under two different formulations of the problem. In the first formulation, we use the conditional covariance of the estimator given the regressors $\{\mathbf{h}_t\}$ to assess its accuracy, and show that the optimum stopping rule is a one-dimensional thresholding on the Fisher information, regardless of the dimension of the unknown parameter vector \mathbf{x} . In the second formulation, following the common practice, we use the (unconditional) covariance of the estimator to assess its accuracy, and show that the complexity of the optimal stopping rule increases prohibitively with the dimension of \mathbf{x} . Our analytical results demonstrate the usefulness of conditioning on ancillary statistics such as $\{\mathbf{h}_t\}$. Although covariance is a generic accuracy measure, conditional covariance is preferred to it in the presence of an ancillary statistic that is independent of the unknown parameters [80].

Then, in the second part of the chapter, from the optimum sequential estimator in the conditional problem, we develop, in Section 3.4, a computationally efficient distributed sequential estimator that meets the timing and stringent energy constraints in a wireless sensor network. We achieve the energy efficiency via level-triggered sampling, a nonuniform sampling technique, and the computational efficiency through a simplification on the optimal estimator. Simulation results show that the simplified distributed estimator attains a very similar performance to those of the unsimplified distributed estimator and the optimal

estimator when the regressors in \mathbf{h}_t are uncorrelated. We also show in the simulation results that the performance gap between the simplified estimator and the unsimplified and optimal estimators increases with the correlation. Nevertheless, the simplified estimator achieves a good performance even in the correlated case. Finally, the chapter is concluded in Section 3.5.

3.2 Problem Formulation and Background

In (3.1), at each time t , we observe the sample y_t and the vector \mathbf{h}_t , hence $\{(y_p, \mathbf{h}_p)\}_{p=1}^t$ are available. We assume $\{w_t\}$ are i.i.d. with $\mathbb{E}[w_t] = 0$ and $\text{Var}(w_t) = \sigma^2$. We are interested in sequentially estimating \mathbf{x} . The least squares (LS) estimator minimizes the sum of squared errors, i.e.,

$$\hat{\mathbf{x}}_t = \arg \min_{\mathbf{x}} \sum_{p=1}^t (y_p - \mathbf{h}_p^T \mathbf{x})^2, \quad (3.2)$$

and is given by

$$\hat{\mathbf{x}}_t = \left(\sum_{p=1}^t \mathbf{h}_p \mathbf{h}_p^T \right)^{-1} \sum_{p=1}^t \mathbf{h}_p y_p = (\mathbf{H}_t^T \mathbf{H}_t)^{-1} \mathbf{H}_t^T \mathbf{y}_t, \quad (3.3)$$

where $\mathbf{H}_t = [\mathbf{h}_1, \dots, \mathbf{h}_t]^T$ and $\mathbf{y}_t = [y_1, \dots, y_t]^T$.

Under the Gaussian noise, $w_t \sim \mathcal{N}(0, \sigma^2)$, the LS estimator coincides with the minimum variance unbiased estimator (MVUE), and achieves the CRLB, i.e., $\text{Cov}(\hat{\mathbf{x}}_t | \mathbf{H}_t) = \text{CRLB}_t$. To compute the CRLB we first write, given \mathbf{x} and \mathbf{H}_t , the log-likelihood of the vector \mathbf{y}_t as

$$L_t = \log f(\mathbf{y}_t | \mathbf{x}, \mathbf{H}_t) = - \sum_{p=1}^t \frac{(y_p - \mathbf{h}_p^T \mathbf{x})^2}{2\sigma^2} - \frac{t}{2} \log(2\pi\sigma^2). \quad (3.4)$$

Then, we have

$$\text{CRLB}_t = \left(\mathbb{E} \left[- \frac{\partial^2}{\partial \mathbf{x}^2} L_t | \mathbf{H}_t \right] \right)^{-1} = \sigma^2 \mathbf{U}_t^{-1}, \quad (3.5)$$

where $\mathbb{E} \left[- \frac{\partial^2}{\partial \mathbf{x}^2} L_t | \mathbf{H}_t \right]$ is the Fisher information matrix and $\mathbf{U}_t \triangleq \mathbf{H}_t^T \mathbf{H}_t$ is a nonsingular matrix. Since $\mathbb{E}[\mathbf{y}_t | \mathbf{H}_t] = \mathbf{H}_t \mathbf{x}$ and $\text{Cov}(\mathbf{y}_t | \mathbf{H}_t) = \sigma^2 \mathbf{I}$, from (3.3) we have $\mathbb{E}[\hat{\mathbf{x}}_t | \mathbf{H}_t] = \mathbf{x}$ and $\text{Cov}(\hat{\mathbf{x}}_t | \mathbf{H}_t) = \sigma^2 \mathbf{U}_t^{-1}$, thus from (3.5) $\text{Cov}(\hat{\mathbf{x}}_t | \mathbf{H}_t) = \text{CRLB}_t$. Note that the maximum likelihood (ML) estimator, that maximizes (3.4), coincides with the LS estimator in (3.3).

In general, the LS estimator is the best linear unbiased estimator (BLUE). In other words, any linear unbiased estimator of the form $\mathbf{A}_t \mathbf{y}_t$ with $\mathbf{A}_t \in \mathbb{R}^{n \times t}$, where $\mathbb{E}[\mathbf{A}_t \mathbf{y}_t | \mathbf{H}_t] =$

\mathbf{x} , has a covariance no smaller than that of the LS estimator in (3.3), i.e., $\text{Cov}(\mathbf{A}_t \mathbf{y}_t | \mathbf{H}_t) \geq \sigma^2 \mathbf{U}_t^{-1}$ in the positive semidefinite sense. To see this result we write $\mathbf{A}_t = (\mathbf{H}_t^T \mathbf{H}_t)^{-1} \mathbf{H}_t^T + \mathbf{B}_t$ for some $\mathbf{B}_t \in \mathbb{R}^{n \times t}$, and then $\text{Cov}(\mathbf{A}_t \mathbf{y}_t | \mathbf{H}_t) = \sigma^2 \mathbf{U}_t^{-1} + \sigma^2 \mathbf{B}_t \mathbf{B}_t^T$, where $\mathbf{B}_t \mathbf{B}_t^T$ is a positive semidefinite matrix.

The recursive least squares (RLS) algorithm enables us to compute $\hat{\mathbf{x}}_t$ in a recursive way as follows

$$\hat{\mathbf{x}}_t = \hat{\mathbf{x}}_{t-1} + K_t (y_t - \mathbf{h}_t^T \hat{\mathbf{x}}_{t-1}) \quad (3.6)$$

where $K_t = \frac{\mathbf{P}_{t-1} \mathbf{h}_t}{1 + \mathbf{h}_t^T \mathbf{P}_{t-1} \mathbf{h}_t}$ and $\mathbf{P}_t = \mathbf{P}_{t-1} - K_t \mathbf{h}_t^T \mathbf{P}_{t-1}$,

where $K_t \in \mathbb{R}^n$ is a gain vector and $\mathbf{P}_t = \mathbf{U}_t^{-1}$. While applying RLS we first initialize $\hat{\mathbf{x}}_0 = 0$ and $\mathbf{P}_0 = \delta^{-1} \mathbf{I}$, where 0 represents a zero vector and δ is a small number, and then at each time t compute K_t , $\hat{\mathbf{x}}_t$ and \mathbf{P}_t as in (3.6).

3.3 Optimum Sequential Estimators

In this section we aim to find the optimal pair $(\mathcal{T}, \hat{\mathbf{x}}_{\mathcal{T}})$ of stopping time and estimator corresponding to the optimum sequential estimator. The stopping time for a sequential estimator is defined as the time it first achieves a target accuracy level. We assess the accuracy of an estimator by using either its covariance matrix $\text{Cov}(\hat{\mathbf{x}}_t)$, which averages also over \mathbf{H}_t , or conditional covariance matrix $\text{Cov}(\hat{\mathbf{x}}_t | \mathbf{H}_t)$. Although traditionally the former is used in general, in the presence of an ancillary statistic whose distribution does not depend on the parameters to be estimated, such as \mathbf{H}_t , the latter was shown to be a better choice in [80] through asymptotic analysis. Specifically, the optimum sequential estimators can be formulated as the following constrained optimization problems,

$$\min_{\mathcal{T}, \hat{\mathbf{x}}_{\mathcal{T}}} \mathbb{E}[\mathcal{T} | \mathbf{H}_{\mathcal{T}}] \quad \text{subject to} \quad f(\text{Cov}(\hat{\mathbf{x}}_{\mathcal{T}} | \mathbf{H}_{\mathcal{T}})) \leq C, \quad (3.7)$$

$$\text{and} \quad \min_{\mathcal{T}, \hat{\mathbf{x}}_{\mathcal{T}}} \mathbb{E}[\mathcal{T}] \quad \text{subject to} \quad f(\text{Cov}(\hat{\mathbf{x}}_{\mathcal{T}})) \leq C, \quad (3.8)$$

under the conditional and unconditional setups, respectively, where $f(\cdot)$ is a function from $\mathbb{R}^{n \times n}$ to \mathbb{R} and $C \in \mathbb{R}$ is the target accuracy level.

Note that the constraint in (3.7) is stricter than the one in (3.8) since it requires that $\hat{\mathbf{x}}_{\mathcal{T}}$ satisfies the target accuracy level for each realization of $\mathbf{H}_{\mathcal{T}}$, whereas in (3.8) it is sufficient

that $\hat{\mathbf{x}}_{\mathcal{T}}$ satisfies the target accuracy level on average. In other words, in (3.8) even if for some realizations of $\mathbf{H}_{\mathcal{T}}$ we have $f(\text{Cov}(\hat{\mathbf{x}}_{\mathcal{T}}|\mathbf{H}_{\mathcal{T}})) > C$, we can still have $f(\text{Cov}(\hat{\mathbf{x}}_{\mathcal{T}})) \leq C$. In fact, we can always have $f(\text{Cov}(\hat{\mathbf{x}}_{\mathcal{T}})) = C$ by using a probabilistic stopping rule such that we sometimes stop above C , i.e., $f(\text{Cov}(\hat{\mathbf{x}}_{\mathcal{T}}|\mathbf{H}_{\mathcal{T}})) > C$, and the rest of the time at or below C , i.e., $f(\text{Cov}(\hat{\mathbf{x}}_{\mathcal{T}}|\mathbf{H}_{\mathcal{T}})) \leq C$. On the other hand, in (3.7) we always have $f(\text{Cov}(\hat{\mathbf{x}}_{\mathcal{T}}|\mathbf{H}_{\mathcal{T}})) \leq C$, and moreover since we observe discrete-time samples, in general we have $f(\text{Cov}(\hat{\mathbf{x}}_{\mathcal{T}}|\mathbf{H}_{\mathcal{T}})) < C$ for each realization of $\mathbf{H}_{\mathcal{T}}$. Hence, the optimal objective value $\text{E}[\mathcal{T}]$ in (3.8) will, in general, be smaller than the optimal objective value $\text{E}[\mathcal{T}|\mathbf{H}_{\mathcal{T}}]$ in (3.7). Note that on the other hand, if we observed continuous-time processes with continuous paths, then we could always have $f(\text{Cov}(\hat{\mathbf{x}}_{\mathcal{T}}|\mathbf{H}_{\mathcal{T}})) = C$ for each realization of $\mathbf{H}_{\mathcal{T}}$, and thus the optimal objective values of (3.7) and (3.8) would be the same.

The accuracy function f should be a monotonic function of the covariance matrices $\text{Cov}(\hat{\mathbf{x}}_{\mathcal{T}}|\mathbf{H}_{\mathcal{T}})$ and $\text{Cov}(\hat{\mathbf{x}}_{\mathcal{T}})$, which are positive semi-definite, in order to make consistent accuracy assessments, e.g., $f(\text{Cov}(\hat{\mathbf{x}}_{\mathcal{T}})) > f(\text{Cov}(\hat{\mathbf{x}}_{\mathcal{S}}))$ for $\mathcal{T} < \mathcal{S}$ since $\text{Cov}(\hat{\mathbf{x}}_{\mathcal{T}}) \succ \text{Cov}(\hat{\mathbf{x}}_{\mathcal{S}})$ in the positive definite sense. Two popular and easy-to-compute choices are the trace $\text{Tr}(\cdot)$, which corresponds to the mean squared error (MSE), and the Frobenius norm $\|\cdot\|_F$. In the sequel we will next treat the two problems in (3.7) and (3.8) separately.

3.3.1 The Optimum Conditional Sequential Estimator

Denote $\{\mathcal{F}_t\}$ as the filtration that corresponds to the samples $\{y_1, \dots, y_t\}$ where $\mathcal{F}_t = \sigma\{y_1, \dots, y_t\}$ is the σ -algebra generated by the samples observed up to time t and \mathcal{F}_0 is the trivial σ -algebra. Similarly we define the filtration $\{\mathcal{H}_t\}$ where $\mathcal{H}_t = \sigma\{\mathbf{h}_1, \dots, \mathbf{h}_t\}$, i.e., the accumulated history related to the coefficient vectors, and \mathcal{H}_0 is again the trivial σ -algebra. It is known that, in general, with discrete-time observations and an unrestricted stopping time, that is $\{\mathcal{F}_t \cup \mathcal{H}_t\}$ -adapted, the sequential CRLB is not attainable under any noise distribution (Gaussian or non-Gaussian) except for the Bernoulli noise [68]. On the other hand, in the case of continuous-time observations with continuous paths the sequential CRLB is attainable by using an $\{\mathcal{H}_t\}$ -adapted stopping time [14]. Moreover, with an $\{\mathcal{H}_t\}$ -adapted stopping time, that depends only on $\mathbf{H}_{\mathcal{T}}$, the LS estimator attains the conditional sequential CRLB as we will show in the following Lemma. Hence, in this paper we restrict

our attention to $\{\mathcal{H}_t\}$ -adapted stopping times as in [69; 14; 23].

Lemma 3. *With a monotonic accuracy function f and an $\{\mathcal{H}_t\}$ -adapted stopping time \mathcal{T} we can write*

$$f(\text{Cov}(\hat{\mathbf{x}}_{\mathcal{T}}|\mathbf{H}_{\mathcal{T}})) \geq f(\sigma^2 \mathbf{U}_{\mathcal{T}}^{-1}) \quad (3.9)$$

for all unbiased estimators under Gaussian noise, and for all linear unbiased estimators under non-Gaussian noise, and the inequality in (3.9) holds with equality for the LS estimator.

The proof is given in Appendix B. Since \mathcal{T} is $\{\mathcal{H}_t\}$ -adapted, i.e., determined by $\mathbf{H}_{\mathcal{T}}$, we have $\mathbb{E}[\mathcal{T}|\mathbf{H}_{\mathcal{T}}] = \mathcal{T}$, and thus from (3.7) we want to find the first time that a member of our class of estimators (i.e., unbiased estimators under Gaussian noise and linear unbiased estimators under non-Gaussian noise) satisfies the constraint $f(\text{Cov}(\hat{\mathbf{x}}_{\mathcal{T}}|\mathbf{H}_{\mathcal{T}})) \leq C$, as well as the estimator that attains this earliest stopping time. From Lemma 3 it is seen that the LS estimator achieves the earliest stopping time among its competitors. Hence, for the conditional problem the optimal pair of stopping time and estimator is $(\mathcal{T}, \hat{\mathbf{x}}_{\mathcal{T}})$ where \mathcal{T} is given by

$$\mathcal{T} = \min\{t \in \mathbb{N} : f(\sigma^2 \mathbf{U}_t^{-1}) \leq C\}, \quad (3.10)$$

and from (3.3),

$$\hat{\mathbf{x}}_{\mathcal{T}} = \mathbf{U}_{\mathcal{T}}^{-1} V_{\mathcal{T}}, \quad V_{\mathcal{T}} \triangleq \mathbf{H}_{\mathcal{T}}^T \mathbf{y}_{\mathcal{T}}, \quad (3.11)$$

which can be computed recursively as in (3.6). The recursive computation of $\mathbf{U}_t^{-1} = \mathbf{P}_t$ in the test statistic in (3.10) is also given in (3.6). Note that for an accuracy function f such that $f(\sigma^2 \mathbf{U}_t^{-1}) = \sigma^2 f(\mathbf{U}_t^{-1})$, e.g., $\text{Tr}(\cdot)$ and $\|\cdot\|_F$, we can use the following stopping time,

$$\mathcal{T} = \min\{t \in \mathbb{N} : f(\mathbf{U}_t^{-1}) \leq C'\}, \quad (3.12)$$

where $C' = \frac{C}{\sigma^2}$ is the relative target accuracy with respect to the noise power. Hence, given C' we do not need to know the noise variance σ^2 to run the test given by (3.12).

Note that $\mathbf{U}_t = \mathbf{H}_t^T \mathbf{H}_t$ is a non-decreasing positive semi-definite matrix, i.e., $\mathbf{U}_t \succeq \mathbf{U}_{t-1}, \forall t$, in the positive semi-definite sense. Thus, from the monotonicity of f , the test statistic $f(\sigma^2 \mathbf{U}_t^{-1})$ is a non-increasing scalar function of time. Specifically, for accuracy

functions $\text{Tr}(\cdot)$ and $\|\cdot\|_F$ we can show that if the minimum eigenvalue of \mathbf{U}_t tends to infinity as $t \rightarrow \infty$, then the stopping time is finite, i.e., $\mathcal{T} < \infty$.

For the special case of scalar parameter estimation, we do not need a function f to assess the accuracy of the estimator since instead of a covariance matrix we now have a variance $\frac{\sigma^2}{u_t}$, where $u_t = \sum_{p=1}^t h_p^2$ and h_t is the scaling coefficient in (3.1). Hence, from (3.12) the stopping time in the scalar case is given by

$$\mathcal{T} = \min \left\{ t \in \mathbb{N} : u_t \geq \frac{1}{C'} \right\}, \quad (3.13)$$

where $\frac{u_t}{\sigma^2}$ is the Fisher information at time t . This result is in accordance with [23, Eq. (3)].

3.3.2 The Optimum Unconditional Sequential Estimator

In this case we assume $\{\mathbf{h}_t\}$ is i.i.d.. From the constrained optimization problem in (3.8), using a Lagrange multiplier λ we obtain the following unconstrained optimization problem,

$$\min_{\mathcal{T}, \hat{\mathbf{x}}_{\mathcal{T}}} \mathbb{E}[\mathcal{T}] + \lambda f(\text{Cov}(\hat{\mathbf{x}}_{\mathcal{T}})). \quad (3.14)$$

We are again interested in $\{\mathcal{H}_t\}$ -adapted stopping times to use the optimality property of the LS estimator in the sequential sense. For simplicity assume a linear accuracy function f so that $f(\mathbb{E}[\cdot]) = \mathbb{E}[f(\cdot)]$, e.g., the trace function $\text{Tr}(\cdot)$. Then, our constraint function becomes the sum of the individual variances, i.e., $\text{Tr}(\text{Cov}(\hat{\mathbf{x}}_{\mathcal{T}})) = \sum_{i=1}^n \text{Var}(\hat{x}_{\mathcal{T}}^i)$. Since $\text{Tr}(\text{Cov}(\hat{\mathbf{x}}_{\mathcal{T}})) = \text{Tr}(\mathbb{E}[\text{Cov}(\hat{\mathbf{x}}_{\mathcal{T}}|\mathbf{H}_{\mathcal{T}})]) = \mathbb{E}[\text{Tr}(\text{Cov}(\hat{\mathbf{x}}_{\mathcal{T}}|\mathbf{H}_{\mathcal{T}}))]$, we rewrite (3.14) as

$$\min_{\mathcal{T}, \hat{\mathbf{x}}_{\mathcal{T}}} \mathbb{E}[\mathcal{T} + \lambda \text{Tr}(\text{Cov}(\hat{\mathbf{x}}_{\mathcal{T}}|\mathbf{H}_{\mathcal{T}}))], \quad (3.15)$$

where the expectation is with respect to $\mathbf{H}_{\mathcal{T}}$.

From Lemma 3, we have $\text{Tr}(\text{Cov}(\hat{\mathbf{x}}_{\mathcal{T}}|\mathbf{H}_{\mathcal{T}})) \geq \text{Tr}(\sigma^2 \mathbf{U}_{\mathcal{T}}^{-1})$ where $\sigma^2 \mathbf{U}_{\mathcal{T}}^{-1}$ is the covariance matrix of the LS estimator at time t . Note that \mathbf{U}_t/σ^2 is the Fisher information matrix at time t [cf. (3.5)]. Using the LS estimator we minimize the objective value in (3.15). Hence, $\hat{\mathbf{x}}_{\mathcal{T}}$ given in (3.11) [cf. (3.6) for recursive computation] is also the optimal estimator for the unconditional problem.

Now, to find the optimal stopping time we need to solve the following optimization problem,

$$\min_{\mathcal{T}} \mathbb{E}[\mathcal{T} + \lambda \text{Tr}(\sigma^2 \mathbf{U}_{\mathcal{T}}^{-1})], \quad (3.16)$$

which can be solved by using the *optimal stopping theory*. Writing (3.16) in the following alternative form

$$\min_{\mathcal{T}} \mathbb{E} \left[\sum_{t=0}^{\mathcal{T}-1} 1 + \lambda \text{Tr}(\sigma^2 \mathbf{U}_{\mathcal{T}}^{-1}) \right], \quad (3.17)$$

we see that the term $\sum_{t=0}^{\mathcal{T}-1} 1$ accounts for the cost of not stopping until time \mathcal{T} and the term $\lambda \text{Tr}(\sigma^2 \mathbf{U}_{\mathcal{T}}^{-1})$ represents the cost of stopping at time \mathcal{T} . Note that $\mathbf{U}_t = \mathbf{U}_{t-1} + \mathbf{h}_t \mathbf{h}_t^T$ and given \mathbf{U}_{t-1} the current state \mathbf{U}_t is (conditionally) independent of all previous states, hence $\{\mathbf{U}_t\}$ is a Markov process. That is, in (3.17), the optimal stopping time for a Markov process is sought, which can be found by solving the following Bellman equation:

$$\mathcal{V}(\mathbf{U}) = \min \left\{ \underbrace{\lambda \text{Tr}(\sigma^2 \mathbf{U}^{-1})}_{F(\mathbf{U})}, \underbrace{1 + \mathbb{E}[\mathcal{V}(\mathbf{U} + \mathbf{h}_1 \mathbf{h}_1^T) | \mathbf{U}]}_{G(\mathbf{U})} \right\}, \quad (3.18)$$

where the expectation is with respect to \mathbf{h}_1 and \mathcal{V} is the optimal cost function [81]. The optimal cost function is obtained by iterating a sequence of functions $\{\mathcal{V}_m\}$ where $\mathcal{V}(\mathbf{U}) = \lim_{m \rightarrow \infty} \mathcal{V}_m(\mathbf{U})$ and

$$\mathcal{V}_m(\mathbf{U}) = \min \left\{ \lambda \text{Tr}(\sigma^2 \mathbf{U}^{-1}), 1 + \mathbb{E}[\mathcal{V}_{m-1}(\mathbf{U} + \mathbf{h}_1 \mathbf{h}_1^T) | \mathbf{U}] \right\}.$$

In the above optimal stopping theory, dynamic programming is used. Specifically, the original complex optimization problem in (3.16) is divided into simpler subproblems given by (3.18). At each time t we are faced with a subproblem consisting of a stopping cost $F(\mathbf{U}_t) = \lambda \text{Tr}(\sigma^2 \mathbf{U}_t^{-1})$ and an expected sampling cost $G(\mathbf{U}_t) = 1 + \mathbb{E}[\mathcal{V}(\mathbf{U}_{t+1}) | \mathbf{U}_t]$ to proceed to time $t + 1$. Since $\{\mathbf{U}_t\}$ is a Markov process, and $\{\mathbf{h}_t\}$ is i.i.d., (3.18) is a general equation holding for all t . The optimal cost function $\mathcal{V}(\mathbf{U}_t)$, selecting the action with minimum cost (i.e., either continue or stop), determines the optimal policy to follow at each time t . That is, we stop the first time the stopping cost is smaller than the average cost of sampling, i.e.,

$$\mathcal{T} = \min\{t \in \mathbb{N} : \mathcal{V}(\mathbf{U}_t) = F(\mathbf{U}_t)\}.$$

We obviously need to analyze the structure of $\mathcal{V}(\mathbf{U}_t)$, i.e., the cost functions $F(\mathbf{U}_t)$ and $G(\mathbf{U}_t)$, to find the optimal stopping time \mathcal{T} .

Note that \mathcal{V} , being a function of the symmetric matrix $\mathbf{U} = [u_{ij}] \in \mathbb{R}^{n \times n}$, is a function of $\frac{n^2+n}{2}$ variables $\{u_{ij} : i \leq j\}$. Analyzing a multi-dimensional optimal cost function proves

intractable, hence we will first analyze the special case of scalar parameter estimation and then provide some numerical results for the two-dimensional vector case, demonstrating how intractable the higher dimensional problems are.

3.3.2.1 Scalar case

For the scalar case, from (3.18) we have the following one-dimensional optimal cost function,

$$\mathcal{V}(u) = \min \left\{ \frac{\lambda\sigma^2}{u}, 1 + \mathbb{E}[\mathcal{V}(u + h_1^2)] \right\}, \quad (3.19)$$

where the expectation is with respect to the scalar coefficient h_1 . Specifically, at time t the optimal cost function is written as $\mathcal{V}(u_t) = \min \left\{ \frac{\lambda\sigma^2}{u_t}, 1 + \mathbb{E}[\mathcal{V}(u_{t+1})] \right\}$, where $u_{t+1} = u_t + h_{t+1}^2$. Writing \mathcal{V} as a function of $z_t \triangleq 1/u_t$ we have $\mathcal{V}(z_t) = \min \left\{ \lambda\sigma^2 z_t, 1 + \mathbb{E}[\mathcal{V}(z_{t+1})] \right\}$, where $z_{t+1} = \frac{z_t}{1+z_t h_{t+1}^2}$, and thus in general

$$\mathcal{V}(z) = \min \left\{ \underbrace{\lambda\sigma^2 z}_{F(z)}, \underbrace{1 + \mathbb{E} \left[\mathcal{V} \left(\frac{z}{1+z h_1^2} \right) \right]}_{G(z)} \right\}. \quad (3.20)$$

We need to analyze the cost functions $F(z) = \lambda\sigma^2 z$ and $G(z) = 1 + \mathbb{E} \left[\mathcal{V} \left(\frac{z}{1+z h_1^2} \right) \right]$. The former is a line, whereas the latter is, in general, a nonlinear function of z . We have the following lemma regarding the structure of $\mathcal{V}(z)$ and $G(z)$. Its proof is given in the Appendix B.

Lemma 4. *The optimal cost \mathcal{V} and the expected sampling cost G , given in (3.20), are non-decreasing, concave and bounded functions of z .*

Following Lemma 4 the theorem below presents the stopping time for the scalar case of the unconditional problem. The proof can be found in Appendix B.

Theorem 5. *The optimal stopping time for the scalar case of the unconditional problem in (3.8) with $\text{Tr}(\cdot)$ as the accuracy function is given by*

$$\mathcal{T} = \min \left\{ t \in \mathbb{N} : u_t \geq \frac{1}{C''} \right\}, \quad (3.21)$$

where C'' is selected so that $\mathbb{E} \left[\frac{\sigma^2}{u_{\mathcal{T}}} \right] = C$, i.e., the variance of the estimator exactly hits the target accuracy level C .

Note that the optimal stopping time in (3.21) is of the same form as that in the scalar case of the conditional problem, where we have $\mathcal{T} = \min \{t \in \mathbb{N} : u_t \geq \frac{1}{C'}\}$ from (3.13). In both conditional and unconditional problems the LS estimator

$$\hat{x}_{\mathcal{T}} = \frac{v_{\mathcal{T}}}{u_{\mathcal{T}}}$$

is the optimal estimator. The fundamental difference between the optimal stopping times

Algorithm 3 The procedure to compute the threshold C'' for given C

```

1: Select  $C''$ 
2: Estimate  $\mathcal{C} = \mathbb{E} \left[ \frac{\sigma^2}{u_{\mathcal{T}}} \right]$  through simulations, where  $u_{\mathcal{T}} = \sum_{t=1}^{\mathcal{T}} h_t^2$ 
3: if  $\mathcal{C} = C$  then
4:   return  $C''$ 
5: else
6:   if  $\mathcal{C} > C$  then
7:     Decrease  $C''$ 
8:   else
9:     Increase  $C''$ 
10:  end if
11:  Go to line 2
12: end if

```

in (3.13) and (3.21) is that the threshold in the conditional problem is written as $C' = \frac{C}{\sigma^2}$, hence known beforehand; whereas the threshold C'' in the unconditional problem needs to be determined through offline simulations following the procedure in Algorithm 3, assuming that some training data $\{h_t\}$ is available or the statistics of h_t is known so that we can generate $\{h_t\}$. We also observe that $C' \leq C''$, hence the optimal objective value $\mathbb{E}[\mathcal{T}]$ of the unconditional problem is in general smaller than that of the conditional problem as noted earlier in this section. This is because the upper bound $\sigma^2 C''$ on the conditional variance $\frac{\sigma^2}{u_{\mathcal{T}}}$ [cf. (3.21)] is also an upper bound for the variance $\mathbb{E} \left[\frac{\sigma^2}{u_{\mathcal{T}}} \right] = C$, and the threshold C' is given by $C' = \frac{C}{\sigma^2}$.

3.3.2.2 Two-dimensional case

We will next show that the multi-dimensional cases are intractable by providing some numerical results for the two-dimensional case. In the two-dimensional case, from (3.18) the

optimal cost function is written as

$$\mathcal{V}(u_{11}, u_{12}, u_{22}) = \min \left\{ \lambda \sigma^2 \frac{u_{11} + u_{22}}{u_{11}u_{22} - u_{12}^2}, 1 + \mathbb{E} [\mathcal{V}(u_{11} + h_{1,1}^2, u_{12} + h_{1,1}h_{1,2}, u_{22} + h_{1,2}^2)] \right\},$$

$$\text{where } \mathbf{U} = \begin{bmatrix} u_{11} & u_{12} \\ u_{12} & u_{22} \end{bmatrix}, \quad \mathbf{h}_1 = \begin{bmatrix} h_{1,1} \\ h_{1,2} \end{bmatrix}$$
(3.22)

and the expectation is with respect to $h_{1,1}$ and $h_{1,2}$. Changing variables we can write \mathcal{V} as a function of $z_{11} \triangleq 1/u_{11}$, $z_{22} \triangleq 1/u_{22}$ and $\rho \triangleq u_{12}/\sqrt{u_{11}u_{22}}$,

$$\mathcal{V}(z_{11}, z_{22}, \rho) =$$

$$\min \left\{ \underbrace{\lambda \sigma^2 \frac{z_{11} + z_{22}}{1 - \rho^2}}_{F(z_{11}, z_{22}, \rho)}, 1 + \mathbb{E} \left[\underbrace{\mathcal{V} \left(\frac{z_{11}}{1 + z_{11}h_{1,1}^2}, \frac{z_{22}}{1 + z_{22}h_{1,2}^2}, \frac{\rho + h_{1,1}h_{1,2}\sqrt{z_{11}z_{22}}}{\sqrt{(1 + z_{11}h_{1,1}^2)(1 + z_{22}h_{1,2}^2)}} \right)}_{G(z_{11}, z_{22}, \rho)} \right] \right\},$$
(3.23)

which can be iteratively computed as follows

$$\mathcal{V}_m(z_{11}, z_{22}, \rho) =$$

$$\min \left\{ \lambda \sigma^2 \frac{z_{11} + z_{22}}{1 - \rho^2}, 1 + \mathbb{E} \left[\mathcal{V}_{m-1} \left(\frac{z_{11}}{1 + z_{11}h_{1,1}^2}, \frac{z_{22}}{1 + z_{22}h_{1,2}^2}, \frac{\rho + h_{1,1}h_{1,2}\sqrt{z_{11}z_{22}}}{\sqrt{(1 + z_{11}h_{1,1}^2)(1 + z_{22}h_{1,2}^2)}} \right) \right] \right\},$$
(3.24)

where $\lim_{m \rightarrow \infty} \mathcal{V}_m = \mathcal{V}$.

Note that ρ is the correlation coefficient, hence we have $\rho \in [-1, 1]$. Following the procedure in Algorithm 4 we numerically compute \mathcal{V} from (3.24) and find the boundary surface

$$\mathcal{S}(\lambda) = \{(z_{11}, z_{22}, \rho) : F(\lambda, z_{11}, z_{22}, \rho) = G(z_{11}, z_{22}, \rho)\},$$

that defines the stopping rule. In Algorithm 4, firstly the three-dimensional grid

$$(n_1 dz, n_2 dz, n_3 dr), \quad n_1, n_2 = 0, \dots, \frac{Rz}{dz}, \quad n_3 = -\frac{1}{dr}, \dots, \frac{1}{dr}$$

is constructed. Then, in lines 5-7 the stopping cost F [cf. (3.23)] and in line 8 the first iteration of the optimal cost function \mathcal{V}_1 with $\mathcal{V}_0 = 0$ are computed over the grid. In

Algorithm 4 The procedure to compute the boundary surface \mathcal{S} for given λ

```

1: Set  $dz, Rz, dr, dh, Rh$ ;  $Nz = \frac{Rz}{dz} + 1$ ;  $Nr = \frac{2}{dr} + 1$ ;  $Nh = \frac{2Rh}{dh} + 1$ 
2:  $z_1 = [0 : dz : Rz]$ ;  $z_2 = z_1$ ;  $\rho = [-1 : dr : 1]$  {all row vectors}
3:  $Z_1 = \mathbf{1}_{Nz} z_1$ ;  $Z_2 = Z_1^T$  { $\mathbf{1}_{Nz}$ : column vector of ones in  $\mathbb{R}^{Nz}$ }
4:  $h = [-Rh : dh : Rh]$ 
5: for  $i = 1 : Nr$  do
6:    $F(:, :, i) = \lambda \frac{Z_1 + Z_2}{1 - \rho(i)^2}$  {stopping cost over the 3D grid}
7: end for
8:  $\mathcal{V} = \min(F, 1)$  {start with  $\mathcal{V}_0 = 0$ }
9:  $dif = \infty$ ;  $Fr = \|\mathcal{V}\|_F$ 
10: while  $dif > \delta Fr$  { $\delta$ : a small threshold} do
11:   for  $i = 1 : Nz^2$  do
12:      $z_{11} = Z_1(i)$ ;  $z_{22} = Z_2(i)$  {linear indexing in matrices}
13:     for  $j = 1 : Nr$  do
14:        $G = 0$  {initialize continuing cost}
15:       for  $k = 1 : Nh$  do
16:          $h_1 = h(k)$  {scalar};  $h_2 = h$  {vector}
17:          $z'_{11} = z_{11}/(1 + z_{11}h_1^2)$  {scalar};  $Z'_{11} = z'_{11}\mathbf{1}_{Nh}$  {vector}
18:          $Z'_{22} = z_{22}/(1 + z_{22}h_2.^2)$  {vector; dot denotes elementwise operation}
19:          $\rho' = [\rho(j) + h_1h_2\sqrt{z_{11}z_{22}}] ./ \sqrt{(1 + z_{11}h_1^2)(1 + z_{22}h_2.^2)}$  {vector}
20:          $I_1 = Z'_{11}/dz + 1$ ;  $I_2 = Z'_{22}/dz + 1$ ;  $I_3 = (\rho' + 1)/dr + 1$  {fractional indices}
21:          $J^{8 \times Nh} =$  linear indices of 8 neighbor points using  $\lfloor I_n \rfloor, \lceil I_n \rceil, n = 1, 2, 3$ 
22:          $D_n = \lceil I_n \rceil - I_n$ ;  $\overline{D}_n = 1 - D_n, n = 1, 2, 3$  {distances to neighbor indices}
23:          $W^{8 \times Nh} =$  weights for neighbors as 8 multiplicative combinations of  $D_n, \overline{D}_n$ 
24:          $V^{Nh \times 1} = \text{diag}(W^T \mathcal{V}(J))$  {average the neighbor  $\mathcal{V}$  values}
25:          $E^{1 \times Nh} = \frac{1}{2\pi} \exp(-\frac{1}{2}(h_1^2 + h_2.^2)) dh^2$  {weights in the integral}
26:          $G = G + E V$  {update continuing cost}
27:       end for
28:        $\ell = i + (j - 1)Nz^2$  {linear index of the point the 3D grid}
29:        $\mathcal{V}'(\ell) = \min(F(\ell), 1 + G)$  {new optimal cost function}
30:     end for
31:   end for
32:    $dif = \|\mathcal{V}' - \mathcal{V}\|_F$ ;  $Fr = \|\mathcal{V}\|_F$ 
33:    $\mathcal{V} = \mathcal{V}'$  {update the optimal cost function}
34: end while
35: Find the points where transition occurs between regions  $\mathcal{V} = F$  and  $\mathcal{V} \neq F$ , i.e.,  $\mathcal{S}$ .

```

lines 10-34, the optimal cost function \mathcal{V} is computed for each point in the grid by iterating \mathcal{V}_m [cf. (3.24)] until no significant change occurs between \mathcal{V}_m and \mathcal{V}_{m+1} . In each iteration, the double integral with respect to $h_{1,1}$ and $h_{1,2}$ corresponding to the expectation in (3.24) is computed in lines 15-27. While computing the integral, since the updated (future)

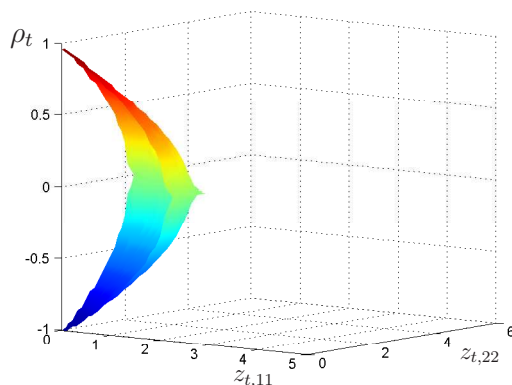


Figure 3.1: The surface that defines the stopping rule for $\lambda = 1$, $\sigma^2 = 1$ and $h_{1,1}, h_{1,2} \sim \mathcal{N}(0, 1)$ in the two-dimensional case.

(z_{11}, z_{22}, ρ) values, i.e, the arguments of \mathcal{V}_{m-1} in (3.24), in general may not correspond to a grid point, we average the \mathcal{V}_{m-1} values of eight neighboring grid points with appropriate weights in lines 21-24 to obtain the desired \mathcal{V}_{m-1} value.

The results for $\lambda \in \{0.01, 1, 100\}$, $\sigma^2 = 1$ and $h_{1,1}, h_{1,2} \sim \mathcal{N}(0, 1)$ are shown in Fig. 3.1 and Fig. 3.2. For $\lambda = 1$, the dome-shaped surface in Fig. 3.1 separates the stopping region from the continuing region. Outside the “dome” $\mathcal{V} = G$, hence we continue. As time progresses $z_{t,11}$ and $z_{t,22}$ decrease, so we move towards the “dome”. And whenever we are inside the “dome”, we stop, i.e., $\mathcal{V} = F$. We obtain similar dome-shaped surfaces for different λ values. However, the cross-sections of the “domes” at specific ρ_t values differ significantly. In particular, we investigate the case of $\rho_t = 0$, where the scaling coefficients $h_{t,1}$ and $h_{t,2}$ are uncorrelated. For small values of λ , e.g., $\lambda = 0.01$, the boundary that separates the stopping and the continuing regions is highly nonlinear as shown in Fig. 3.2(a). In Fig. 3.2(b) and 3.2(c), it is seen that the boundary tends to become more and more linear as λ increases.

Now let us explain the meaning of the λ value. Firstly, note from (3.23) that F and G are functions of z_{11}, z_{22} for fixed ρ , and the boundary is the solution to $F(\lambda, z_{11}, z_{22}) = G(z_{11}, z_{22})$. When λ is small, the region where $F < G$, i.e., the stopping region, is large, hence we stop early as shown in Fig. 3.2(a)¹. Conversely, for large λ the stopping region is

¹Note that the axis scales in Fig. 3.2(a) are on the order of hundreds and $z_{t,11}, z_{t,22}$ decrease as t

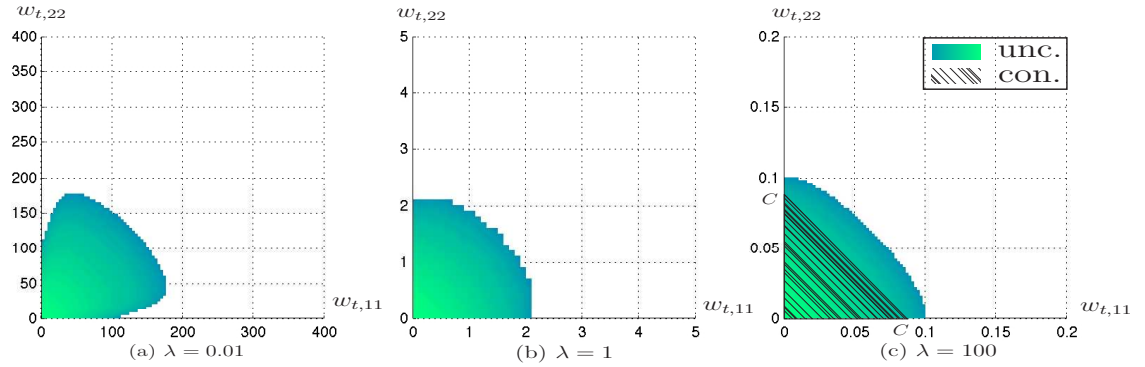


Figure 3.2: The stopping regions for $\rho_t = 0$, $\sigma^2 = 1$ and $h_{t,1}, h_{t,2} \sim \mathcal{N}(0, 1), \forall t$ in the unconditional problem with (a) $\lambda = 0.01$, (b) $\lambda = 1$, (c) $\lambda = 100$. That of the conditional problem is also shown in (c).

small, hence the stopping time is large [cf. Fig. 3.2(c)]. In fact, the Lagrange multiplier λ is

Algorithm 5 The procedure to compute the boundary surface \mathcal{S}

- 1: Select λ
 - 2: Compute $\mathcal{S}(\lambda)$ as in Algorithm 4
 - 3: Estimate $C = \mathbb{E} \left[\sigma^2 \frac{z_{\mathcal{T},11} + z_{\mathcal{T},22}}{1 - \rho_{\mathcal{T}}^2} \right]$ through simulations, where $z_{t,11} = 1/u_{t,11}$, $z_{t,22} = 1/u_{t,22}$, $\rho_t = u_{t,12} / \sqrt{u_{t,11} u_{t,22}}$ and $\mathcal{T} = \min\{t \in \mathbb{N} : (z_{t,11}, z_{t,22}, \rho_t) \text{ is between } \mathcal{S} \text{ and the origin}\}$
 - 4: **if** $C = C$ **then**
 - 5: return \mathcal{S}
 - 6: **else**
 - 7: **if** $C > C$ **then**
 - 8: Increase λ
 - 9: **else**
 - 10: Decrease λ
 - 11: **end if**
 - 12: Go to line 2
 - 13: **end if**
-

selected through simulations following the procedure in Algorithm 5 so that the constraint $\text{Tr} \left(\mathbb{E} [\sigma^2 \mathbf{U}_{\mathcal{T}}^{-1}] \right) = \mathbb{E} \left[\sigma^2 \frac{z_{\mathcal{T},11} + z_{\mathcal{T},22}}{1 - \rho_{\mathcal{T}}^2} \right] = C$ is satisfied. Note that line 2 of Algorithm 5 uses Algorithm 4 to compute the boundary surface \mathcal{S} .

In general, in the unconditional problem we need to numerically compute the stopping rule offline, i.e., the hypersurface that separates the stopping and the continuing regions, for

increases.

a given target accuracy level C . This becomes a quite intractable task as the dimension n of the vector to be estimated increases since the computation of G in (3.23) involves computing an n -dimensional integral, which is then used to find the separating hypersurface in a $\frac{n^2+n}{2}$ -dimensional space. On the other hand, in the conditional problem we have a simple stopping rule given in (3.12), which uses the target accuracy level $\frac{C}{\sigma^2}$ as its threshold, hence known beforehand for any n . Specifically, in the two-dimensional case of the conditional problem the optimal stopping time is given by $\mathcal{T} = \min \left\{ t \in \mathbb{N} : \frac{z_{t,11} + z_{t,22}}{1 - \rho_t^2} \leq \frac{C}{\sigma^2} \right\}$, which is a function of $z_{t,11} + z_{t,22}$ for fixed ρ_t . In Fig. 3.2(c), where $\rho_t = 0$ and $\sigma^2 = 1$, the stopping region of the conditional problem, which is characterized by a line, is shown to be smaller than that of the unconditional problem due to the same reasoning in the scalar case.

3.4 Distributed Sequential Estimator

In this section, we propose a computationally efficient scheme based on level-triggered sampling to implement the conditional sequential estimator in a distributed way. Consider a network of K distributed sensors and a fusion center (FC) which is responsible for computing the stopping time and the estimate. In practice, due to the stringent energy constraints, sensors should *infrequently* convey *low-rate* information to the FC, which is the main concern in the design of a distributed sequential estimator.

As in (3.1) each sensor k observes

$$y_t^k = (\mathbf{h}_t^k)^T \mathbf{x} + w_t^k, \quad t \in \mathbb{N}, \quad k = 1, \dots, K \quad (3.25)$$

as well as the coefficient vector $\mathbf{h}_t^k = [h_{t,1}^k, \dots, h_{t,n}^k]^T$ at time t , where $\{w_t^k\}_{k,t}$ ² are independent, zero-mean, i.e., $\mathbb{E}[w_t^k] = 0$, $\forall k, t$, and $\text{Var}(w_t^k) = \sigma_k^2$, $\forall t$. In other words, we allow for different noise variances at different sensors. Then, similar to (3.3) the weighted least squares (WLS) estimator

$$\hat{\mathbf{x}}_t = \arg \min_{\mathbf{x}} \sum_{k=1}^K \sum_{p=1}^t \frac{(y_p^k - (\mathbf{h}_p^k)^T \mathbf{x})^2}{\sigma_k^2}$$

²The subscripts k and t in the set notation denote $k = 1, \dots, K$ and $t \in \mathbb{N}$.

is given by

$$\hat{\mathbf{x}}_t = \left(\sum_{k=1}^K \sum_{p=1}^t \frac{\mathbf{h}_p^k (\mathbf{h}_p^k)^T}{\sigma_k^2} \right)^{-1} \sum_{k=1}^K \sum_{p=1}^t \frac{\mathbf{h}_p^k y_p^k}{\sigma_k^2} = \bar{\mathbf{U}}_t^{-1} \bar{\mathbf{V}}_t \quad (3.26)$$

where $\bar{\mathbf{U}}_t^k \triangleq \frac{1}{\sigma_k^2} \sum_{p=1}^t \mathbf{h}_p^k (\mathbf{h}_p^k)^T$, $\bar{\mathbf{V}}_t^k \triangleq \frac{1}{\sigma_k^2} \sum_{p=1}^t \mathbf{h}_p^k y_p^k$, $\bar{\mathbf{U}}_t = \sum_{k=1}^K \bar{\mathbf{U}}_t^k$ and $\bar{\mathbf{V}}_t = \sum_{k=1}^K \bar{\mathbf{V}}_t^k$. As before it can be shown that the WLS estimator $\hat{\mathbf{x}}_t$ in (3.26) is the BLUE under the general noise distributions. Moreover, in the Gaussian noise case, where $w_t^k \sim \mathcal{N}(0, \sigma_k^2) \forall t$ for each k , $\hat{\mathbf{x}}_t$ is also the MVUE. Note that $\hat{\mathbf{x}}_t$ in (3.26) coincides the ML estimator in the Gaussian case.

Following the steps in Section 3.3.1 it is straightforward to show that $(\mathcal{T}, \hat{\mathbf{x}}_{\mathcal{T}})$ is the optimum sequential estimator where

$$\mathcal{T} = \min \left\{ t \in \mathbb{N} : f \left(\bar{\mathbf{U}}_t^{-1} \right) \leq C \right\}, \quad (3.27)$$

is the stopping time and the estimator $\hat{\mathbf{x}}_t$ is given in (3.26). Note that $(\mathcal{T}, \hat{\mathbf{x}}_{\mathcal{T}})$ is achievable only in the centralized case, where all local observations until time t , i.e., $\{(y_p^k, \mathbf{h}_p^k)\}_{k,p}^3$, are available to the FC. Local processes $\{\bar{\mathbf{U}}_t^k\}_{k,t}$ and $\{\bar{\mathbf{V}}_t^k\}_{k,t}$ are used to compute the stopping time and the estimator as in (3.27) and (3.26), respectively. On the other hand, in a distributed system the FC can compute approximations $\tilde{\mathbf{U}}_t^k$ and $\tilde{\mathbf{V}}_t^k$ at each time t , and then use these approximations to compute the stopping time and the estimator as in (3.27) and (3.26), respectively.

3.4.1 Key Approximations in Distributed Approach

Before proceeding to explain the proposed distributed scheme, we note that the RLS estimator is a special case of the Kalman filter, which is easily distributed through its inverse covariance form, namely the information filter. In the information filter, an $n \times n$ matrix, namely the information matrix, and an $n \times 1$ vector, namely the information vector, are used at each time, similar to $\bar{\mathbf{U}}_t$ and $\bar{\mathbf{V}}_t$ in the LS estimator, respectively. Distributed implementations of the information filter in the literature, e.g., [82], require the transmission of local information matrices and information vectors from sensors to the FC at each time

³The subscript p in the set notation denotes $p = 1, \dots, t$.

t , which may not be practical, especially for large n , since it requires transmission of $O(n^2)$ terms.

Considering $\text{Tr}(\cdot)$ as the accuracy function f in (3.27), that is, assuming an MSE constraint, we propose to transmit only the n diagonal entries of $\bar{\mathbf{U}}_t^k$ for each k , giving us a computationally tractable scheme with linear complexity, i.e., $O(n)$, instead of quadratic complexity, i.e., $O(n^2)$. Using the diagonal entries of $\bar{\mathbf{U}}_t$ we define the diagonal matrix

$$\mathbf{D}_t \triangleq \text{diag}(d_{t,1}, \dots, d_{t,n})$$

$$\text{where } d_{t,i} = \sum_{k=1}^K \sum_{p=1}^t \frac{(h_{p,i}^k)^2}{\sigma_k^2}, \quad i = 1, \dots, n. \quad (3.28)$$

We further define the correlation matrix

$$\mathbf{R} = \begin{bmatrix} 1 & r_{12} & \cdots & r_{1n} \\ r_{12} & 1 & \cdots & r_{2n} \\ \vdots & \vdots & \ddots & \vdots \\ r_{1n} & r_{2n} & \cdots & 1 \end{bmatrix}, \quad (3.29)$$

$$\text{where } r_{ij} = \frac{\sum_{k=1}^K \frac{\mathbb{E}[h_{t,i}^k h_{t,j}^k]}{\sigma_k^2}}{\sqrt{\sum_{k=1}^K \frac{\mathbb{E}[(h_{t,i}^k)^2]}{\sigma_k^2} \sum_{k=1}^K \frac{\mathbb{E}[(h_{t,j}^k)^2]}{\sigma_k^2}}}, \quad i, j = 1, \dots, n.$$

Proposition 3. *For sufficiently large t , we can make the following approximations,*

$$\bar{\mathbf{U}}_t \cong \mathbf{D}_t^{1/2} \mathbf{R} \mathbf{D}_t^{1/2}$$

$$\text{and } \text{Tr}(\bar{\mathbf{U}}_t^{-1}) \cong \text{Tr}(\mathbf{D}_t^{-1} \mathbf{R}^{-1}). \quad (3.30)$$

The proof of Proposition 3 is provided in Appendix B. Then, assuming that the FC knows *a priori* the correlation matrix \mathbf{R} , i.e., $\{\mathbb{E}[h_{t,i}^k h_{t,j}^k]\}_{i,j,k}$ ⁴ and $\{\sigma_k^2\}$ [cf. (3.29)], it can compute the approximations in (3.30) if sensors report their local processes $\{\mathbf{D}_t^k\}_{k,t}$ to the

⁴The subscripts i and j in the set notation denote $i = 1, \dots, n$ and $j = i, \dots, n$. In the special case where $\mathbb{E}[(h_{t,i}^k)^2] = \mathbb{E}[(h_{t,i}^m)^2]$, $k, m = 1, \dots, K$, $i = 1, \dots, n$, the correlation coefficients

$$\left\{ \xi_{ij}^k = \frac{\mathbb{E}[h_{t,i}^k h_{t,j}^k]}{\sqrt{\mathbb{E}[(h_{t,i}^k)^2] \mathbb{E}[(h_{t,j}^k)^2]}} : i = 1, \dots, n-1, j = i+1, \dots, n \right\}_k$$

together with $\{\sigma_k^2\}$ are sufficient statistics since $r_{ij} = \frac{\sum_{k=1}^K \xi_{ij}^k / \sigma_k^2}{\sum_{k=1}^K 1 / \sigma_k^2}$ from (B.19).

FC, where $\mathbf{D}_t = \sum_{k=1}^K \mathbf{D}_t^k$. Note that each local process $\{\mathbf{D}_t^k\}_t$ is n -dimensional, and its entries at time t are given by $\left\{d_{t,i}^k = \sum_{p=1}^t \frac{(h_{p,i}^k)^2}{\sigma_k^2}\right\}_i$ [cf. (3.28)]. Hence, we propose that each sensor k sequentially reports the local processes $\{\mathbf{D}_t^k\}_t$ and $\{\bar{\mathbf{V}}_t^k\}_t$ to the FC, achieving linear complexity $O(n)$. On the other side, the FC, using the information received from sensors, computes the approximations $\{\tilde{\mathbf{D}}_t\}$ and $\{\tilde{\mathbf{V}}_t\}$, which are then used to compute the stopping time

$$\tilde{\mathcal{T}} = \min \left\{ t \in \mathbb{N} : \text{Tr} \left(\tilde{\mathbf{U}}_t^{-1} \right) \leq \tilde{C} \right\}, \quad (3.31)$$

and the estimator

$$\tilde{\mathbf{x}}_{\tilde{\mathcal{T}}} = \tilde{\mathbf{U}}_{\tilde{\mathcal{T}}}^{-1} \tilde{\mathbf{V}}_{\tilde{\mathcal{T}}} \quad (3.32)$$

similar to (3.27) and (3.26), respectively. The approximations $\text{Tr} \left(\tilde{\mathbf{U}}_t^{-1} \right)$ in (3.31) and $\tilde{\mathbf{U}}_{\tilde{\mathcal{T}}}$ in (3.32) are computed using $\tilde{\mathbf{D}}_t$ as in (3.30). The threshold \tilde{C} is selected through simulations to satisfy the constraint in (3.7) with equality, i.e., $\text{Tr} \left(\text{Cov}(\tilde{\mathbf{x}}_{\tilde{\mathcal{T}}} | \mathbf{H}_{\tilde{\mathcal{T}}}) \right) = C$.

3.4.2 Proposed Estimator Based on Level-triggered Sampling

Level-triggered sampling provides a very convenient way of information transmission in distributed systems as recently shown in [12; 20; 21; 14; 23]. Methods based on level-triggered sampling, sending infrequently small number of bits, e.g., one bit, from sensors to the FC, enables highly accurate approximations and thus high performance schemes at the FC. They significantly outperform canonical sampling-and-quantizing methods which sample local processes using the conventional uniform-in-time sampling and send the quantized versions of samples to the FC [20]. On the other hand, level-triggered sampling, which is a non-uniform sampling technique, naturally outputs single-bit information. Moreover, the FC can effectively recover the samples of local processes by using these low-rate information from sensors.

All of the references above that propose schemes based on level-triggered sampling deal with one-dimensional, i.e., scalar, local processes. However, in our case $\{\bar{\mathbf{V}}_t^k\}_t$ is n -dimensional and even worse $\{\bar{\mathbf{U}}_t^k\}_t$ is $\frac{n^2+n}{2}$ -dimensional⁵ for each k . Applying a scheme that was proposed for one-dimensional processes in a straightforward fashion for each dimension,

⁵This is because $\bar{\mathbf{U}}_t^k$ is symmetric.

i.e., entry, of $\bar{\mathbf{U}}_t^k$ becomes cumbersome, especially when n is large. Hence, in this paper we propose to use the approximations introduced in the previous subsection, achieving linear complexity $O(n)$.

We will next describe the distributed scheme based on level-triggered sampling in which each sensor non-uniformly samples the local processes $\{\mathbf{D}_t^k\}_t$ and $\{\bar{\mathbf{V}}_t^k\}_t$, transmits a single pulse for each sample to the FC, and the FC computes $\{\tilde{\mathbf{D}}_t\}$ and $\{\tilde{\mathbf{V}}_t\}$ using received information. Our scheme employs a novel algorithm to transmit a one-dimensional process, separately for each dimension of $\{\mathbf{D}_t^k\}_t$ and $\{\bar{\mathbf{V}}_t^k\}_t$. In other words, our scheme at each sensor k consists of, in total, $2n$ level-triggered samplers running in parallel.

3.4.2.1 Sampling and Recovery of \mathbf{D}_t^k

Each sensor k samples each entry $d_{t,i}^k$ of \mathbf{D}_t^k at a sequence of random times $\{s_{m,i}^k\}_m$ ⁶ given by

$$s_{m,i}^k \triangleq \min \left\{ t \in \mathbb{N} : d_{t,i}^k - d_{s_{m-1,i}^k}^k \geq \Delta_i^k \right\}, \quad s_{0,i}^k = 0, \quad (3.33)$$

where $d_{t,i}^k = \sum_{p=1}^t \frac{(h_{p,i}^k)^2}{\sigma_k^2}$, $d_{0,i}^k = 0$ and $\Delta_i^k > 0$ is a constant threshold that controls the average sampling interval. Note that the sampling times $\{s_{m,i}^k\}_m$ in (3.33) are dynamically determined by the signal to be sampled, i.e., realizations of $d_{t,i}^k$. Hence, they are random, whereas sampling times in the conventional uniform-in-time sampling are deterministic with a certain period. According to the sampling rule in (3.33), a sample is taken whenever the signal level $d_{t,i}^k$ increases by at least Δ_i^k since the last sampling time. Note that $d_{t,i}^k = \sum_{p=1}^t \frac{(h_{p,i}^k)^2}{\sigma_k^2}$ is non-decreasing in t .

At each sampling time $s_{m,i}^k$, sensor k transmits a single pulse to the FC at time $t_{m,i}^k \triangleq s_{m,i}^k + \delta_{m,i}^k$, indicating that $d_{t,i}^k$ has increased by at least Δ_i^k since the last sampling time $s_{m-1,i}^k$. The value of the transmitted pulse is not important since it only indicates $d_{s_{m,i}^k}^k - d_{s_{m-1,i}^k}^k \geq \Delta_i^k$. The delay $\delta_{m,i}^k$ between the transmission time and the sampling time is used to linearly encode the overshoot

$$q_{m,i}^k \triangleq \left(d_{s_{m,i}^k}^k - d_{s_{m-1,i}^k}^k \right) - \Delta_i^k < \theta_d, \quad \forall k, m, i \quad (3.34)$$

⁶The subscript m in the set notation denotes $m \in \mathbb{N}^+$.

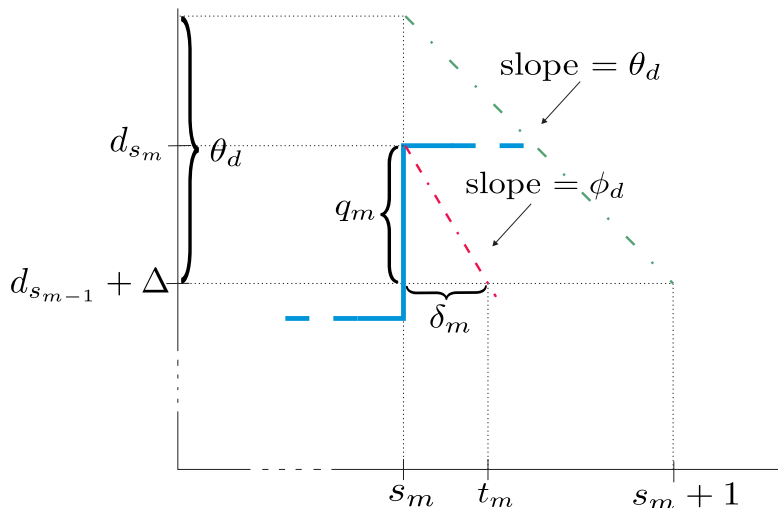


Figure 3.3: Illustration of sampling time s_m , transmission time t_m , transmission delay δ_m and overshoot q_m . We encode $q_m = (d_{s_m} - d_{s_{m-1}}) - \Delta < \theta_d$ in $\delta_m = t_m - s_m < 1$ using the slope $\phi_d > \theta_d$.

and given by

$$\delta_{m,i}^k = \frac{q_{m,i}^k}{\phi_d} \in [0, 1), \quad (3.35)$$

where ϕ_d^{-1} is the slope of the linear encoding function (cf. Fig. 3.3), known to sensors and the FC.

Assume a global clock, that is, the time index $t \in \mathbb{N}$ is the same for all sensors and the FC, meaning that the FC knows the potential sampling times. Assume further ultra-wideband (UWB) channels between sensors and the FC, in which the FC can determine the time of flight of pulses transmitted from sensors. Then, FC can measure the transmission delay $\delta_{m,i}^k$ if it is bounded by unit time, i.e., $\delta_{m,i}^k \in [0, 1)$. To ensure this, from (3.35), we need to have $\phi_d > q_{m,i}^k, \forall k, m, i$. Assuming a bound for overshoots, i.e., $q_{m,i}^k < \theta_d, \forall k, m, i$, we can achieve this by setting $\phi_d > \theta_d$ ⁷. Consequently, the FC can uniquely decode the overshoot by computing $q_{m,i}^k = \phi_d \delta_{m,i}^k$ (cf. Fig. 3.3), using which it can also find the increment occurred in $d_{t,i}^k$ during the interval $(s_{m-1,i}^k, s_{m,i}^k]$ as $d_{s_{m,i}^k,i}^k - d_{s_{m-1,i}^k,i}^k = \Delta_i^k + q_{m,i}^k$ from (3.34). It is then possible to reach the signal level $d_{s_{m,i}^k,i}^k$ by accumulating the increments occurred

⁷In fact, by setting the slope ϕ_d arbitrarily large we can make the transmission delay arbitrarily small.

until the m -th sampling time, i.e.,

$$d_{s_{m,i},i}^k = \sum_{\ell=1}^m (\Delta_i^k + q_{\ell,i}^k) = m\Delta_i^k + \sum_{\ell=1}^m q_{\ell,i}^k. \quad (3.36)$$

Using $\{d_{s_{m,i},i}^k\}_m$ the FC computes the staircase approximation $\tilde{d}_{t,i}^k$ as

$$\tilde{d}_{t,i}^k = d_{s_{m,i},i}^k, \quad t \in [t_{m,i}^k, t_{m+1,i}^k), \quad (3.37)$$

which is updated when a new pulse is received from sensor k , otherwise kept constant. Such approximate local signals of different sensors are next combined to obtain the approximate global signal $\tilde{d}_{t,i}$ as

$$\tilde{d}_{t,i} = \sum_{k=1}^K \tilde{d}_{t,i}^k. \quad (3.38)$$

In practice, when the m -th pulse in the global order regarding dimension i is received from sensor k_m at time $t_{m,i}$, instead of computing (3.36)–(3.38) the FC only updates $\tilde{d}_{t,i}$ as

$$\tilde{d}_{t_m,i} = \tilde{d}_{t_{m-1},i} + \Delta_i^{k_m} + q_{m,i}, \quad \tilde{d}_{0,i} = \epsilon, \quad (3.39)$$

and keeps it constant when no pulse arrives. We initialize $\tilde{d}_{t,i}$ to a small constant ϵ to prevent dividing by zero while computing the test statistic [cf. (3.40)]. Note that in general $\tilde{d}_{t_m,i} \neq d_{s_{m,i},i}$ unlike (3.37) since all sensors do not necessarily sample and transmit at the same time. The approximations $\{\tilde{d}_{t,i}\}_i$ form $\tilde{\mathbf{D}}_t = \text{diag}(\tilde{d}_{t,1}, \dots, \tilde{d}_{t,n})$, which is used in (3.31) and (3.32) to compute the stopping time and the estimator, respectively. Note that to determine the stopping time as in (3.31) we need to compute $\text{Tr}(\tilde{\mathbf{U}}_t^{-1})$ using (3.30) at times $\{t_m\}$ when a pulse is received from any sensor regarding any dimension. Fortunately, when the m -th pulse in the global order is received from sensor k_m at time t_m regarding dimension i_m we can compute $\text{Tr}(\tilde{\mathbf{U}}_{t_m}^{-1})$ recursively as follows

$$\text{Tr}(\tilde{\mathbf{U}}_{t_m}^{-1}) = \text{Tr}(\tilde{\mathbf{U}}_{t_{m-1}}^{-1}) - \frac{\kappa_{i_m}(\Delta_{i_m}^{k_m} + q_m)}{\tilde{d}_{t_m,i_m}\tilde{d}_{t_{m-1},i_m}}, \quad \text{Tr}(\tilde{\mathbf{U}}_0^{-1}) = \sum_{i=1}^n \frac{\kappa_i}{\epsilon}, \quad (3.40)$$

where κ_i is the i -th diagonal element of the inverse correlation matrix \mathbf{R}^{-1} , known to the FC. In (3.40) pulse arrival times are assumed to be distinct for the sake of simplicity. In case multiple pulses arrive at the same time, the update rule will be similar to (3.40) except that it will consider all new arrivals together.

3.4.2.2 Sampling and Recovery of \bar{V}_t^k

Similar to (3.33) each sensor k samples each entry $\bar{v}_{t,i}^k$ of \bar{V}_t^k at a sequence of random times $\{\alpha_{m,i}^k\}_m$ written as

$$\alpha_{m,i}^k \triangleq \min \left\{ t \in \mathbb{N} : |\bar{v}_{t,i}^k - \bar{v}_{\alpha_{m-1,i}^k}^k| \geq \gamma_i^k \right\}, \quad \alpha_{0,i}^k = 0, \quad (3.41)$$

where $\bar{v}_{t,i}^k = \sum_{p=1}^t \frac{h_{p,i}^k y_p^k}{\sigma_k^2}$ and γ_i^k is a constant threshold, available to both sensor k and the FC. It has been shown in [20, Section IV-B] that γ_i^k is determined by

$$\gamma_i^k \tanh(\gamma_i^k/2) = T \sum_{k=1}^K \frac{\mathbb{E}[\bar{v}_{t,i}^k]}{K}$$

to ensure the average sampling interval T . Since $\bar{v}_{t,i}^k$ is neither increasing nor decreasing, we use two thresholds γ_i^k and $-\gamma_i^k$ in the sampling rule given in (3.41). Specifically, a sample is taken whenever $\bar{v}_{t,i}^k$ increases or decreases by at least γ_i^k since the last sampling time. Then, sensor k at time $p_{m,i}^k \triangleq \alpha_{m,i}^k + \beta_{m,i}^k$ transmits a single pulse $b_{m,i}^k$ to the FC, indicating whether $\bar{v}_{t,i}^k$ has changed by at least γ_i^k or $-\gamma_i^k$ since the last sampling time $\alpha_{m-1,i}^k$. We can simply write $b_{m,i}^k$ as

$$b_{m,i}^k = \text{sign}(\bar{v}_{\alpha_{m,i}^k}^k - \bar{v}_{\alpha_{m-1,i}^k}^k), \quad (3.42)$$

where $b_{m,i}^k = 1$ implies that $\bar{v}_{\alpha_{m,i}^k}^k - \bar{v}_{\alpha_{m-1,i}^k}^k \geq \gamma_i^k$ and $b_{m,i}^k = -1$ indicates that $\bar{v}_{\alpha_{m,i}^k}^k - \bar{v}_{\alpha_{m-1,i}^k}^k \leq -\gamma_i^k$. The overshoot $\eta_{m,i}^k \triangleq |\bar{v}_{\alpha_{m,i}^k}^k - \bar{v}_{\alpha_{m-1,i}^k}^k| - \gamma_i^k$ is linearly encoded in the transmission delay as before. Similar to (3.35) the transmission delay is written as $\beta_{m,i}^k = \frac{\eta_{m,i}^k}{\phi_v}$, where ϕ_v^{-1} is the slope of the encoding function, available to sensors and the FC. Assume again that (i) there exists a global clock among sensors and the FC, (ii) the FC determines channel delay (i.e., time of flight), and (iii) overshoots are bounded by a constant, i.e., $\eta_{m,i}^k < \theta_v$, $\forall k, m, i$, and we set $\phi_v > \theta_v$. With these assumptions we ensure that the FC can measure the transmission delay $\beta_{m,i}^k$, and accordingly decode the overshoot as $\eta_{m,i}^k = \phi_v \beta_{m,i}^k$. Then, upon receiving the m -th pulse $b_{m,i}$ regarding dimension i from sensor k_m at time $p_{m,i}$ the FC performs the following update,

$$\tilde{v}_{p_{m,i},i} = \tilde{v}_{p_{m-1,i},i} + b_{m,i}(\gamma_i^{k_m} + \eta_{m,i}), \quad (3.43)$$

where $\{\tilde{v}_{t,i}\}_i$ compose the approximation $\tilde{V}_t = [\tilde{v}_{t,1}, \dots, \tilde{v}_{t,n}]^T$. Recall that the FC employs \tilde{V}_t to compute the estimator as in (3.32).

Algorithm 6 The level-triggered sampling procedure at the k -th sensor for the i -th dimension

- 1: Initialization: $t \leftarrow 0$, $m \leftarrow 0$, $\ell \leftarrow 0$, $\chi \leftarrow 0$, $\psi \leftarrow 0$
 - 2: **while** $\chi < \Delta_i^k$ **and** $\psi \in (-\gamma_i^k, \gamma_i^k)$ **do**
 - 3: $t \leftarrow t + 1$
 - 4: $\chi \leftarrow \chi + \frac{(h_{t,i}^k)^2}{\sigma_k^2}$
 - 5: $\psi \leftarrow \psi + \frac{h_{t,i}^k y_t^k}{\sigma_k^2}$
 - 6: **end while**
 - 7: **if** $\chi \geq \Delta_i^k$ {sample $d_{t,i}^k$ } **then**
 - 8: $m \leftarrow m + 1$
 - 9: $s_{m,i}^k = t$
 - 10: Send a pulse to the FC through channel $\text{ch}_{k,i}^d$ at time instant $t_{m,i}^k = s_{m,i}^k + \frac{\chi - \Delta_i^k}{\phi_d}$
 - 11: $\chi \leftarrow 0$
 - 12: **end if**
 - 13: **if** $\psi \notin (-\gamma_i^k, \gamma_i^k)$ {sample $\bar{v}_{t,i}^k$ } **then**
 - 14: $\ell \leftarrow \ell + 1$
 - 15: $\alpha_{\ell,i}^k = t$
 - 16: Send $b_{\ell,i}^k = \text{sign}(\psi)$ to the FC through channel $\text{ch}_{k,i}^v$ at time instant $p_{\ell,i}^k = \alpha_{\ell,i}^k + \frac{|\psi| - \gamma_i^k}{\phi_v}$
 - 17: $\psi \leftarrow 0$
 - 18: **end if**
 - 19: Stop if the FC instructs so; otherwise go to line 2.
-

The level-triggered sampling procedure at each sensor k for each dimension i is summarized in Algorithm 6. Each sensor k runs n of these procedures in parallel. The sequential estimation procedure at the FC is also summarized in Algorithm 7. We assumed, for the sake of clarity, that each sensor transmits pulses to the FC for each dimension through a separate channel, i.e., parallel architecture. On the other hand, in practice the number of parallel channels can be decreased to two by using identical sampling thresholds Δ and γ for all sensors and for all dimensions in (3.33) and (3.41), respectively. Moreover, sensors can even employ a single channel to convey information about local processes $\{d_{t,i}^k\}$ and $\{\bar{v}_{t,i}^k\}$ by sending ternary digits to the FC. This is possible since pulses transmitted for $\{d_{t,i}^k\}$ are unsigned.

3.4.3 Discussions

We introduced the distributed estimator in Section 3.4.2 initially for a continuous-time system with infinite precision. In practice, due to bandwidth constraints, discrete-time

Algorithm 7 The sequential estimation procedure at the fusion center

- 1: Initialization: $\text{Tr} \leftarrow \sum_{i=1}^n \frac{\kappa_i}{\epsilon}$, $m \leftarrow 1$, $\ell \leftarrow 1$, $\tilde{d}_i \leftarrow \epsilon \forall i$, $\tilde{v}_i \leftarrow 0 \forall i$
 - 2: **while** $\text{Tr} < \tilde{C}$ **do**
 - 3: Listen to the channels $\{\text{ch}_{k,i}^d\}_{k,i}$ and $\{\text{ch}_{k,i}^v\}_{k,i}$, and wait to receive a pulse
 - 4: **if** m -th pulse arrives through ch_{k_m,i_m}^d at time t_m **then**
 - 5: $q_m = \phi_d(t_m - \lfloor t_m \rfloor)$
 - 6: $\text{Tr} \leftarrow \text{Tr} - \frac{\kappa_{i_m}(\Delta_{i_m}^{k_m} + q_m)}{\tilde{d}_{i_m}(\tilde{d}_{i_m} + \Delta_{i_m}^{k_m} + q_m)}$
 - 7: $\tilde{d}_{i_m} = \tilde{d}_{i_m} + \Delta_{i_m}^{k_m} + q_m$
 - 8: $m \leftarrow m + 1$
 - 9: **end if**
 - 10: **if** ℓ -th pulse b_ℓ arrives through $\text{ch}_{p_\ell,j_\ell}^v$ at time p_ℓ **then**
 - 11: $\eta_\ell = \phi_v(p_\ell - \lfloor p_\ell \rfloor)$
 - 12: $\tilde{v}_{j_\ell} = \tilde{v}_{j_\ell} + b_\ell(\gamma_{j_\ell}^{p_\ell} + \eta_\ell)$
 - 13: $\ell \leftarrow \ell + 1$
 - 14: **end if**
 - 15: **end while**
 - 16: Stop at time $\tilde{\mathcal{T}} = t_m$
 - 17: $\tilde{\mathbf{D}} = \text{diag}(\tilde{d}_1, \dots, \tilde{d}_n)$, $\tilde{\mathbf{U}}^{-1} = \tilde{\mathbf{D}}^{-1/2} \mathbf{R}^{-1} \tilde{\mathbf{D}}^{-1/2}$, $\tilde{\mathbf{V}} = [\tilde{v}_1, \dots, \tilde{v}_n]^T$
 - 18: $\tilde{\mathbf{x}} = \tilde{\mathbf{U}}^{-1} \tilde{\mathbf{V}}$
 - 19: Instruct sensors to stop
-

systems with finite precision are of interest. For example, in such systems, the overshoot $q_{m,i}^k \in \left[j \frac{\theta_d}{N}, (j+1) \frac{\theta_d}{N} \right)$, $j = 0, 1, \dots, N-1$, is quantized into $\hat{q}_{m,i}^k = \left(j + \frac{1}{2} \right) \frac{\theta_d}{N}$ where N is the number of quantization levels. More specifically, a pulse is transmitted at time $t_{m,i}^k = s_{m,i}^k + \frac{j+1/2}{N}$, where the transmission delay $\frac{j+1/2}{N} \in (0, 1)$ encodes $\hat{q}_{m,i}^k$. This transmission scheme is called pulse position modulation (PPM).

In UWB and optical communication systems, PPM is effectively employed. In such systems, N , which denotes the precision, can be easily made large enough so that the quantization error $|\hat{q}_{m,i}^k - q_{m,i}^k|$ becomes insignificant. Compared to conventional transmission techniques which convey information by varying the power level, frequency, and/or phase of a sinusoidal wave, PPM (with UWB) is extremely energy efficient at the expense of high bandwidth usage. Hence, PPM suits well to energy-constrained sensor network systems.

3.4.4 Simulation Results

We next provide simulation results to compare the performances of the proposed scheme with linear complexity, given in Algorithm 6 and Algorithm 7, the unsimplified version of the proposed scheme with quadratic complexity and the optimal centralized scheme. A wireless sensor network with 10 identical sensors and an FC is considered to estimate a five-dimensional deterministic vector of parameters, i.e., $n = 5$. We assume i.i.d. Gaussian noise with unit variance at all sensors, i.e., $w_t^k \sim \mathcal{N}(0, 1), \forall k, t$. We set the correlation coefficients $\{r_{ij}\}$ [cf. (B.19)] of the vector \mathbf{h}_t^k to different values in $[0, 1)$. In Fig. 3.4 and Fig. 3.5, they are set to 0 and 0.5 to test the performance of the proposed scheme in the uncorrelated and correlated cases, respectively. We compare the average stopping time performance of the proposed scheme with linear complexity to those of the other two schemes for different MSE values. In Fig. 3.4 and Fig. 3.5, the horizontal axis represents the MSE normalized by the square of the Euclidean norm of the vector to be estimated, i.e., $\text{nMSE} \triangleq \frac{\text{MSE}}{\|\mathbf{x}\|_2^2}$.

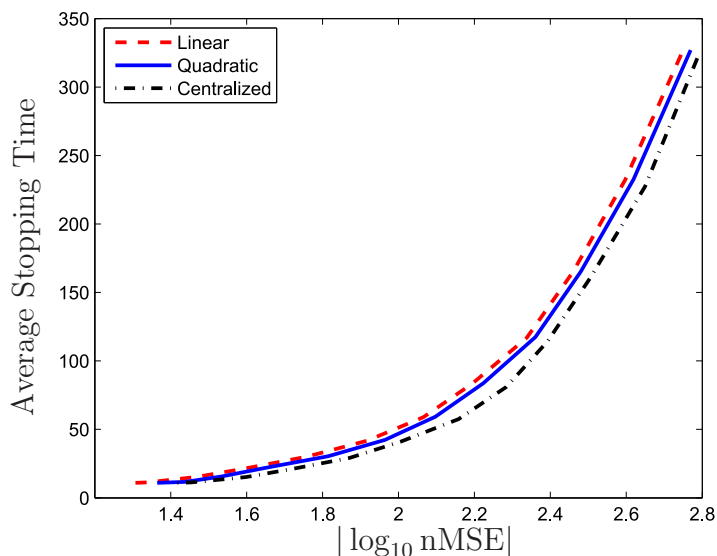


Figure 3.4: Average stopping time performances of the optimal centralized scheme and the distributed schemes based on level-triggered sampling with quadratic and linear complexity vs. normalized MSE values when scaling coefficients are uncorrelated, i.e., $r_{ij} = 0, \forall i, j$.

In the uncorrelated case, where $r_{ij} = 0, \forall i, j, i \neq j$, the proposed scheme with linear

complexity nearly attains the performance of the unsimplified scheme with quadratic complexity as seen in Fig. 3.4. This result is rather expected since in this case $\bar{\mathbf{U}}_t \cong \mathbf{D}_t$ for sufficiently large t , where $\bar{\mathbf{U}}_t$ and \mathbf{D}_t are used to compute the stopping time and the estimator in the unsimplified and simplified schemes, respectively. Strikingly the distributed schemes (simplified and unsimplified) achieve very close performances to that of the optimal centralized scheme, which is obviously unattainable in a distributed system, thanks to the efficient information transmission through level-triggered sampling. It is seen in Fig. 3.5

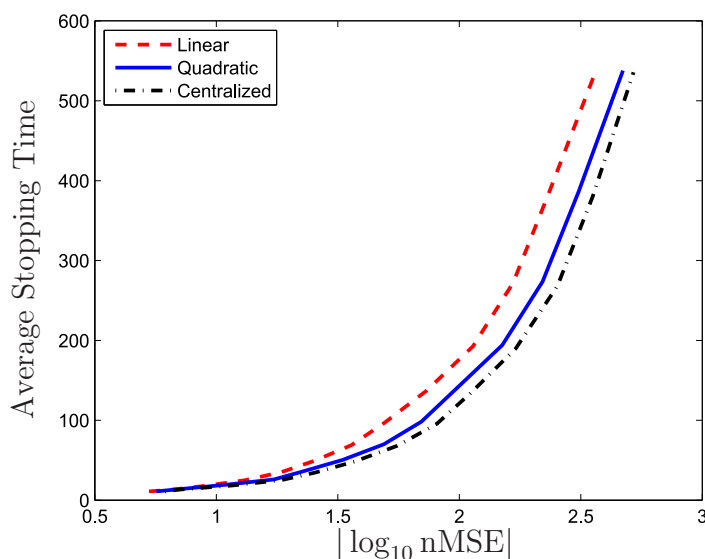


Figure 3.5: Average stopping time performances of the optimal centralized scheme and the distributed schemes based on level-triggered sampling with quadratic and linear complexity vs. normalized MSE values when scaling coefficients are correlated with $r_{ij} = 0.5, \forall i, j$.

that the proposed simplified scheme exhibits an average stopping time performance close to those of the unsimplified scheme and the optimal centralized scheme even when the scaling coefficients $\{h_{t,i}^k\}_i$ are correlated with $r_{ij} = 0.5, \forall i, j, i \neq j$, justifying the simplification proposed in Section 3.4.1 to obtain linear complexity.

Finally, in Fig. 3.6 we fix the normalized MSE value at 10^{-2} and plot average stopping time against the correlation coefficient r where $r_{ij} = r, \forall i, j, i \neq j$. We observe an exponential growth in average stopping time of each scheme as r increases. The average stopping time of each scheme becomes infinite at $r = 1$ since in this case only some multiples

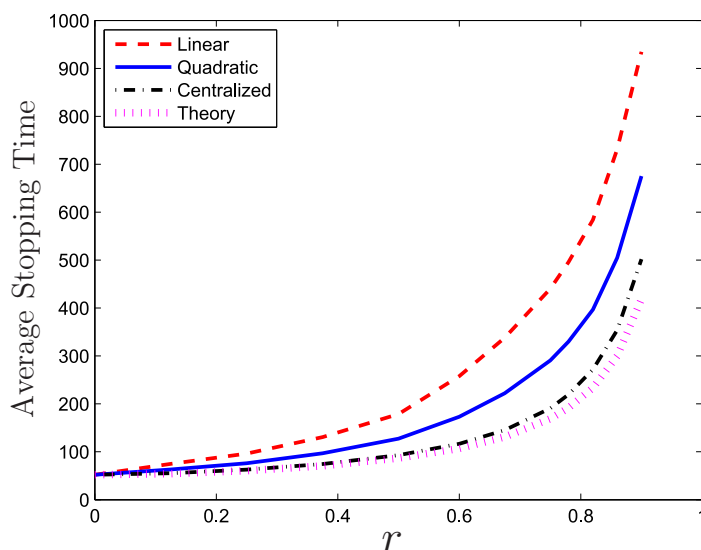


Figure 3.6: Average stopping time performances of the optimal centralized scheme and the distributed schemes based on level-triggered sampling with quadratic and linear complexity vs. correlation coefficient for normalized MSE fixed to 10^{-2} .

of a certain linear combination of the parameters to be estimated, i.e., $h_{t,1}^k \sum_{i=1}^n c_i x_i$, are observed under the noise w_t^k at each sensor k at each time t , hence it is not possible to recover the individual parameters. Specifically, it can be shown that $c_i = \sqrt{\frac{\mathbb{E}[(h_{t,i}^k)^2]}{\mathbb{E}[(h_{t,1}^k)^2]}}$, which is the same for all sensors as we assume identical sensors. To see the mechanism that causes the exponential growth consider the computation of $\text{Tr}(\bar{\mathbf{U}}_t^{-1})$, which is used to determine the stopping time in the optimal centralized scheme. From (3.30) we write

$$\text{Tr}(\bar{\mathbf{U}}_t^{-1}) \cong \text{Tr}(\mathbf{D}_t^{-1} \mathbf{R}^{-1}) = \sum_{i=1}^n \frac{\kappa_i}{d_{t,i}} \quad (3.44)$$

for sufficiently large t , where $d_{t,i}$ and κ_i are the i -th diagonal elements of the matrices \mathbf{D}_t and \mathbf{R}^{-1} , respectively. For instance, we have $\kappa_i = 1, \forall i$, $\kappa_i = 8.0435, \forall i$ and $\kappa_i = \infty$ when $r = 0$, $r = 0.9$ and $r = 1$, respectively. Assuming that the scaling coefficients have the same mean and variance when $r = 0$ and $r = 0.9$, we have similar $d_{t,i}$ values [cf. (3.28)] in (3.44), hence the stopping time of $r = 0.9$ is approximately 8 times that of $r = 0$ for the same accuracy level. Since $\text{MSE} = \mathbb{E}[\|\hat{\mathbf{x}}_{\mathcal{T}} - \mathbf{x}\|_2^2] = \text{Tr}(\bar{\mathbf{U}}_t^{-1})$ in the centralized scheme, using κ_i for different r values we can approximately know how the average stopping time

changes as r increases for a given MSE value. As shown in Fig. 3.6 with the label “Theory” this theoretical curve is in a good match with the numerical result. The small discrepancy at high r values is due to the high sensitivity of the WLS estimator in (3.26) to numerical errors when the stopping time is large. The high sensitivity is due to multiplying the matrix $\bar{U}_{\mathcal{T}}^{-1}$ with very small entries by the vector $\bar{V}_{\mathcal{T}}$ with very large entries while computing the estimator $\hat{x}_{\mathcal{T}}$ in (3.26) for a large \mathcal{T} . The distributed schemes suffer from a similar high sensitivity problem [cf. (3.32)] much more than the centralized scheme since making error is inherent in a distributed system. Moreover, in the distributed schemes the MSE is not given by the stopping time statistic $\text{Tr}(\tilde{U}_t^{-1})$, hence “Theory” does not match well the curves for the distributed schemes. Although it cannot be used to estimate the rates of the exponential growths of the distributed schemes, it is still useful to explain the mechanism behind them as the distributed schemes are derived from the centralized scheme.

To summarize, with identical sensors any estimator (centralized or distributed) experiences an exponential growth in its average stopping time as the correlation between scaling coefficients increases since in the extreme case of full correlation, i.e., $r = 1$, each sensor k , at each time t , observes a noisy sample of the linear combination $\sum_{i=1}^n x_i \sqrt{\frac{\mathbb{E}[(h_{t,i}^k)^2]}{\mathbb{E}[(h_{t,1}^k)^2]}}$, and thus the stopping time is infinite. As a result of exponentially growing stopping time, the WLS estimator, which is also the ML estimator and the MVUE, i.e., the optimal estimator, in our case, and the distributed estimators derived from it become highly sensitive to errors as r increases. In either uncorrelated or mildly correlated cases, which are of practical importance, the proposed distributed scheme with linear complexity performs very close to the optimal centralized scheme as shown in Fig. 3.4 and Fig. 3.5, respectively.

3.5 Conclusion

We have treated the problem of sequential vector parameter estimation under both centralized and distributed settings. In the centralized setting two different formulations, which use unconditional and conditional covariances of the estimator respectively to assess the estimation accuracy, are considered and the corresponding sequential estimators are derived. The conditional formulation, having a simple stopping rule for any number of parame-

ters, was shown to be preferable to the unconditional formulation, whose stopping rule can only be found by complicated numerical computations even for a small number of parameters. Moreover, following the optimum conditional sequential estimator we have developed a computationally efficient distributed sequential estimator based on level-triggered sampling. Simulation results have shown that the proposed scheme with linear complexity has a similar performance to that of the optimal centralized scheme.

Part III

Joint Detection and Estimation

Chapter 4

Sequential Joint Detection and Estimation

4.1 Introduction

Detection and estimation problems appear simultaneously in a wide range of fields, such as wireless communications, power systems, image processing, genetics, and finance. For instance, to achieve effective and reliable dynamic spectrum access in cognitive radio, a secondary user needs to detect primary user transmissions, and if detected estimate the cross channels that may cause interference to primary users [26]. In power grid monitoring, it is essential to detect the correct topological model, and at the same time estimate the system state [83]. Some other important examples are detecting and estimating objects from images [84], target detection and parameter estimation in radar [85], and detection and estimation of periodicities in DNA sequences [86].

In all these applications, detection and estimation problems are intrinsically coupled, and are both of primary importance. Hence, a jointly optimum method, that maximizes the overall performance, is required. Classical approaches either treat the two subproblems separately with the corresponding optimum solutions, or solve them together, as a composite hypothesis testing problem, using the generalized likelihood ratio test (GLRT). It is well known that such approaches do not yield the optimum overall result [87; 25]. In the former approach, for example, the likelihood ratio test (LRT) is performed by averaging

over the unknown parameters to solve the detection subproblem optimally, and then relying on the detection decision the Bayes estimators are used to solve the estimation subproblem. On the other hand, in GLRT, the maximum likelihood (ML) estimates of all unknown parameters are computed, and then using these estimates LRT is performed as in a simple hypothesis testing problem. In GLRT, the primary emphasis is on the detection performance and the estimation performance is of secondary importance. GLRT is very popular due to its simplicity. However, it is not always optimal in terms of the detection performance in the Neyman-Pearson sense [88], and also the overall performance under mixed Bayesian/Neyman-Pearson [89] and pure Bayesian [87] setups.

Although there is a number of works on joint detection and estimation, e.g., [87; 90; 91; 92; 89; 93; 86; 83; 25], this important topic is not sufficiently treated in the literature. The first systematic theory on joint detection and estimation appeared in [87]. This initial work, in a Bayesian framework, derives optimum joint detector and estimator structures for different levels of coupling between the two subproblems. [90] extends the results of [87] on binary hypothesis testing to the multi-hypothesis case. In [91], different from [87; 90], the case with unknown parameters under the null hypothesis is considered. [91] does not present an optimum joint detector and estimator, but shows that, even in the classical separate treatment of the two subproblems, LRT implicitly uses the posterior distributions of unknown parameters, which characterize the Bayesian estimation. [92] deals with joint multi-hypothesis testing and non-Bayesian estimation considering a finite discrete parameter set and the minimax approach. [89] and [93] study Bayesian estimation under different Neyman-Pearson-like formulations, and derive the corresponding optimum joint detection and estimation schemes. [86], in a minimax sense, extends the analysis in [93] to the general case with unknown parameters in both hypotheses. [83] handles the joint multi-hypothesis testing and state estimation problem for linear models with Gaussian noise. It finds the joint posterior distribution of the hypotheses and the system states, which can be used to identify the optimum joint detector and estimator for a specific performance criterion in a unified Bayesian approach.

Most of the today's engineering applications are subject to resource (e.g., time, energy, bandwidth) constraints. For that reason, it is essential to minimize the number of observa-

tions used to perform a task (e.g., detection, estimation) due to the cost of taking a new observation, and also latency constraints. Sequential statistical methods are designed to minimize the average number of observations for a given accuracy level. They are equipped with a stopping rule to achieve optimal stopping, unlike fixed-sample-size methods. Specifically, we cannot stop taking samples too early due to the performance constraints, and do not want to stop too late to save critical resources, such as time and energy. Optimal stopping theory handles this trade-off through sequential methods. For more information on sequential methods we refer to the original work [56] by Wald, and a more recent work [94]. The majority of existing works on joint detection and estimation consider only the fixed-sample-size problem. Although [91] discusses the case where observations are taken sequentially, it lacks a discussion on optimal stopping, limiting the scope of the work to the iterative computation of sufficient statistics. The only work that treats the joint detection and estimation problem in a “real” sequential manner is [25]. It provides the exact optimum triplet of stopping time, detector, and estimator for a linear scalar observation model with Gaussian noise.

In this chapter, following the methodology presented in [25], we develop a general framework for optimum sequential joint detection and estimation in Section 4.2. In particular, we extend [25] in five directions: We consider (i) a general non-linear signal model (ii) for vector observations (iii) with a universal noise model, and also (iv) a general problem formulation with unknown parameters under both hypotheses. Moreover, (v) we extend our analysis to the multi-hypothesis case in the smart grid application. After presenting the general theory, we pave the way for applications by systematically analyzing more specific cases. We then apply the developed theory to two popular concepts, namely cognitive radio and smart grid in Sections 4.3 and 4.4, respectively. Finally, the concluding remarks are given in Section 4.5.

4.2 Optimum Sequential Joint Detection and Estimation

4.2.1 Problem Formulation

Consider a general model

$$\mathbf{y}_t = f(\mathbf{x}, \mathbf{H}_t) + \mathbf{w}_t, \quad t = 1, 2, \dots, \quad (4.1)$$

where $\mathbf{y}_t \in \mathbb{R}^M$ is the measurement vector taken at time t ; $\mathbf{x} \in \mathbb{R}^N$ is the unknown vector of parameters that we want to estimate; \mathbf{H}_t is the observation matrix that relates \mathbf{x} to \mathbf{y}_t ; $f : \mathbb{R}^M \rightarrow \mathbb{R}^M$ is a (possibly nonlinear) function of \mathbf{x} and \mathbf{H}_t ; and $\mathbf{w}_t \in \mathbb{R}^M$ is the noise vector.

In addition to estimation, we would like to detect the true hypothesis (H_0 or H_1) in a binary hypothesis testing setup, in which \mathbf{x} is distributed according to a specific probability distribution under each hypothesis, i.e.,

$$\begin{aligned} H_0 : \mathbf{x} &\sim \pi_0, \\ H_1 : \mathbf{x} &\sim \pi_1. \end{aligned} \quad (4.2)$$

Here, we do not assume specific probability distributions for \mathbf{x} , \mathbf{H}_t , \mathbf{w}_t , or a specific system model f . We only assume π_0 and π_1 are known, and $\{\mathbf{y}_t, \mathbf{H}_t\}$ are observed at each time t . Note that we allow for correlated noise \mathbf{w}_t and correlated \mathbf{H}_t .

Since we want to both detect and estimate, we use a combined cost function

$$\begin{aligned} \mathcal{C}(T, d_T, \hat{\mathbf{x}}_T^0, \hat{\mathbf{x}}_T^1) &= a_0 \mathbf{P}_0(d_T = 1 | \mathcal{H}_T) + a_1 \mathbf{P}_1(d_T = 0 | \mathcal{H}_T) \\ &+ b_{00} \mathbf{E}_0 [J(\hat{\mathbf{x}}_T^0, \mathbf{x}) \mathbb{1}_{\{d_T=0\}} | \mathcal{H}_T] + b_{01} \mathbf{E}_0 [J(\hat{\mathbf{x}}_T^1, \mathbf{x}) \mathbb{1}_{\{d_T=1\}} | \mathcal{H}_T] \\ &+ b_{10} \mathbf{E}_1 [J(\hat{\mathbf{x}}_T^0, \mathbf{x}) \mathbb{1}_{\{d_T=0\}} | \mathcal{H}_T] + b_{11} \mathbf{E}_1 [J(\hat{\mathbf{x}}_T^1, \mathbf{x}) \mathbb{1}_{\{d_T=1\}} | \mathcal{H}_T] \end{aligned} \quad (4.3)$$

where T is the stopping time, d_T is the detection function, $\{\hat{\mathbf{x}}_T^0, \hat{\mathbf{x}}_T^1\}$ are the estimators when we decide on H_0 and H_1 , respectively, $J(\hat{\mathbf{x}}_T, \mathbf{x})$ is a general estimation cost function, e.g., $\|\hat{\mathbf{x}}_T - \mathbf{x}\|^2$, and $\{a_i, b_{ij}\}_{i,j=0,1}$ are some constants. We denote with \mathcal{H}_t and $\{\mathcal{H}_t\}$ the sigma-algebra and filtration generated by the history of the observation matrices $\{\mathbf{H}_1, \dots, \mathbf{H}_t\}$, respectively, and with \mathbf{P}_i and \mathbf{E}_i the probability measure and expectation under H_i . The indicator function $\mathbb{1}_{\{A\}}$ takes the value 1 if the event A is true, or 0 otherwise. In (4.3),

the first two terms are the detection cost, and the remaining ones are the estimation cost. Writing (4.3) in the following alternative form

$$\begin{aligned} \mathcal{C}(T, d_T, \hat{\mathbf{x}}_T^0, \hat{\mathbf{x}}_T^1) &= \mathbb{E}_0 [b_{00}J(\hat{\mathbf{x}}_T^0, \mathbf{x})\mathbb{1}_{\{d_T=0\}} + \{a_0 + b_{01}J(\hat{\mathbf{x}}_T^1, \mathbf{x})\}\mathbb{1}_{\{d_T=1\}}|\mathcal{H}_T] \\ &+ \mathbb{E}_1 [\{a_1 + b_{10}J(\hat{\mathbf{x}}_T^0, \mathbf{x})\}\mathbb{1}_{\{d_T=0\}} + b_{11}J(\hat{\mathbf{x}}_T^1, \mathbf{x})\mathbb{1}_{\{d_T=1\}}|\mathcal{H}_T] \end{aligned} \quad (4.4)$$

it is clear that our cost function corresponds to the Bayes risk given $\{\mathbf{H}_1, \dots, \mathbf{H}_t\}$.

In a sequential setup, in general, the expected stopping time (i.e., the average number of samples) is minimized subject to a constraint on the cost function. In the presence of an ancillary statistic, such as \mathcal{H}_t , conditioning is known to have significant advantages [80; 24], hence the cost function in (4.3) is conditioned on \mathcal{H}_t . Intuitively, there is no need to average the performance measure $\mathcal{C}(T, d_T, \hat{\mathbf{x}}_T^0, \hat{\mathbf{x}}_T^1)$ over \mathcal{H}_t , which is a reliable statistic (i.e., does not include noise). Conditioning on \mathcal{H}_t also facilitates finding an optimum sequential scheme [24], and frees our formulation from assuming statistical descriptions (e.g., probability distribution, independence, stationarity) on the observation matrix \mathbf{H}_t . As a result, our objective is to minimize $\mathbb{E}[T|\mathcal{H}_t]$ subject to a constraint on $\mathcal{C}(T, d_T, \hat{\mathbf{x}}_T^0, \hat{\mathbf{x}}_T^1)$.

Let \mathcal{F}_t and $\{\mathcal{F}_t\}$ denote the sigma-algebra and filtration generated by the complete history of observations $\{(\mathbf{y}_1, \mathbf{H}_1), \dots, (\mathbf{y}_t, \mathbf{H}_t)\}$, respectively, thus $\mathcal{H}_t \subset \mathcal{F}_t$. In the pure detection and pure estimation problems, it is well known that serious analytical complications arise if we consider a general $\{\mathcal{F}_t\}$ -adapted stopping time, that depends on the complete history of observations. Specifically, in the pure estimation problem, finding the optimum sequential estimator that attains the sequential Cramer-Rao lower bound (CRLB) is not a tractable problem if T is adapted to the complete observation history $\{\mathcal{F}_t\}$ [68; 95]. Similarly, in the pure detection problem with an $\{\mathcal{F}_t\}$ -adapted stopping time, we end up with a two-dimensional optimal stopping problem which is impossible to solve (analytically) since the thresholds for the running likelihood ratio depend on the sequence $\{\mathbf{H}_t\}$. Alternatively, in [69; 14; 24; 23; 25], T is restricted to $\{\mathcal{H}_t\}$ -adapted stopping times, which facilitates finding an optimal solution. In this paper, we are interested in $\{\mathcal{H}_t\}$ -adapted stopping times as well. Hence, $\mathbb{E}[T|\mathcal{H}_t] = T$ and we aim to solve the following optimization problem,

$$\min_{T, d_T, \hat{\mathbf{x}}_T^0, \hat{\mathbf{x}}_T^1} T \quad \text{s.t.} \quad \mathcal{C}(T, d_T, \hat{\mathbf{x}}_T^0, \hat{\mathbf{x}}_T^1) \leq \alpha, \quad (4.5)$$

where α is a target accuracy level.

Above, from a theoretical point of view, we explained why we unconventionally minimize T instead of $\mathbf{E}[T]$, which is the usual practice in classical optimal stopping problems. From an operational point of view, we start with the following stopping rule: stop the first time the target accuracy level α is achieved, i.e., the inequality $\mathcal{C}(T, d_T, \hat{\mathbf{x}}_T^0, \hat{\mathbf{x}}_T^1) \leq \alpha$ is satisfied. This operational problem statement gives us the problem formulation in (4.5), which in turn defines an $\{\mathcal{H}_t\}$ -adapted stopping time T . This is because T is solely determined by $\mathcal{C}(T, d_T, \hat{\mathbf{x}}_T^0, \hat{\mathbf{x}}_T^1)$, which, as seen in (4.3), averages over $\{\mathbf{y}_t\}$ and thus is a function of only $\{\mathbf{H}_t\}$. The stopping rule considered here is a natural extension of the one commonly used in sequential estimation problems, e.g., [69; 23], and is optimum for $\{\mathcal{H}_t\}$ -adapted stopping times, as shown in (4.5). Note that the solution sought in (4.5) is optimum for each realization of $\{\mathbf{H}_t\}$, and not on average with respect to this sequence.

4.2.2 Optimum Solution

4.2.2.1 Optimum Estimators

Let us begin our analysis with optimum estimators. Grouping the terms with the same estimator in (4.3), we can write the optimum estimators as

$$\begin{aligned}\hat{\mathbf{x}}_T^0 &= \arg \min_{\hat{\mathbf{x}}_T^0} b_{00} \mathbf{E}_0 [J(\hat{\mathbf{x}}_T^0, \mathbf{x}) \mathbb{1}_{\{d_T=0\}} | \mathcal{H}_T] + b_{10} \mathbf{E}_1 [J(\hat{\mathbf{x}}_T^0, \mathbf{x}) \mathbb{1}_{\{d_T=0\}} | \mathcal{H}_T] \\ \hat{\mathbf{x}}_T^1 &= \arg \min_{\hat{\mathbf{x}}_T^1} b_{01} \mathbf{E}_0 [J(\hat{\mathbf{x}}_T^1, \mathbf{x}) \mathbb{1}_{\{d_T=1\}} | \mathcal{H}_T] + b_{11} \mathbf{E}_1 [J(\hat{\mathbf{x}}_T^1, \mathbf{x}) \mathbb{1}_{\{d_T=1\}} | \mathcal{H}_T].\end{aligned}$$

Since both estimators can be found in the same way, we will only focus on $\hat{\mathbf{x}}_T^0$. Recall that \mathcal{F}_t denotes the sigma-algebra generated by the complete history of observations $\{(\mathbf{y}_1, \mathbf{H}_1), \dots, (\mathbf{y}_t, \mathbf{H}_t)\}$. Then, we can write

$$\begin{aligned}\hat{\mathbf{x}}_T^0 &= \arg \min_{\hat{\mathbf{x}}_T^0} \sum_{t=0}^{\infty} \mathbf{E}_0 \left[(b_{00} + b_{10} \bar{L}_t) J(\hat{\mathbf{x}}_T^0, \mathbf{x}) \mathbb{1}_{\{d_t=0\}} | \mathcal{H}_t \right] \mathbb{1}_{\{T=t\}}, \\ &= \arg \min_{\hat{\mathbf{x}}_T^0} \sum_{t=0}^{\infty} \mathbf{E}_0 \left[(b_{00} \mathbf{E}_0 [J(\hat{\mathbf{x}}_T^0, \mathbf{x}) | \mathcal{F}_t] + b_{10} L_t \mathbf{E}_1 [J(\hat{\mathbf{x}}_T^0, \mathbf{x}) | \mathcal{F}_t]) \mathbb{1}_{\{d_t=0\}} | \mathcal{H}_t \right] \mathbb{1}_{\{T=t\}},\end{aligned}\tag{4.6}$$

where $\bar{L}_t \triangleq \frac{p_1(\{\mathbf{y}_s\}_{s=1}^t, \mathbf{x}|\mathcal{H}_t)}{p_0(\{\mathbf{y}_s\}_{s=1}^t, \mathbf{x}|\mathcal{H}_t)}$ and $L_t \triangleq \frac{p_1(\{\mathbf{y}_s\}_{s=1}^t|\mathcal{H}_t)}{p_0(\{\mathbf{y}_s\}_{s=1}^t|\mathcal{H}_t)}$ are likelihood ratios. To write (4.6) we used the facts that $\bar{L}_t = L_t \frac{p_1(\mathbf{x}|\{\mathbf{y}_s\}_{s=1}^t, \mathcal{H}_t)}{p_0(\mathbf{x}|\{\mathbf{y}_s\}_{s=1}^t, \mathcal{H}_t)} = L_t \frac{p_1(\mathbf{x}|\mathcal{F}_t)}{p_0(\mathbf{x}|\mathcal{F}_t)}$ and d_t is \mathcal{F}_t -measurable (i.e., d_t is deterministic given \mathcal{F}_t).

Define a new probability distribution $p_2 \triangleq \frac{b_{00}p_0 + b_{10}L_t p_1}{b_{00} + b_{10}L_t}$. We are, in fact, searching for an estimator that minimizes $\mathbf{E}_2 [J(\hat{\mathbf{x}}_T^0, \mathbf{x})|\mathcal{F}_t]$, i.e.,

$$\hat{\mathbf{x}}_T^i = \arg \min_{\hat{\mathbf{x}}_T^i} \mathbf{E}_2 [J(\hat{\mathbf{x}}_T^i, \mathbf{x})|\mathcal{F}_t], \quad i = 0, 1. \quad (4.7)$$

Note that for a large class of cost functions [96, pp. 239–241], including the mean square error (MSE) $\mathbf{E}_i [\|\hat{\mathbf{x}}_T^0 - \mathbf{x}\|^2|\mathcal{F}_t]$, the optimum estimator is given by the conditional mean $\mathbf{E}_i[\mathbf{x}|\mathcal{F}_t]$, which we will consider throughout the paper whenever a specification is needed. Hence, for MSE and many other cost functions

$$\hat{\mathbf{x}}_T^0 = \mathbf{E}_2[\mathbf{x}|\mathcal{F}_T] = \frac{b_{00}\mathbf{E}_0[\mathbf{x}|\mathcal{F}_T] + b_{10}L_T\mathbf{E}_1[\mathbf{x}|\mathcal{F}_T]}{b_{00} + b_{10}L_T}. \quad (4.8)$$

Similarly, we can write

$$\hat{\mathbf{x}}_T^1 = \frac{b_{01}\mathbf{E}_0[\mathbf{x}|\mathcal{F}_T] + b_{11}L_T\mathbf{E}_1[\mathbf{x}|\mathcal{F}_T]}{b_{01} + b_{11}L_T}. \quad (4.9)$$

We see that the optimum estimators in (4.8) and (4.9) are weighted averages of the minimum MSE (MMSE) estimators under \mathbf{H}_0 and \mathbf{H}_1 . Note that typically the likelihood ratio L_T is smaller than 1 under \mathbf{H}_0 and larger than 1 under \mathbf{H}_1 , that is, $\hat{\mathbf{x}}_T^i$ is close to $\mathbf{E}_i[\mathbf{x}|\mathcal{F}_T]$.

With the optimum estimators given in (4.7) the cost function in (4.3) becomes

$$\begin{aligned} \mathcal{C}(T, d_T) &= a_0\mathbf{P}_0(d_T = 1|\mathcal{H}_T) + a_1\mathbf{P}_1(d_T = 0|\mathcal{H}_T) \\ &+ b_{00}\mathbf{E}_0 \left[\underbrace{\mathbf{E}_0 [J(\hat{\mathbf{x}}_T^0, \mathbf{x})|\mathcal{F}_T]}_{\Delta_T^{00}} \mathbb{1}_{\{d_T=0\}}|\mathcal{H}_T \right] + b_{01}\mathbf{E}_0 \left[\underbrace{\mathbf{E}_0 [J(\hat{\mathbf{x}}_T^1, \mathbf{x})|\mathcal{F}_T]}_{\Delta_T^{01}} \mathbb{1}_{\{d_T=1\}}|\mathcal{H}_T \right] \\ &+ b_{10}\mathbf{E}_1 \left[\underbrace{\mathbf{E}_1 [J(\hat{\mathbf{x}}_T^0, \mathbf{x})|\mathcal{F}_T]}_{\Delta_T^{10}} \mathbb{1}_{\{d_T=0\}}|\mathcal{H}_T \right] + b_{11}\mathbf{E}_1 \left[\underbrace{\mathbf{E}_1 [J(\hat{\mathbf{x}}_T^1, \mathbf{x})|\mathcal{F}_T]}_{\Delta_T^{11}} \mathbb{1}_{\{d_T=1\}}|\mathcal{H}_T \right], \end{aligned} \quad (4.10)$$

where Δ_t^{ij} is the posterior expected estimation cost when \mathbf{H}_j is decided under \mathbf{H}_i .

Considering the conditional mean as the optimum estimator, from (4.8) and (4.9),

$$\begin{aligned} \Delta_t^{ij} &= \mathbf{E}_i [\|\mathbf{x} - \mathbf{E}_i[\mathbf{x}|\mathcal{F}_t]\|^2|\mathcal{F}_t] + \mathbf{E}_i [\|\mathbf{E}_i[\mathbf{x}|\mathcal{F}_t] - \hat{\mathbf{x}}_t^j\|^2|\mathcal{F}_t] \\ &= \text{Tr}(\text{Cov}_i[\mathbf{x}|\mathcal{F}_t]) + \delta_{ij}\|\mathbf{E}_0[\mathbf{x}|\mathcal{F}_t] - \mathbf{E}_1[\mathbf{x}|\mathcal{F}_t]\|^2, \end{aligned} \quad (4.11)$$

where $\text{Tr}(\cdot)$ is the trace of a matrix, $\delta_{0j} = \left(\frac{b_{1j}L_t}{b_{0j}+b_{1j}L_t}\right)^2$ and $\delta_{1j} = \left(\frac{b_{0j}}{b_{0j}+b_{1j}L_t}\right)^2$. In other words, Δ_t^{ij} is the MMSE under H_i plus the distance between our estimator $\hat{\mathbf{x}}_t^j$ and the optimum estimator under H_i . The latter is the penalty we pay for not knowing the true hypothesis.

Note that for $b_{00} = b_{10}$ and $b_{01} = b_{11}$ (e.g., the case $b_{ij} = b \forall i, j$, where we do not differentiate between estimation errors), the optimum estimators in (4.8) and (4.9) coincide, and as a result $\delta_{00} = \delta_{01} = \frac{L_t}{1+L_t}$ and $\delta_{10} = \delta_{11} = \frac{1}{1+L_t}$ in (4.11). In other words, we use the estimator $\hat{\mathbf{x}}_T = \frac{\mathbb{E}_0[\mathbf{x}|\mathcal{F}_T] + L_T \mathbb{E}_1[\mathbf{x}|\mathcal{F}_T]}{1+L_T}$ regardless of the detection decision.

4.2.2.2 Optimum Detector

We now search for the optimum decision function d_T that minimizes (4.10). Combining all the terms under \mathbb{E}_0 we write

$$d_T = \arg \min_{d_T} \sum_{t=0}^{\infty} \mathbb{E}_0 [a_0 \mathbb{1}_{\{d_t=1\}} + a_1 L_t \mathbb{1}_{\{d_t=0\}} + b_{00} \Delta_t^{00} \mathbb{1}_{\{d_t=0\}} + b_{01} \Delta_t^{01} \mathbb{1}_{\{d_t=1\}} + b_{10} L_t \Delta_t^{10} \mathbb{1}_{\{d_t=0\}} + b_{11} L_t \Delta_t^{11} \mathbb{1}_{\{d_t=1\}} | \mathcal{H}_t] \mathbb{1}_{\{T=t\}}, \quad (4.12)$$

where $L_t = \frac{p_1(\{\mathbf{y}_s\}_{s=1}^t | \mathcal{H}_t)}{p_0(\{\mathbf{y}_s\}_{s=1}^t | \mathcal{H}_t)}$. Since $\mathbb{1}_{\{d_t=0\}} = 1 - \mathbb{1}_{\{d_t=1\}}$,

$$d_T = \arg \min_{d_T} \sum_{t=0}^{\infty} \mathbb{E}_0 [\{a_0 + b_{01} \Delta_t^{01} - b_{00} \Delta_t^{00} - (a_1 + b_{10} \Delta_t^{10} - b_{11} \Delta_t^{11}) L_t\} \mathbb{1}_{\{d_t=1\}} | \mathcal{H}_t] \mathbb{1}_{\{T=t\}} + a_1 + b_{00} \mathbb{E}_0[\Delta_T^{00} | \mathcal{H}_T] + b_{10} \mathbb{E}_1[\Delta_T^{10} | \mathcal{H}_T]. \quad (4.13)$$

Note that $a_1 + b_{00} \mathbb{E}_0[\Delta_T^{00} | \mathcal{H}_T] + b_{10} \mathbb{E}_1[\Delta_T^{10} | \mathcal{H}_T]$ does not depend on d_T , and the term inside the expectation is minimized by

$$d_t = \begin{cases} 1 & \text{if } L_t (a_1 + b_{10} \Delta_t^{10} - b_{11} \Delta_t^{11}) \geq a_0 + b_{01} \Delta_t^{01} - b_{00} \Delta_t^{00} \\ 0 & \text{otherwise.} \end{cases} \quad (4.14)$$

The optimum decision function d_t is coupled with the estimators $\hat{\mathbf{x}}_t^0, \hat{\mathbf{x}}_t^1$ through the posterior estimation costs $\{\Delta_t^{ij}\}$ due to our joint formulation [cf. (4.3)]. Specifically, while making a decision, it takes into account all possible estimation costs that may result from the true hypothesis and its decision. In the detection-only problem with $b_{ij} = 0, \forall i, j$, the coupling disappears, and d_t boils down to the well-known likelihood ratio test.

4.2.2.3 Complete Solution

We can now identify the optimum stopping time T , and as a result the complete solution $(T, d_T, \hat{\mathbf{x}}_T^0, \hat{\mathbf{x}}_T^1)$ to the optimization problem in (4.5).

Theorem 6. *The optimum sequential joint detector and estimator $(T, d_T, \hat{\mathbf{x}}_T^0, \hat{\mathbf{x}}_T^1)$ that solves the problem in (4.5) is given by*

$$T = \min\{t \in \mathbb{N} : C_t \leq \alpha\} \quad (4.15)$$

$$d_T = \begin{cases} 1 & \text{if } L_T (a_1 + b_{10}\Delta_T^{10} - b_{11}\Delta_T^{11}) \geq a_0 + b_{01}\Delta_T^{01} - b_{00}\Delta_T^{00} \\ 0 & \text{otherwise.} \end{cases} \quad (4.16)$$

$$\hat{\mathbf{x}}_T^i = \arg \min_{\hat{\mathbf{x}}_T^i} \mathbf{E}_{2i} [J(\hat{\mathbf{x}}_T^i, \mathbf{x}) | \mathcal{F}_T], \quad i = 0, 1, \quad (4.17)$$

$$\left(\text{e.g., } \hat{\mathbf{x}}_T^i = \frac{b_{0i}\mathbf{E}_0[\mathbf{x} | \mathcal{F}_T] + b_{1i}L_T\mathbf{E}_1[\mathbf{x} | \mathcal{F}_T]}{b_{0i} + b_{1i}L_T} \text{ for } J(\hat{\mathbf{x}}_T^i, \mathbf{x}) = \|\hat{\mathbf{x}}_T^i - \mathbf{x}\|^2, \text{ etc.} \right)$$

where

$$C_t \triangleq \mathbf{E}_0 \left[\{a_0 + b_{01}\Delta_t^{01} - b_{00}\Delta_t^{00} - (a_1 + b_{10}\Delta_t^{10} - b_{11}\Delta_t^{11}) L_t\}^- + a_1 L_t + b_{00}\Delta_t^{00} + b_{10}L_t\Delta_t^{10} | \mathcal{H}_t \right] \quad (4.18)$$

is the optimal cost at time t , \mathbf{E}_{2i} is the expectation with respect to the probability measure $p_{2i} = \frac{b_{0i}p_0 + b_{1i}L_t p_1}{b_{0i} + b_{1i}L_t}$ and $A^- = \min(A, 0)$.

Proof. In (4.7)–(4.9), we showed that $\hat{\mathbf{x}}_T^0$ and $\hat{\mathbf{x}}_T^1$ minimize the cost function in (4.3) for any stopping time T and decision function d_T , i.e., $\mathcal{C}(T, d_T, \hat{\mathbf{x}}_T^0, \hat{\mathbf{x}}_T^1) \leq \mathcal{C}(T, d_T, \hat{\mathbf{x}}_T^0, \hat{\mathbf{x}}_T^1)$. Later in (4.14), we showed that $\mathcal{C}(T, d_T, \hat{\mathbf{x}}_T^0, \hat{\mathbf{x}}_T^1) \leq \mathcal{C}(T, d_T, \hat{\mathbf{x}}_T^0, \hat{\mathbf{x}}_T^1)$. Hence, from (4.5), the optimum stopping time is the first time $C_t \triangleq \mathcal{C}(t, d_t, \hat{\mathbf{x}}_t^0, \hat{\mathbf{x}}_t^1)$ achieves the target accuracy level α , as shown in (4.15). From (4.13) and (4.14), we write the optimal cost C_t as in (4.18). \square

According to Theorem 6, the optimum scheme, at each time t , computes C_t [cf. (4.18)], and then compares it to α . When $C_t \leq \alpha$, it stops and makes a decision using (4.16). Finally, it estimates \mathbf{x} using (4.17). Considering the conditional mean as the optimum estimator a pseudo-code for this scheme is given in Algorithm 8.

Since the results in Theorem 6 are universal in the sense that they hold for all probability distributions and system models, in Algorithm 8 we provide a general procedure that

Algorithm 8 The procedure for the optimum scheme in Theorem 6

```

1: Initialization:  $t \leftarrow 0, \mathcal{C} \leftarrow \infty$ 
2: while  $\mathcal{C} > \alpha$  do
3:    $t \leftarrow t + 1$ 
4:    $L = \frac{p_1(\{\mathbf{y}_s\}_{s=1}^t | \mathcal{H}_t)}{p_0(\{\mathbf{y}_s\}_{s=1}^t | \mathcal{H}_t)}$ 
5:    $\mathbf{e}_i = \mathbf{E}_i[\mathbf{x} | \mathcal{F}_t], i = 0, 1$ 
6:    $\text{MMSE}_i = \text{Tr}(\text{Cov}_i[\mathbf{x} | \mathcal{F}_t]), i = 0, 1$ 
7:    $\Delta^{0j} = \text{MMSE}_0 + \left(\frac{b_{1j}L}{b_{0j} + b_{1j}L}\right)^2 \|\mathbf{e}_0 - \mathbf{e}_1\|^2, j = 0, 1$ 
8:    $\Delta^{1j} = \text{MMSE}_1 + \left(\frac{b_{0j}}{b_{0j} + b_{1j}L}\right)^2 \|\mathbf{e}_0 - \mathbf{e}_1\|^2, j = 0, 1$ 
9:   Cost:  $\mathcal{C}$  as in (4.18)
10: end while
11: Stop:  $\mathsf{T} = t$ 
12: if  $L(a_1 + b_{10}\Delta^{10} - b_{11}\Delta^{11}) \geq a_0 + b_{01}\Delta^{01} - b_{00}\Delta^{00}$  then
13:   Decide:  $\mathbf{d} = 1$ 
14:   Estimate:  $\hat{\mathbf{x}} = \frac{b_{01}\mathbf{e}_0 + b_{11}L\mathbf{e}_1}{b_{01} + b_{11}L}$ 
15: else
16:   Decide:  $\mathbf{d} = 0$ 
17:   Estimate:  $\hat{\mathbf{x}} = \frac{b_{00}\mathbf{e}_0 + b_{10}L\mathbf{e}_1}{b_{00} + b_{10}L}$ 
18: end if

```

requires computation of some statistics (cf. lines 4,5,6,9). In specific cases, such statistics may be easily computed. However, in many cases they cannot be written in closed forms, hence intense computation is required to estimate them (e.g., a multi-dimensional integral). The fact that such computation is performed online (i.e., as new observations arrive at each time t) is the bottleneck of the generic algorithm given in Algorithm 8.

4.2.3 Separated Detection and Estimation Costs

In the combined cost function, given by (4.3), if we penalize the wrong decisions only with the detection costs, i.e., $b_{01} = b_{10} = 0$, we get the following simplified alternative cost function

$$\begin{aligned} \mathcal{E}(T, d_T, \hat{\mathbf{x}}_T^0, \hat{\mathbf{x}}_T^1) &= a_0 \mathbf{P}_0(d_T = 1 | \mathcal{H}_T) + a_1 \mathbf{P}_1(d_T = 0 | \mathcal{H}_T) \\ &\quad + b_{00} \mathbf{E}_0 [J(\hat{\mathbf{x}}_T^0, \mathbf{x}) \mathbb{1}_{\{d_T=0\}} | \mathcal{H}_T] + b_{11} \mathbf{E}_1 [J(\hat{\mathbf{x}}_T^1, \mathbf{x}) \mathbb{1}_{\{d_T=1\}} | \mathcal{H}_T]. \end{aligned} \quad (4.19)$$

In this alternative form, detection and estimation costs are used to penalize separate cases. Specifically, under H_i , the wrong decision case is penalized with the constant detection

cost a_i , and the correct decision case is penalized with the estimation cost $\mathbb{E}_i[J(\hat{\mathbf{x}}_T^i, \mathbf{x})|\mathcal{H}_t]$. Since a_i is the only cost to penalize the wrong decision case, it is typically assigned a larger number here than in (4.3).

Substituting $b_{01} = b_{10} = 0$ in (4.7)–(4.9) yields the following optimum estimators

$$\hat{\mathbf{x}}_T^i = \arg \min_{\hat{\mathbf{x}}_T^i} \mathbb{E}_i [J(\hat{\mathbf{x}}_T^i, \mathbf{x})|\mathcal{F}_T], \quad i = 0, 1, \quad (4.20)$$

$$\left(\text{e.g., } \hat{\mathbf{x}}_T^i = \mathbb{E}_i[\mathbf{x}|\mathcal{F}_T] \text{ for } J(\hat{\mathbf{x}}_T^i, \mathbf{x}) = \|\hat{\mathbf{x}}_T^i - \mathbf{x}\|^2 \right), \quad (4.21)$$

which we use when \mathbf{H}_i is decided. According to (4.21), when we decide on \mathbf{H}_i , we use the MMSE estimator under \mathbf{H}_i , as opposed to (4.8) and (4.9), which are mixtures of the MMSE estimators under both hypotheses. Consequently, from (4.11), the posterior estimation cost

$$\Delta_t^{ii} = \text{Tr}(\text{Cov}_i[\mathbf{x}|\mathcal{F}_t]) = \text{MMSE}_t^i. \quad (4.22)$$

Moreover, with $b_{01} = b_{10} = 0$, the optimum decision function in (4.14) becomes

$$\mathbf{d}_t = \begin{cases} 1 & \text{if } L_t(a_1 - b_{11}\Delta_t^{11}) \geq a_0 - b_{00}\Delta_t^{00} \\ 0 & \text{otherwise.} \end{cases} \quad (4.23)$$

The above decision function is biased towards the hypothesis with better estimation performance. Specifically, when the MMSE under \mathbf{H}_1 is smaller than that under \mathbf{H}_0 (i.e., $\Delta_t^{11} < \Delta_t^{00}$), it is easier to satisfy the inequality $L_t(a_1 - b_{11}\Delta_t^{11}) \geq a_0 - b_{00}\Delta_t^{00}$, and thus to decide in favor of \mathbf{H}_1 . Conversely, \mathbf{H}_0 is favored when $\Delta_t^{00} < \Delta_t^{11}$. Since the detector in (4.23) uses the maximum likelihood (ML) criterion, as in the likelihood ratio test, together with the MMSE criterion, we can call it ML & MMSE detector. On the other hand, the detector in (4.14) similarly favors the hypothesis that can decrease the general estimation cost [cf. (4.3)] more.

Finally, the optimum stopping time in this special case is still given by (4.15), where

$$\begin{aligned} \mathcal{C}_t &= \mathbb{E}_0 \left[(a_1 L_t + b_{00} \Delta_t^{00}) \mathbb{1}_{\{\mathbf{d}_t=0\}} + (a_0 + b_{11} L_t \Delta_t^{11}) \mathbb{1}_{\{\mathbf{d}_t=1\}} | \mathcal{H}_t \right] \\ &= \mathbb{E}_0 \left[\{a_0 - b_{00} \Delta_t^{00} - (a_1 - b_{11} \Delta_t^{11}) L_t\}^- + a_1 L_t + b_{00} \Delta_t^{00} | \mathcal{H}_t \right], \end{aligned} \quad (4.24)$$

with $\Delta_t^{ii} = \text{MMSE}_t^i$ for the conditional mean optimum estimator.

4.2.4 Linear Quadratic Gaussian (LQG) Model

We next consider, as a special case, the quadratic estimation cost $J(\hat{\mathbf{x}}_T^i, \mathbf{x}) = \|\hat{\mathbf{x}}_T^i - \mathbf{x}\|^2$, and the linear system model

$$\mathbf{y}_t = \mathbf{H}_t \mathbf{x} + \mathbf{w}_t, \quad (4.25)$$

where \mathbf{w}_t is the white Gaussian noise with covariance $\sigma^2 \mathbf{I}$, and \mathbf{x} is Gaussian under both hypotheses, i.e.,

$$\begin{aligned} \mathbf{H}_0 : \mathbf{x} &\sim \mathcal{N}(\boldsymbol{\mu}_0, \boldsymbol{\Sigma}_0), \\ \mathbf{H}_1 : \mathbf{x} &\sim \mathcal{N}(\boldsymbol{\mu}_1, \boldsymbol{\Sigma}_1). \end{aligned} \quad (4.26)$$

In this case, we compute

$$\begin{aligned} p_i(\{\mathbf{y}_s\}_{s=1}^t | \mathcal{H}_t) &= \int_{\mathbb{R}^N} p_i(\{\mathbf{y}_s\}_{s=1}^t, \mathbf{x} | \mathcal{H}_t) \, d\mathbf{x} \\ &= \int_{\mathbb{R}^N} \underbrace{\frac{\exp\left(-\frac{1}{2\sigma^2} \sum_{s=1}^t \|\mathbf{y}_s - \mathbf{H}_s \mathbf{x}\|^2\right)}{(2\pi)^{mt/2} \sigma^{mt}}}_{p_i(\{\mathbf{y}_s\}_{s=1}^t | \mathcal{H}_t, \mathbf{x})} \underbrace{\frac{\exp\left(-\frac{1}{2} \|\mathbf{x} - \boldsymbol{\mu}_i\|_{\boldsymbol{\Sigma}_i^{-1}}^2\right)}{(2\pi)^{n/2} |\boldsymbol{\Sigma}_i|^{1/2}}}_{\pi_i} \, d\mathbf{x} \\ &= \frac{\exp\left[-\frac{1}{2} \left(\sum_{s=1}^t \frac{\|\mathbf{y}_s\|^2}{\sigma^2} + \|\boldsymbol{\mu}_i\|_{\boldsymbol{\Sigma}_i^{-1}}^2 - \left\| \frac{\mathbf{v}_t}{\sigma^2} + \boldsymbol{\Sigma}_i^{-1} \boldsymbol{\mu}_i \right\|_{\left(\frac{\mathbf{U}_t}{\sigma^2} + \boldsymbol{\Sigma}_i^{-1}\right)^{-1}}^2 \right)\right]}{(2\pi)^{mt/2} \sigma^{mt} |\boldsymbol{\Sigma}_i|^{1/2} \left| \frac{\mathbf{U}_t}{\sigma^2} + \boldsymbol{\Sigma}_i^{-1} \right|^{1/2}} \\ &\quad \underbrace{\int_{\mathbb{R}^N} \frac{\exp\left(-\frac{1}{2} \left\| \mathbf{x} - \left(\frac{\mathbf{U}_t}{\sigma^2} + \boldsymbol{\Sigma}_i^{-1}\right)^{-1} \left(\frac{\mathbf{v}_t}{\sigma^2} + \boldsymbol{\Sigma}_i^{-1} \boldsymbol{\mu}_i\right) \right\|_{\frac{\mathbf{U}_t}{\sigma^2} + \boldsymbol{\Sigma}_i^{-1}}^2\right)}{(2\pi)^{n/2} \left| \left(\frac{\mathbf{U}_t}{\sigma^2} + \boldsymbol{\Sigma}_i^{-1}\right)^{-1} \right|^{1/2}} \, d\mathbf{x}}_{=1} \quad (4.27) \end{aligned}$$

where $\mathbf{U}_t \triangleq \sum_{s=1}^t \mathbf{H}'_s \mathbf{H}_s$, $\mathbf{v}_t \triangleq \sum_{s=1}^t \mathbf{H}'_s \mathbf{y}_s$, and $\|\mathbf{x}\|_{\boldsymbol{\Sigma}}^2 = \mathbf{x}' \boldsymbol{\Sigma} \mathbf{x}$. As a result, the likelihood ratio $L_t = \frac{p_1(\{\mathbf{y}_s\}_{s=1}^t | \mathcal{H}_1)}{p_0(\{\mathbf{y}_s\}_{s=1}^t | \mathcal{H}_0)}$ is given by

$$\begin{aligned} L_t &= \sqrt{\frac{|\boldsymbol{\Sigma}_0| \left| \frac{\mathbf{U}_t}{\sigma^2} + \boldsymbol{\Sigma}_0^{-1} \right|}{|\boldsymbol{\Sigma}_1| \left| \frac{\mathbf{U}_t}{\sigma^2} + \boldsymbol{\Sigma}_1^{-1} \right|}} \exp \left[\frac{1}{2} \left(\left\| \frac{\mathbf{v}_t}{\sigma^2} + \boldsymbol{\Sigma}_1^{-1} \boldsymbol{\mu}_1 \right\|_{\left(\frac{\mathbf{U}_t}{\sigma^2} + \boldsymbol{\Sigma}_1^{-1}\right)^{-1}}^2 - \left\| \frac{\mathbf{v}_t}{\sigma^2} + \boldsymbol{\Sigma}_0^{-1} \boldsymbol{\mu}_0 \right\|_{\left(\frac{\mathbf{U}_t}{\sigma^2} + \boldsymbol{\Sigma}_0^{-1}\right)^{-1}}^2 \right. \right. \\ &\quad \left. \left. + \|\boldsymbol{\mu}_0\|_{\boldsymbol{\Sigma}_0^{-1}}^2 - \|\boldsymbol{\mu}_1\|_{\boldsymbol{\Sigma}_1^{-1}}^2 \right) \right]. \quad (4.28) \end{aligned}$$

From (4.27), it is seen that the posterior distribution $p_i(\mathbf{x}|\mathcal{F}_t) = \frac{p_i(\{\mathbf{y}_s\}_{s=1}^t, \mathbf{x}|\mathcal{H}_t)}{p_i(\{\mathbf{y}_s\}_{s=1}^t|\mathcal{H}_t)}$ is

$$\mathcal{N}\left(\underbrace{\left(\frac{\mathbf{U}_t}{\sigma^2} + \boldsymbol{\Sigma}_i^{-1}\right)^{-1} \left(\frac{\mathbf{v}_t}{\sigma^2} + \boldsymbol{\Sigma}_i^{-1} \boldsymbol{\mu}_i\right)}_{\mathbf{E}_i[\mathbf{x}|\mathcal{F}_t]}, \underbrace{\left(\frac{\mathbf{U}_t}{\sigma^2} + \boldsymbol{\Sigma}_i^{-1}\right)^{-1}}_{\mathbf{Cov}_i[\mathbf{x}|\mathcal{F}_t]}\right). \quad (4.29)$$

The closed form expressions for the necessary and sufficient statistics in Algorithm 8, namely L_t , $\mathbf{E}_i[\mathbf{x}|\mathcal{F}_t]$ and $\mathbf{Cov}_i[\mathbf{x}|\mathcal{F}_t]$, are given in (4.28) and (4.29). Note that these statistics, and thus the posterior estimation cost Δ_t^{ij} [cf. (4.11)] are functions of \mathbf{U}_t and \mathbf{v}_t only. Hence, in (4.18), given \mathbf{U}_t the expectation is taken over $\mathbf{v}_t = \mathbf{U}_t \mathbf{x} + \sum_{s=1}^t \mathbf{H}'_s \mathbf{w}_s$, which is distributed as $\mathcal{N}(\mathbf{U}_t \boldsymbol{\mu}_i, \mathbf{U}_t \boldsymbol{\Sigma}_i \mathbf{U}_t + \sigma^2 \mathbf{U}_t)$ under \mathbf{H}_i . As a result, \mathcal{C}_t and the optimum stopping time T [cf. (4.15)] are functions of \mathbf{U}_t only, which is in fact the Fisher information matrix. At each time t , for the corresponding \mathbf{U}_t , we can easily estimate the optimal cost \mathcal{C}_t [cf. (4.18)] through Monte Carlo simulations. Specifically, given \mathbf{U}_t we generate realizations of \mathbf{v}_t , compute the expression inside the expectation in (4.18), and average them.

The above scheme performs online simulations to estimate \mathcal{C}_t for the specific \mathbf{U}_t value at time t . Alternatively, for a large number of \mathbf{U} values, $\mathcal{C}(\mathbf{U})$ can be computed offline to obtain a stopping rule based on \mathbf{U} , reducing the online computation considerably. In particular, a hyper-surface $\mathcal{Q} = \{\mathbf{U} : \mathcal{C}(\mathbf{U}) = \alpha\}$ that separates the continuation region $\mathcal{R} = \{\mathbf{U} : \mathcal{C}(\mathbf{U}) > \alpha\}$ and stopping region $\mathcal{S} = \{\mathbf{U} : \mathcal{C}(\mathbf{U}) < \alpha\}$ in an $\frac{N^2+N}{2}$ -dimensional space determines the optimal stopping rule. Although $\mathbf{U}_t = \sum_{s=1}^t \mathbf{H}'_s \mathbf{H}_s$ has N^2 entries, it is in fact $\frac{N^2+N}{2}$ -dimensional due to symmetry. Such a hyper-surface can be found through offline Monte Carlo simulations. This alternative method significantly reduces the amount of online computations since at each time t we only need to check whether \mathbf{U}_t is in the continuation or stopping region. On the other hand, to decrease the amount of online computations it performs exhaustive offline computations. Hence, it should be preferred in the cases where offline resources are cheap. The procedure for the alternative optimum scheme is summarized in Algorithm 9.

4.2.5 Independent LQG Model

Here, we further assume in (4.25) that the entries of \mathbf{x} are independent (i.e., $\boldsymbol{\Sigma}_0$ and $\boldsymbol{\Sigma}_1$ are diagonal), and \mathbf{H}_t is diagonal. Note that in this case $M = N$, and the entries of \mathbf{y}_t are

Algorithm 9 The procedure for the optimum scheme with offline computation

- 1: Initialization: $t \leftarrow 0, \mathbf{U} \leftarrow 0, \mathbf{v} \leftarrow 0$
 - 2: Compute the continuation region \mathcal{R}
 - 3: **while** $\mathbf{U} \in \mathcal{R}$ **do**
 - 4: $t \leftarrow t + 1$
 - 5: $\mathbf{U} \leftarrow \mathbf{U} + \mathbf{H}'_t \mathbf{H}_t; \mathbf{v} \leftarrow \mathbf{v} + \mathbf{H}'_t \mathbf{y}_t$
 - 6: **end while**
 - 7: Stop: $\mathbb{T} = t$
 - 8: $\mathbf{A}_i = \frac{\mathbf{U}}{\sigma^2} + \boldsymbol{\Sigma}_i^{-1}; \mathbf{b}_i = \frac{\mathbf{v}}{\sigma^2} + \boldsymbol{\Sigma}_i^{-1} \boldsymbol{\mu}_i, i = 0, 1$
 - 9: $L = \sqrt{\frac{|\boldsymbol{\Sigma}_0| |\mathbf{A}_0|}{|\boldsymbol{\Sigma}_1| |\mathbf{A}_1|}} \exp \left[\frac{1}{2} (\mathbf{b}'_1 \mathbf{A}_1 \mathbf{b}_1 - \mathbf{b}'_0 \mathbf{A}_0 \mathbf{b}_0 + \boldsymbol{\mu}'_0 \boldsymbol{\Sigma}_0^{-1} \boldsymbol{\mu}_0 - \boldsymbol{\mu}'_1 \boldsymbol{\Sigma}_1^{-1} \boldsymbol{\mu}_1) \right]$
 - 10: $\mathbf{e}_i = \mathbf{A}_i^{-1} \mathbf{b}_i$
 - 11: $\text{MMSE}_i = \text{Tr}(\mathbf{A}_i^{-1})$
 - 12: $\Delta^{0j} = \text{MMSE}_0 + \left(\frac{b_{1j} L}{b_{0j} + b_{1j} L} \right)^2 \|\mathbf{e}_0 - \mathbf{e}_1\|^2, j = 0, 1$
 - 13: $\Delta^{1j} = \text{MMSE}_1 + \left(\frac{b_{0j}}{b_{0j} + b_{1j} L} \right)^2 \|\mathbf{e}_0 - \mathbf{e}_1\|^2$
 - 14: **if** $L (a_1 + b_{10} \Delta^{10} - b_{11} \Delta^{11}) \geq a_0 + b_{01} \Delta^{01} - b_{00} \Delta^{00}$ **then**
 - 15: Decide: $\mathbf{d} = 1$
 - 16: Estimate: $\hat{\mathbf{x}} = \frac{b_{01} \mathbf{e}_0 + b_{11} L \mathbf{e}_1}{b_{01} + b_{11} L}$
 - 17: **else**
 - 18: Decide: $\mathbf{d} = 0$
 - 19: Estimate: $\hat{\mathbf{x}} = \frac{b_{00} \mathbf{e}_0 + b_{10} L \mathbf{e}_1}{b_{00} + b_{10} L}$
 - 20: **end if**
-

independent. This may be the case in a distributed system (e.g., wireless sensor network) in which each node (e.g., sensor) takes noisy measurements of a local parameter, and there is a global event whose occurrence changes the probability distributions of local parameters. In such a setup, nodes collaborate through a fusion center to jointly detect the global event and estimate the local parameters. To find the optimal scheme we assume that all the observations collected at nodes are available to the fusion center.

Due to spatial independence we have $p_i(\{\mathbf{y}_s\}_{s=1}^t | \mathcal{H}_t) = \prod_{n=1}^N p_i(\{y_{s,n}\}_{s=1}^t | \mathcal{H}_t^n)$, where

$p_i(\{y_{s,n}\}_{s=1}^t | \mathcal{H}_t^n)$ is given by the scalar version of (4.27), i.e.,

$$p_i(\{y_{s,n}\}_{s=1}^t | \mathcal{H}_t^n) = \frac{\exp \left[-\frac{1}{2} \left(\sum_{s=1}^t \frac{y_{s,n}^2}{\sigma^2} + \frac{\mu_{i,n}^2}{\rho_{i,n}^2} - \frac{\left(\frac{v_{t,n}}{\sigma^2} + \frac{\mu_{i,n}}{\rho_{i,n}^2} \right)^2}{\frac{u_{t,n}}{\sigma^2} + \frac{1}{\rho_{i,n}^2}} \right) \right]}{(2\pi)^{t/2} \sigma^t \rho_{i,n} \sqrt{\frac{u_{t,n}}{\sigma^2} + \frac{1}{\rho_{i,n}^2}}} \underbrace{\int_{\mathbb{R}} \frac{\exp \left[-\frac{\left(x_n - \frac{\frac{v_{t,n}}{\sigma^2} + \frac{\mu_{i,n}}{\rho_{i,n}^2}}{\frac{u_{t,n}}{\sigma^2} + \frac{1}{\rho_{i,n}^2}} \right)^2}{\frac{u_{t,n}}{\sigma^2} + \frac{1}{\rho_{i,n}^2}} \right]}{\sqrt{\frac{2\pi}{\frac{u_{t,n}}{\sigma^2} + \frac{1}{\rho_{i,n}^2}}}} dx}_{=1}, \quad (4.30)$$

where the subscript n denotes the n -th entry of the corresponding vector, $\rho_{i,n}^2$ is the n -th diagonal entry of Σ_i , $u_{t,n} = \sum_{s=1}^t h_{s,n}^2$ and $v_{t,n} = \sum_{s=1}^t h_{s,n} y_{s,n}$. As a result, the posterior distribution $p_i(x_n | \mathcal{F}_t^n) = \frac{p_i(\{y_{s,n}\}_{s=1}^t, x_n | \mathcal{H}_t^n)}{p_i(\{y_{s,n}\}_{s=1}^t | \mathcal{H}_t^n)}$ of each local parameter x_n is

$$\mathcal{N} \left(\frac{\frac{v_{t,n}}{\sigma^2} + \frac{\mu_{i,n}}{\rho_{i,n}^2}}{\frac{u_{t,n}}{\sigma^2} + \frac{1}{\rho_{i,n}^2}}, \frac{1}{\frac{u_{t,n}}{\sigma^2} + \frac{1}{\rho_{i,n}^2}} \right), \quad (4.31)$$

and thus the MMSE estimator and MMSE under H_i are

$$\mathbb{E}_i[x_n | \mathcal{F}_t^n] = \frac{\frac{v_{t,n}}{\sigma^2} + \frac{\mu_{i,n}}{\rho_{i,n}^2}}{\frac{u_{t,n}}{\sigma^2} + \frac{1}{\rho_{i,n}^2}} \quad \text{and} \quad \text{MMSE}_{t,n}^i = \frac{1}{\frac{u_{t,n}}{\sigma^2} + \frac{1}{\rho_{i,n}^2}},$$

respectively. Note that $\text{MMSE}_t^i = \sum_{n=1}^N \text{MMSE}_{t,n}^i$. The global likelihood ratio is given by the product of the local ones, i.e., $L_t = \prod_{n=1}^N L_t^n$, where from (4.30) $L_t^n = \frac{p_1(\{y_{s,n}\}_{s=1}^t | \mathcal{H}_t^n)}{p_0(\{y_{s,n}\}_{s=1}^t | \mathcal{H}_t^n)}$ is written as

$$L_t^n = \frac{\rho_{0,n}}{\rho_{1,n}} \sqrt{\frac{\frac{u_{t,n}}{\sigma^2} + \frac{1}{\rho_{0,n}^2}}{\frac{u_{t,n}}{\sigma^2} + \frac{1}{\rho_{1,n}^2}}} \exp \left[\frac{1}{2} \left(\frac{\left(\frac{v_{t,n}}{\sigma^2} + \frac{\mu_{1,n}}{\rho_{1,n}^2} \right)^2}{\frac{u_{t,n}}{\sigma^2} + \frac{1}{\rho_{1,n}^2}} - \frac{\left(\frac{v_{t,n}}{\sigma^2} + \frac{\mu_{0,n}}{\rho_{0,n}^2} \right)^2}{\frac{u_{t,n}}{\sigma^2} + \frac{1}{\rho_{0,n}^2}} + \frac{\mu_{0,n}^2}{\rho_{0,n}^2} - \frac{\mu_{1,n}^2}{\rho_{1,n}^2} \right) \right]. \quad (4.32)$$

In this case, the optimal cost \mathcal{C}_t and thus the optimum stopping time \mathbb{T} (cf. Theorem 6) are functions of the local entities $\{u_{t,n}\}_{n=1}^N$ only since L_t , $\{\mathbb{E}_i[x_n | \mathcal{F}_t^n]\}$, MMSE_i , and accordingly Δ_t^{ij} are functions of $\{u_{t,n}, v_{t,n}\}_{n=1}^N$ only. Hence, here the continuation and stopping regions that determine the optimal stopping rule can be found through offline simulations in an N -dimensional space, which is much smaller than the $\frac{N^2+N}{2}$ -dimensional

space under the general LQG model. Consequently, the scheme that finds the optimal stopping rule through offline simulations is more viable here. In simulations, we generate the realizations of each entry $v_{t,n}$ of \mathbf{v}_t independently and according to $\mathcal{N}(\mu_{i,n}u_{t,n}, \rho_{i,n}^2u_{t,n}^2 + \sigma^2u_{t,n})$.

4.3 Dynamic Spectrum Access in Cognitive Radio Networks

4.3.1 Background

Dynamic spectrum access is a fundamental problem in cognitive radio, in which secondary users (SUs) are allowed to utilize a wireless spectrum band (i.e., communication channel) that is licensed to primary users (PUs) without affecting the PU quality of service (QoS) [79]. Spectrum sensing plays a key role in maximizing the SU throughput, and at the same time protecting the PU QoS. In spectrum sensing, if no PU communication is detected, then SU can opportunistically utilize the band [97; 98]. Otherwise, it has to meet some strict interference constraints. Nevertheless, it can still use the band in an underlay fashion with a transmit power that does not violate the maximum allowable interference level [99; 100]. Methods for combining the underlay and opportunistic access approaches have also been proposed, e.g., [101; 102; 26]. In such combined methods, the SU senses the spectrum band, as in opportunistic access, and controls its transmit power using the sensing result, which allows SU to coexist with PU, as in underlay.

The interference at the PU receiver is a result of the SU transmit power, and also the power gain of the channel between the SU transmitter and PU receiver. Hence, SU needs to estimate the channel coefficient to keep its transmit power within allowable limits. As a result, channel estimation, in addition to PU detection, is an integral part of an effective dynamic spectrum access scheme in cognitive radio. In spectrum access methods it is customary to assume perfect channel state information (CSI) at the SU, e.g., [99; 101; 100]. Recently, in [26], the joint problem of PU detection and channel estimation has been addressed.

It is also crucial to minimize the sensing time for maximizing the SU throughput. Specifically, decreasing the sensing period, that is used to determine the transmit power, saves

time for data communication, increasing the SU throughput. Consequently, dynamic spectrum access in cognitive radio is intrinsically a sequential joint detection and estimation problem.

4.3.2 Problem Formulation

We consider a cognitive radio network consisting of K SUs, and a pair of PUs. In PU communication, a preamble takes place before data communication for synchronization and channel estimation purposes. In particular, during the preamble both PUs transmit random pilot symbols simultaneously through full duplexing. Pilot signals are often used in channel estimation, e.g., [103], and also in spectrum sensing, e.g., [104]. We assume each SU observes such pilot symbols (e.g., it knows the seed of the random number generator) so that it can estimate the channels that connect it to PUs. Moreover, SUs cooperate to detect the PU communication, through a fusion center (FC), which can be one of the SUs. To find the optimal scheme we again assume a centralized setup where all of the observations collected at SUs are available to the FC. In practice, under stringent energy and bandwidth constraints SUs can report to the FC using level-triggered sampling, a non-uniform sampling technique known to achieve asymptotic optimality while satisfying such constraints [20].

When the channel is idle (i.e., no PU communication), there is no interference constraint, and as a result an SU can transmit with full power P_{\max} . In this case, SUs receive pure noise. On the other hand, in the presence of PU communication, to satisfy the peak interference power constraints I_1 and I_2 of PU 1 and PU 2, respectively, SU k should transmit with power $P_k = \min \left\{ P_{\max}, \frac{I_1}{x_{1k}^2}, \frac{I_2}{x_{2k}^2} \right\}$, where x_{jk} is the channel coefficient between PU j and SU k . Hence, firstly the presence/absence of PU communication is detected. If no PU communication is detected, then a designated SU transmits data with P_{\max} . Otherwise, the channels between PUs and SUs are estimated to determine transmission powers, and then the SU with the highest transmission power starts data communication.

We can model this sequential joint detection and estimation problem using (4.25). Here, the vector $\mathbf{x} = [x_{11}, \dots, x_{1K}, x_{21}, \dots, x_{2K}]'$ holds the channel coefficients; the diagonal matrix

$$\mathbf{H}_t = \text{diag}(h_{t,1}, \dots, h_{t,1}, h_{t,2}, \dots, h_{t,2})$$

holds the pilot signals; \mathbf{y}_t and \mathbf{w}_t are the observation and noise vectors in \mathbb{R}^{2K} , respectively. Then, we have the following binary hypothesis testing problem

$$\begin{aligned} \mathbf{H}_0 : \mathbf{x} &= 0, \\ \mathbf{H}_1 : \mathbf{x} &\sim \mathcal{N}(\boldsymbol{\mu}, \boldsymbol{\Sigma}), \end{aligned} \quad (4.33)$$

where $\boldsymbol{\mu} = [\mu_{11}, \dots, \mu_{2K}]'$, $\boldsymbol{\Sigma} = \text{diag}(\rho_{11}^2, \dots, \rho_{2K}^2)$ with μ_{jk} and ρ_{jk}^2 being the mean and variance of the channel coefficient x_{jk} , respectively.

Since channel estimation is meaningful only under \mathbf{H}_1 , we do not assign estimation cost to \mathbf{H}_0 , and perform estimation only when \mathbf{H}_1 is decided. In other words, we use the cost function

$$\begin{aligned} \mathcal{C}(T, d_T, \hat{\mathbf{x}}_T) &= a_0 \mathbf{P}_0(d_T = 1 | \mathcal{H}_T) + a_1 \mathbf{P}_1(d_T = 0 | \mathcal{H}_T) \\ &\quad + \mathbf{E}_1 [b_{11} \|\hat{\mathbf{x}}_T - \mathbf{x}\|^2 \mathbb{1}_{\{d_T=1\}} + b_{10} \|\mathbf{x}\|^2 \mathbb{1}_{\{d_T=0\}} | \mathcal{H}_T], \end{aligned} \quad (4.34)$$

which is a special case of (4.3). When \mathbf{H}_0 is decided, it is like we set $\hat{\mathbf{x}}_T = 0$. Similar to (4.5), we want to solve the following problem

$$\min_{T, d_T, \hat{\mathbf{x}}_T} T \quad \text{s.t.} \quad \mathcal{C}(T, d_T, \hat{\mathbf{x}}_T) \leq \alpha, \quad (4.35)$$

for which the optimum solution follows from Section 4.2.2.

4.3.3 Optimum Solution

We write the optimum estimator as

$$\hat{\mathbf{x}}_T = \mathbf{E}_1[\mathbf{x} | \mathcal{F}_T] \quad (4.36)$$

by substituting $b_{01} = 0$ into (4.9). Then, from (4.10), the posterior estimation costs are given by

$$\begin{aligned} \Delta_T^{11} &= \text{Tr}(\text{Cov}_1[\mathbf{x} | \mathcal{F}_T]) \\ \Delta_T^{10} &= \sum_{j=1}^2 \sum_{k=1}^K \mathbf{E}_i[x_{jk}^2 | \mathcal{F}_T^{jk}] = \sum_{j=1}^2 \sum_{k=1}^K \left\{ \left(\mathbf{E}_i[x_{jk} | \mathcal{F}_T^{jk}] \right)^2 + \text{Var}_1[x_{jk} | \mathcal{F}_T^{jk}] \right\} \\ &= \|\hat{\mathbf{x}}_T\|^2 + \text{Tr}(\text{Cov}_1[\mathbf{x} | \mathcal{F}_T]). \end{aligned}$$

As a result, we get the optimum detector, from (4.14), as

$$d_T = \begin{cases} 1 & \text{if } L_T [a_1 + b_{10}\|\hat{\mathbf{x}}_T\|^2 + (b_{10} - b_{11})\text{Tr}(\text{Cov}_1[\mathbf{x}|\mathcal{F}_T])] \geq a_0 \\ 0 & \text{otherwise} \end{cases} \quad (4.37)$$

since $b_{00} = b_{01} = 0$ here. In practice, a single weight is used for the estimation error regardless of the detection decision. Hence, assuming $b_{10} = b_{11} = b_1$ we obtain the following optimum solution.

Corollary 1. *The optimum sequential joint detector and estimator that solves (4.35) is given by*

$$T = \min\{t \in \mathbb{N} : \mathcal{C}_t \leq \alpha\} \quad (4.38)$$

$$d_T = \begin{cases} 1 & \text{if } L_T \geq \frac{a_0}{a_1 + b_1\|\hat{\mathbf{x}}_T\|^2} \\ 0 & \text{otherwise} \end{cases} \quad (4.39)$$

$$\hat{\mathbf{x}}_T = \mathbb{E}_1[\mathbf{x}|\mathcal{F}_T], \quad (4.40)$$

where

$$\mathcal{C}_t \triangleq \mathbb{E}_0 \left[\{a_0 - (a_1 + b_1\|\hat{\mathbf{x}}_t\|^2) L_t\}^- | \mathcal{H}_t \right] + b_1 \mathbb{E}_1 [\|\hat{\mathbf{x}}_t\|^2 + \text{Tr}(\text{Cov}_1[\mathbf{x}|\mathcal{F}_t]) | \mathcal{H}_t] + a_1 \quad (4.41)$$

is the optimal cost at time t .

Proof. Since for any stopping time T we showed in (4.36) and (4.37) that $\mathcal{C}(T, d_T, \hat{\mathbf{x}}_T) \leq \mathcal{C}(T, d_T, \hat{\mathbf{x}}_T)$, the optimum stopping time T is the first time $\mathcal{C}_t \triangleq \mathcal{C}(t, d_t, \hat{\mathbf{x}}_t)$ achieves the target accuracy level α , proving (4.38). Finally, (4.39), (4.40), (4.41) directly follow from (4.37), (4.36), (4.18), respectively. \square

From (4.31), the posterior distribution of each channel coefficient x_{jk} under \mathbb{H}_1 is known to be Gaussian with mean and variance

$$\mathbb{E}_1[x_{jk}|\mathcal{F}_t^{jk}] = \frac{\frac{v_{t,jk}}{\sigma^2} + \frac{\mu_{jk}}{\rho_{jk}^2}}{\frac{u_{t,j}}{\sigma^2} + \frac{1}{\rho_{jk}^2}}, \quad \text{and} \quad \text{Var}_1[x_{jk}|\mathcal{F}_t^{jk}] = \frac{1}{\frac{u_{t,j}}{\sigma^2} + \frac{1}{\rho_{jk}^2}}, \quad j = 1, 2, \quad k = 1, \dots, K, \quad (4.42)$$

where $u_{t,j} = \sum_{s=1}^t h_{s,j}^2$ and $v_{t,jk} = \sum_{s=1}^t h_{s,j} y_{s,jk}$. Note that the entries of $\hat{\mathbf{x}}_t$, and $\text{Tr}(\text{Cov}_1[\mathbf{x}|\mathcal{F}_t]) = \sum_{j=1}^2 \sum_{k=1}^K \text{Var}_1[x_{jk}|\mathcal{F}_t^{jk}]$ are given in (4.42). Since the received signal

under H_0 is white Gaussian noise, and the likelihood $p_1(\{y_{s,jk}\}_{s=1}^t | \mathcal{H}_t^{jk})$ is given by (4.30), we write the local and global likelihood ratios $L_t^{jk} = \frac{p_1(\{y_{s,jk}\}_{s=1}^t | \mathcal{H}_t^{jk})}{p_0(\{y_{s,jk}\}_{s=1}^t | \mathcal{H}_t^{jk})}$ and L_t as

$$L_t^{jk} = \frac{\exp \left[\frac{1}{2} \left(\frac{\left(\frac{v_{t,jk} + \frac{\mu_{jk}}{\rho_{jk}^2}}{\sigma^2 + \frac{1}{\rho_{jk}^2}} \right)^2}{\frac{u_{t,j}}{\sigma^2} + \frac{1}{\rho_{jk}^2}} - \frac{\mu_{jk}^2}{\rho_{jk}^2} \right) \right]}{\rho_{jk} \sqrt{\frac{u_{t,j}}{\sigma^2} + \frac{1}{\rho_{jk}^2}}}, \quad L_t = \prod_{j=1}^2 \prod_{k=1}^K L_t^{jk}. \quad (4.43)$$

The necessary and sufficient statistics for the optimum schemes given in Algorithm 8 and Algorithm 9 are provided in (4.42) and (4.43). Similar to Section 4.2.5, in (online/offline) Monte Carlo simulations for estimating the optimal cost, we generate the realizations of $v_{t,jk}$ independently for each pair (j, k) and according to $\mathcal{N}(0, \sigma^2 u_{t,j})$ and $\mathcal{N}(\mu_{jk} u_{t,j}, \rho_{jk}^2 u_{t,j}^2 + \sigma^2 u_{t,j})$ under H_0 and H_1 , respectively.

4.3.4 Discussions

Since the statistics in (4.42) and (4.43) are functions of $\{u_{t,j}, v_{t,jk}\}_{j,k}$ only, and the expectations in (4.41) are conditioned on $\{h_{s,j}\}_{s,j}$ for $s = 1, \dots, t$, the optimal cost \mathcal{C}_t is a function of the Fisher information $u_{t,1}$ and $u_{t,2}$ only. Hence, the continuation and stopping regions that determine the optimal stopping rule can be easily found through offline simulations in a 2-dimensional space, compared with the N -dimensional and $\frac{N^2+N}{2}$ -dimensional spaces in Section 4.2.5 and Section 4.2.4, respectively. That is, in this problem, Algorithm 9, which considerably decreases the amount of online computation by finding offline the optimum stopping rule for $\{u_{t,1}, u_{t,2}\}$, is preferred over Algorithm 8, which estimates \mathcal{C}_t online at each time t .

The optimum estimator, given by (4.40), is the posterior expected value, i.e., MMSE estimator, of the channel coefficient vector under H_1 as channel estimation is meaningful only when PU communication takes place. The optimum detector, given in (4.39), uses the side information provided by the estimator. Specifically, the farther away the estimates are from zero, i.e., $\|\hat{\mathbf{x}}_T\|^2 \gg 0$, the easier it is to decide for H_1 . For $b_1 = 0$, i.e., in the pure detection problem, it boils down to the well-known likelihood ratio test (LRT). Note that the proposed scheme in Corollary 1 can be used in parallel to dynamically access to multiple spectrum bands.

In the conventional approach, the detection and estimation problems are treated separately with a combination of either sequential detector and fixed-sample-size estimator or sequential estimator and fixed-sample-size detector, as opposed to the sequential joint detector and estimator (SJDE) given in Corollary 1. An important example to the former is the combination of sequential probability ratio test (SPRT) and MMSE estimator. In the pure detection problem, SPRT is the optimum sequential detector for i.i.d. observations $\{y_{t,jk}\}$, which is not the case here. Since it is the most common sequential detector, we consider it here. In SPRT, we continue taking new observations as long as the likelihood ratio is between two thresholds, and stop the first time it crosses a threshold. At the stopping time, H_1 (resp. H_0) is decided if the upper (resp. lower) threshold is crossed [56], and finally the MMSE estimator of \mathbf{x} under H_1 (resp. H_0) is computed. On the other hand, since the accuracy of channel estimation is crucial in satisfying the PU interference constraints under H_1 , in SJDE, the cost function, and as a result the stopping time and decision function involve the estimator. To verify the involvement of the estimator in the decision function we also compare SJDE with the combination of the stopping time given in (4.38) for SJDE, the LRT detector, and the MMSE estimator.

In Fig. 4.1, we numerically show the superior performance of SJDE over i) the combined SPRT detector and MMSE estimator (SPRT & Est.), and ii) the sequential LRT detector and MMSE estimator (SLRT & Est.), which are described above. The α value on the horizontal axis is the target accuracy level that we want to achieve in terms of the combined detection and estimation cost in (4.34), i.e., $\mathcal{C}(T, d_T, \hat{\mathbf{x}}_T) \leq \alpha$. The combined SLRT detector and MMSE estimator is equipped with the stopping rule of SJDE to demonstrate the advantage of incorporating the side information from estimation into the decision function. SJDE is specifically designed to minimize the stopping time subject to a constraint on the combined cost, thus expectedly achieves the best performance in Fig. 4.1. Since SLRT & Est. uses the optimum stopping time, given by (4.38), for the problem in (4.35), it outperforms SPRT & Est., in which the detector and estimator are completely separated, and the stopping time is solely determined by the detector, following a conventional approach.

In our problem of interest, it is crucial that SUs do not violate the maximum interference constraint, which in turn ensures an admissible PU outage probability. In case of

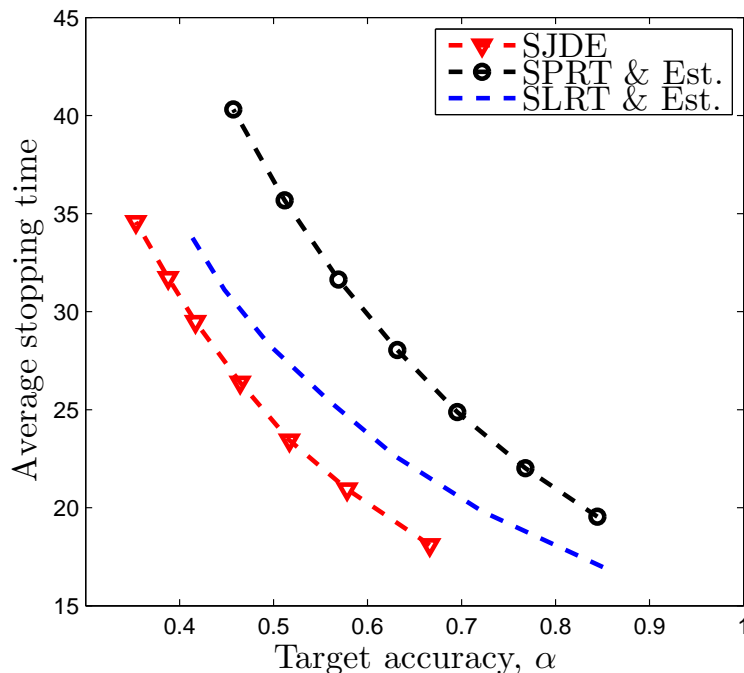


Figure 4.1: Average stopping time vs. target accuracy level for SJDE in Corollary 1, the conventional SPRT detector & MMSE estimator, and the sequential LRT detector & MMSE estimator equipped with the stopping rule of SJDE.

mis-detection the SU transmits with maximum power, which may cause the violation of outage constraint. Even when the SU correctly detects PU communication, poor channel estimate may still cause the SU to transmit with a non-admissible power. On the other hand, the false alarm, which corresponds to deciding on H_1 under H_0 , is not related to the outage constraint, but only degrades the SU throughput. Therefore, in the combined cost expression in (4.34) the second and third terms are more important than the first term. Accordingly, in Fig. 4.1 we use $a_0 = a_1 = 0.2$ and $b_{11} = b_{10} = b_1 = 0.6$. Since the second part of the third term in (4.34) already penalizes mis-detection, we do not differentiate between the coefficients, a_0 and a_1 , of the detection error probabilities. In Fig. 4.1, referring to (4.33) we use $\mu_{jk} = 0$, i.e., Rayleigh fading channel x_{jk} , and $\rho_{jk}^2 = \sigma^2 = \mathbb{E}[|h_{t,j}^2|] = 1$, where $j = 1, 2$ and $k = 1, \dots, 5$ are the PU and SU indices, respectively.

4.4 State Estimation in Smart Grid with Topological Uncertainty

4.4.1 Background and Problem Formulation

State estimation is a vital task in real-time monitoring of smart grid [105]. In the widely used linear model

$$\mathbf{y}_t = \mathbf{H}\mathbf{x} + \mathbf{w}_t, \quad (4.44)$$

the state vector $\mathbf{x} = [\theta_1, \dots, \theta_N]'$ holds the bus voltage phase angles; the measurement matrix $\mathbf{H} \in \mathbb{R}^{M \times N}$ represents the network topology; $\mathbf{y}_t \in \mathbb{R}^M$ holds the power flow and injection measurements; and $\mathbf{w}_t \in \mathbb{R}^M$ is the white Gaussian measurement noise vector. We assume a pseudo-static state estimation problem, i.e., \mathbf{x} does not change during the estimation period. For the above linear model to be valid it is assumed that the differences between phase angles are small. Hence, we can model θ_n , $n = 1, \dots, N$ using a Gaussian prior with a small variance, as in [106; 83].

The measurement matrix \mathbf{H} is also estimated periodically using the status data from switching devices in the power grid, and assumed to remain unchanged until the next estimation instance. However, in practice, such status data is also noisy, like the power flow measurements in (4.44), and thus the estimate of \mathbf{H} may include some error. Since the elements of \mathbf{H} take the values $\{-1, 0, 1\}$, there is a finite number of possible errors. Another source of topological uncertainty is the power outage, in which protective devices automatically isolate the faulty area from the rest of the grid. Specifically, an outage changes the grid topology, i.e., \mathbf{H} , and also the prior on \mathbf{x} . We model the topological uncertainty using multiple hypotheses, as in [83; 107; 108; 109]. In (4.44), under hypothesis j we have

$$\mathbf{H}_j : \mathbf{H} = \mathbf{H}_j, \mathbf{x} \sim \mathcal{N}(\boldsymbol{\mu}_j, \boldsymbol{\Sigma}_j), j = 0, 1, \dots, J, \quad (4.45)$$

where \mathbf{H}_0 corresponds to the normal-operation (i.e., no estimation error or outage) case.

Note that in this case, for large J , in (4.3) there will be a large number of cross estimation costs $b_{ji} \mathbb{E}_j[\|\hat{\mathbf{x}}_T^i - \mathbf{x}\|^2 \mathbb{1}_{\{d_T=i\}} | \mathcal{H}_T]$, $i \neq j$ that penalize the wrong decisions under \mathbf{H}_j . For simplicity, following the formulation in Section 4.2.3, we here penalize the wrong decisions only with the detection costs, i.e., $b_{ji} = 0$, $i \neq j$, and $b_{jj} = b_j > 0$. Hence, generalizing the

cost function in (4.19) to the mulihypothesis case, we use the following cost function

$$\mathcal{C}(T, d_T, \{\hat{\mathbf{x}}_T^j\}) = \sum_{j=0}^J \left\{ a_j \mathbf{P}(d_T \neq j) + b_j \mathbf{E}_j \left[\|\hat{\mathbf{x}}_T^j - \mathbf{x}\|^2 \mathbb{1}_{\{d_T=j\}} \right] \right\}. \quad (4.46)$$

Here we do not need the conditioning on \mathcal{H}_t as the measurement matrices $\{\mathbf{H}_j\}$ are deterministic and known. As a result the optimum stopping time T is deterministic and can be computed offline.

4.4.2 Optimum Solution

Similar to (4.21), the optimum estimators are given by

$$\begin{aligned} \hat{\mathbf{x}}_T^j &= \mathbf{E}_j[\mathbf{x} | \mathcal{F}_T], \quad j = 0, \dots, J, \\ &= \left(\frac{\mathbf{U}_t^j}{\sigma^2} + \boldsymbol{\Sigma}_j^{-1} \right)^{-1} \left(\frac{\mathbf{v}_t^j}{\sigma^2} + \boldsymbol{\Sigma}_j^{-1} \boldsymbol{\mu}_j \right), \end{aligned} \quad (4.47)$$

where the closed form expression follows from (4.29) with $\mathbf{U}_t^j = t\mathbf{H}'_j\mathbf{H}_j$ and $\mathbf{v}_t^j = \mathbf{H}'_j \sum_{s=1}^t \mathbf{y}_s$.

We use the estimator $\hat{\mathbf{x}}_T^j$ when \mathbf{H}_j is decided. Substituting $\{\hat{\mathbf{x}}_T^j\}$ in (4.46) we have

$$\mathcal{C}(d_T) = \sum_{j=0}^J \mathbf{E}_j \left[(a_j - b_j \Delta_T^j) \mathbb{1}_{\{d_T \neq j\}} \right] + b_j \Delta_T^j, \quad (4.48)$$

where $\Delta_t^j = \text{Tr}(\text{Cov}_j[\mathbf{x} | \mathcal{F}_t]) = \text{Tr} \left(\left(\frac{\mathbf{U}_t^j}{\sigma^2} + \boldsymbol{\Sigma}_j^{-1} \right)^{-1} \right)$ from (4.22) and (4.29), respectively.

Hence,

$$d_T = \arg \min_{d_T} \sum_{j=0}^J \int \cdots \int_{\mathcal{A}_j(d_T)} (a_j - b_j \Delta_T^j) p_j(\{\mathbf{y}_t\}_{t=1}^T) d\mathbf{y}_1 \cdots d\mathbf{y}_T, \quad (4.49)$$

where $\mathcal{A}_j(d_T)$ is the region where \mathbf{H}_j is rejected, i.e., $d_T \neq j$, under \mathbf{H}_j . To minimize the summation over all hypotheses, the optimum detector, for each observation set $\{\mathbf{y}_t\}$, omits the largest $(a_j - b_j \Delta_T^j) p_j(\{\mathbf{y}_t\}_{t=1}^T)$ in the integral calculation by choosing the corresponding hypothesis. That is, the optimum detector is given by

$$d_T = \arg \max_j (a_j - b_j \Delta_T^j) p_j(\{\mathbf{y}_t\}_{t=1}^T), \quad (4.50)$$

where $\Delta_{\mathbb{T}}^j = \text{Tr} \left(\left(\frac{\mathbf{U}_{\mathbb{T}}}{\sigma^2} + \boldsymbol{\Sigma}_j^{-1} \right)^{-1} \right)$ and, from (4.27),

$$p_j \left(\{\mathbf{y}_t\}_{t=1}^{\mathbb{T}} \right) = \frac{\exp \left[-\frac{1}{2} \left(\sum_{t=1}^{\mathbb{T}} \frac{\|\mathbf{y}_t\|^2}{\sigma^2} + \|\boldsymbol{\mu}_j\|_{\boldsymbol{\Sigma}_j^{-1}}^2 - \left\| \frac{\mathbf{v}_{\mathbb{T}}}{\sigma^2} + \boldsymbol{\Sigma}_j^{-1} \boldsymbol{\mu}_j \right\|^2 \left(\frac{\mathbf{U}_{\mathbb{T}}}{\sigma^2} + \boldsymbol{\Sigma}_j^{-1} \right)^{-1} \right) \right]}{(2\pi)^{m\mathbb{T}/2} \sigma^{m\mathbb{T}} |\boldsymbol{\Sigma}_j|^{1/2} \left| \frac{\mathbf{U}_{\mathbb{T}}}{\sigma^2} + \boldsymbol{\Sigma}_j^{-1} \right|^{1/2}}.$$

Finally, from (4.48) and (4.50), the optimal cost $\mathcal{C}_t = \mathcal{C}(\mathbf{d}_t)$ is given by

$$\mathcal{C}_t = \sum_{j=0}^J (a_j - b_j \Delta_t^j) \mathbf{P}_j(\mathbf{d}_t \neq j) + b_j \Delta_t^j, \quad (4.51)$$

which can be numerically computed offline for all t by estimating the sufficient statistics $\{\mathbf{P}_j(\mathbf{d}_t \neq j)\}_{t,j}$ through Monte Carlo simulations. Once the sequence $\{\mathcal{C}_t\}$ is obtained, the optimum detection and estimation time is found offline using $\mathbb{T} = \min\{t : \mathcal{C}_t \leq \alpha\}$. In simulations, we generate the realizations of \mathbf{y}_t according to $\mathcal{N}(\mathbf{H}_j \boldsymbol{\mu}_j, \mathbf{H}_j \boldsymbol{\Sigma}_j \mathbf{H}_j' + \sigma^2 \mathbf{I})$; find \mathbf{d}_t using (4.50); and average $\mathbb{1}_{\{\mathbf{d}_t \neq j\}}$ over the realizations. Since the correct hypothesis is unknown, the individual average costs under each hypothesis are summed to yield the overall average cost in (4.51). According to the optimum stopping rule we stop taking new observations and perform detection and estimation (in a joint manner) when this overall average cost is as small as the target value α .

4.4.3 Discussions

Similar to Section 4.2.3, the optimum detector in (4.50) is biased towards the hypothesis with best estimation performance (i.e., smallest MMSE), hence is an ML & MMSE detector.

We next present numerical results for the proposed scheme using the IEEE-4 bus system (c.f. Fig. 4.2). Note that in this case the state status is characterized by a 3-dimensional vector, i.e., $\mathbf{x} \in \mathbb{R}^3$ (the phase angle of bus 1 is taken as the reference). In Fig. 4.2, it is seen that there are eight measurements collected by meters, thus the topology is characterized by a 8-by-3 matrix, i.e., $\mathbf{H} \in \mathbb{R}^{8 \times 3}$.

Since the impedances of all links are known beforehand, we assume that they are of unit values without loss of generality. Here, instead of considering all possible forms of \mathbf{H} , we narrow down the candidate grid topologies to the outage scenarios. In particular, as given

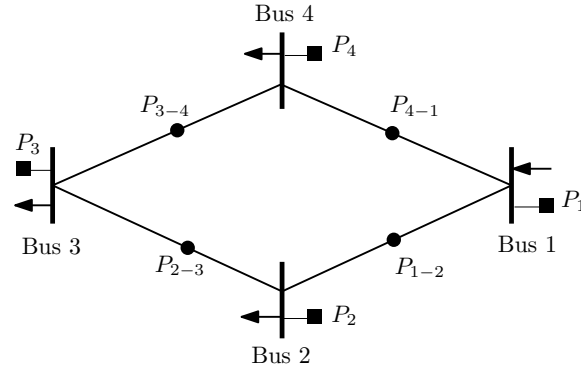


Figure 4.2: Illustration for the IEEE-4bus system and the power injection (square) and power flow (circle) measurements.

in (4.52), \mathbf{H}_0 represents the default topology matrix, and $\{\mathbf{H}_i, i = 1, 2, 3, 4\}$ correspond to the scenarios where the links $l_{1-2}, l_{2-3}, l_{3-4}, l_{4-1}$ (l_{i-j} denotes the link between bus i and bus j) break down, respectively.

We use the following distributions for the state vector \mathbf{x} under the hypotheses $\{\mathbf{H}_i\}$.

$$\begin{aligned} \mathbf{H}_0 : \mathbf{x} &\sim \mathcal{N}(\pi/5 \times \mathbf{1}, \pi^2/9 \times \mathbf{I}), & \mathbf{H}_1 : \mathbf{x} &\sim \mathcal{N}(2\pi/5 \times \mathbf{1}, \pi^2/16 \times \mathbf{I}), \\ \mathbf{H}_2 : \mathbf{x} &\sim \mathcal{N}(3\pi/5 \times \mathbf{1}, \pi^2/25 \times \mathbf{I}), & \mathbf{H}_3 : \mathbf{x} &\sim \mathcal{N}(4\pi/5 \times \mathbf{1}, \pi^2/36 \times \mathbf{I}), \\ \mathbf{H}_4 : \mathbf{x} &\sim \mathcal{N}(\pi \times \mathbf{1}, \pi^2/4 \times \mathbf{I}), \end{aligned}$$

where $a_i = 0.2$, $b_i = 0.8, \forall i$, $\mathbf{1}$ is the vector of ones and \mathbf{I} is the identity matrix. The measurements are contaminated by the white Gaussian noise $\mathbf{w}_t \sim \mathcal{N}(\mathbf{0}, \mathbf{I})$. The goal is to decide among the five candidate grid topologies, and meanwhile, to estimate the state

vector.

$$\begin{aligned}
 \mathbf{H}_0 = & \begin{matrix} & \theta_2 & \theta_3 & \theta_4 \\ \begin{matrix} P_1 \\ P_{1-2} \\ P_2 \\ P_{2-3} \\ P_3 \\ P_{3-4} \\ P_4 \\ P_{4-1} \end{matrix} & \begin{pmatrix} -1 & 0 & -1 \\ -1 & 0 & 0 \\ 2 & -1 & 0 \\ 1 & -1 & 0 \\ -1 & 2 & -1 \\ 0 & 1 & -1 \\ 0 & -1 & 2 \\ 0 & 0 & 1 \end{pmatrix} & , & \mathbf{H}_1 = \begin{pmatrix} 0 & 0 & -1 \\ 0 & 0 & 0 \\ 1 & -1 & 0 \\ 1 & -1 & 0 \\ -1 & 2 & -1 \\ 0 & 1 & -1 \\ 0 & -1 & 2 \\ 0 & 0 & 1 \end{pmatrix} & , \end{matrix} \quad (4.52) \\
 \mathbf{H}_2 = & \begin{pmatrix} -1 & 0 & -1 \\ -1 & 0 & 0 \\ 1 & 0 & 0 \\ 0 & 0 & 0 \\ 0 & 1 & -1 \\ 0 & 1 & -1 \\ 0 & -1 & 2 \\ 0 & 0 & 1 \end{pmatrix} & , & \mathbf{H}_3 = \begin{pmatrix} -1 & 0 & -1 \\ -1 & 0 & 0 \\ 2 & -1 & 0 \\ 1 & -1 & 0 \\ -1 & 1 & 0 \\ 0 & 0 & 0 \\ 0 & 0 & 1 \\ 0 & 0 & 1 \end{pmatrix} & , & \mathbf{H}_4 = \begin{pmatrix} -1 & 0 & 0 \\ -1 & 0 & 0 \\ 2 & -1 & 0 \\ 1 & -1 & 0 \\ -1 & 2 & -1 \\ 0 & 1 & -1 \\ 0 & -1 & 1 \\ 0 & 0 & 0 \end{pmatrix} . \quad (4.53)
 \end{aligned}$$

Since SPRT is not applicable in the multi-hypothesis case, we compare the proposed SJDE scheme with the combination of SLRT detector and MMSE estimator, equipped the stopping time given in (4.15). Fig. 4.3 illustrates that SJDE significantly outperforms this combination. We see that SJDE requires smaller average number of samples than SLRT & Est. to achieve the same target accuracy. Specifically, with small average sample size (i.e., stopping time), the improvement of SJDE is substantial. This is because smaller sample size causes larger estimation cost Δ_T^j , which in turn emphasizes the advantage of the proposed detector, given by (4.50), over the conventional LRT detector. In fact, in smart grid monitoring, the typical sample size is small since the system state evolves quickly, and thus there is limited time for the control center to estimate the current state.

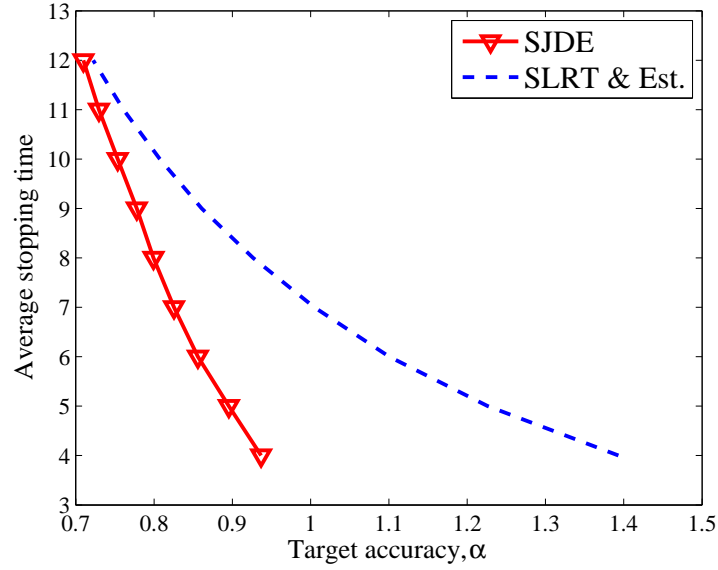


Figure 4.3: Average stopping time vs. target accuracy level for SJDE and the combination of sequential LRT detector & MMSE estimator equipped with the stopping rule of SJDE.

4.5 Conclusion

We have developed a general framework for optimum sequential joint detection and estimation. More specific cases have also been analyzed for application purposes. Applying the developed theory to two popular problems, namely dynamic spectrum sensing in cognitive radio networks, and state estimation in smart grid with topological uncertainties, we have proposed optimum sequential procedures, and numerically analyzed their performances. Numerical results show considerable performance gains over the conventional methods.

Part IV

Conclusions

Chapter 5

Conclusions

In this thesis, we have considered sequential detection, estimation, and joint detection and estimation, and their applications to decentralized systems, such as wireless sensor networks, cognitive radio, and smart grid. We have designed optimum sequential schemes for estimation, and joint detection and estimation. An event-based sampling technique called level-triggered sampling has been used as a means of information transmission in decentralized systems with stringent energy and bandwidth constraints. The sequential decentralized schemes designed in this thesis are compatible with the existing hardware based on conventional A/D conversion. Rigorous analyses have been performed to show that the developed decentralized schemes achieve a strong type of asymptotic optimality called order-2 asymptotic optimality. We have shown both analytically and numerically that the proposed schemes based on level-triggered sampling significantly outperform their counterparts based on conventional uniform sampling in terms of minimizing the average sample size, i.e., decision time.

Part V

Bibliography

Bibliography

- [1] H. V. Poor, *An Introduction to Signal Detection and Estimation*. New York, NY: Springer, 1994.
- [2] J. W. Mark and T. Todd, "A nonuniform sampling approach to data compression," *Communications, IEEE Transactions on*, vol. 29, pp. 24–32, Jan 1981.
- [3] P. Ellis, "Extension of phase plane analysis to quantized systems," *Automatic Control, IRE Transactions on*, vol. 4, pp. 43–54, Nov 1959.
- [4] K. Astrom and B. Bernhardsson, "Comparison of riemann and lebesgue sampling for first order stochastic systems," in *Decision and Control, 2002, Proceedings of the 41st IEEE Conference on*, vol. 2, pp. 2011–2016 vol.2, Dec 2002.
- [5] E. Kofman and J. Braslavsky, "Level crossing sampling in feedback stabilization under data-rate constraints," in *Decision and Control, 2006 45th IEEE Conference on*, pp. 4423–4428, Dec 2006.
- [6] K. M. Guan, S. S. Kozat, and A. C. Singer, "Adaptive reference levels in a level-crossing analog-to-digital converter," *EURASIP J. Adv. Signal Process*, vol. 2008, pp. 183:1–183:11, Jan. 2008.
- [7] Y. Tsividis, "Event-driven data acquisition and digital signal processing—a tutorial," *Circuits and Systems II: Express Briefs, IEEE Transactions on*, vol. 57, pp. 577–581, Aug 2010.

- [8] A. Lazar and L. Toth, "Perfect recovery and sensitivity analysis of time encoded bandlimited signals," *Circuits and Systems I: Regular Papers, IEEE Transactions on*, vol. 51, pp. 2060–2073, Oct 2004.
- [9] M. Miskowicz, "Send-on-delta concept: an event-based data reporting strategy," *Sensors*, vol. 6, pp. 49–63, 2006.
- [10] M. Miskowicz, "Asymptotic effectiveness of the event-based sampling according to the integral criterion," *Sensors*, vol. 7, pp. 16–37, 2007.
- [11] Y. S. Suh, "Send-on-delta sensor data transmission with a linear predictor," *Sensors*, vol. 7, no. 4, pp. 537–547, 2007.
- [12] G. Fellouris and G. Moustakides, "Decentralized sequential hypothesis testing using asynchronous communication," *Information Theory, IEEE Transactions on*, vol. 57, pp. 534–548, Jan 2011.
- [13] K. Guan and A. Singer, "Opportunistic sampling by level-crossing," in *Acoustics, Speech and Signal Processing, 2007. ICASSP 2007. IEEE International Conference on*, vol. 3, pp. III–1513–III–1516, April 2007.
- [14] G. Fellouris, "Asymptotically optimal parameter estimation under communication constraints," *Ann. Statist.*, vol. 40, pp. 2239–2265, Aug 2012.
- [15] D. Drazen, P. Lichtsteiner, P. Hafziger, T. Delbruck, and A. Jensen, "Toward real-time particle tracking using an event-based dynamic vision sensor," *Experiments in Fluids*, vol. 51, no. 5, pp. 1465–1469, 2011.
- [16] M. Hofstatter, M. Litzberger, D. Matolin, and C. Posch, "Hardware-accelerated address-event processing for high-speed visual object recognition," in *Electronics, Circuits and Systems (ICECS), 2011 18th IEEE International Conference on*, pp. 89–92, Dec 2011.
- [17] A. Lazar and E. Pnevmatikakis, "Video time encoding machines," *Neural Networks, IEEE Transactions on*, vol. 22, pp. 461–473, March 2011.

- [18] J. Fromm and S. Lautner, “Electrical signals and their physiological significance in plants,” *Plant, Cell & Environment*, vol. 30, no. 3, pp. 249–257, 2007.
- [19] B. Moser and T. Natschlager, “On stability of distance measures for event sequences induced by level-crossing sampling,” *Signal Processing, IEEE Transactions on*, vol. 62, pp. 1987–1999, April 2014.
- [20] Y. Yilmaz, G. Moustakides, and X. Wang, “Cooperative sequential spectrum sensing based on level-triggered sampling,” *Signal Processing, IEEE Transactions on*, vol. 60, pp. 4509–4524, Sept 2012.
- [21] Y. Yilmaz, G. Moustakides, and X. Wang, “Channel-aware decentralized detection via level-triggered sampling,” *Signal Processing, IEEE Transactions on*, vol. 61, pp. 300–315, Jan 2013.
- [22] Y. Yilmaz and X. Wang, “Sequential distributed detection in energy-constrained wireless sensor networks,” *Signal Processing, IEEE Transactions on*, vol. 62, pp. 3180–3193, June 2014.
- [23] Y. Yilmaz and X. Wang, “Sequential decentralized parameter estimation under randomly observed fisher information,” *Information Theory, IEEE Transactions on*, vol. 60, pp. 1281–1300, Feb 2014.
- [24] Y. Yilmaz, G. Moustakides, and X. Wang, “Sequential vector parameter estimation for linear models with application to distributed systems,” *Signal Processing, IEEE Transactions on*, available at <http://arxiv.org/pdf/1301.5701v3.pdf> to be published.
- [25] Y. Yilmaz, G. Moustakides, and X. Wang, “Sequential joint detection and estimation,” *SIAM Theory Probab. Appl.*, available at <http://arxiv.org/pdf/1302.6058v4.pdf> to be published.
- [26] Y. Yilmaz, Z. Guo, and X. Wang, “Sequential joint spectrum sensing and channel estimation for dynamic spectrum access,” *Selected Areas in Communications, IEEE Journal on*, vol. 32, Nov 2014.

- [27] R. Tenney and N. R. Sandell, "Detection with distributed sensors," *Aerospace and Electronic Systems, IEEE Transactions on*, vol. AES-17, pp. 501–510, July 1981.
- [28] Z. Chair and P. Varshney, "Optimal data fusion in multiple sensor detection systems," *Aerospace and Electronic Systems, IEEE Transactions on*, vol. AES-22, pp. 98–101, Jan 1986.
- [29] S. C. A. Thomopoulos, R. Viswanathan, and D. Bougoulas, "Optimal decision fusion in multiple sensor systems," *Aerospace and Electronic Systems, IEEE Transactions on*, vol. AES-23, pp. 644–653, Sept 1987.
- [30] J. Tsitsiklis, "Decentralized detection by a large number of sensors," *Mathematics of Control, Signals, and Systems*, pp. 167–182, 1988.
- [31] V. Aalo and R. Viswanathou, "On distributed detection with correlated sensors: two examples," *Aerospace and Electronic Systems, IEEE Transactions on*, vol. 25, pp. 414–421, May 1989.
- [32] P. Willett, P. Swaszek, and R. Blum, "The good, bad and ugly: distributed detection of a known signal in dependent gaussian noise," *Signal Processing, IEEE Transactions on*, vol. 48, pp. 3266–3279, Dec 2000.
- [33] V. Veeravalli, T. Basar, and H. Poor, "Decentralized sequential detection with a fusion center performing the sequential test," *Information Theory, IEEE Transactions on*, vol. 39, pp. 433–442, Mar 1993.
- [34] Y. Mei, "Asymptotic optimality theory for decentralized sequential hypothesis testing in sensor networks," *Information Theory, IEEE Transactions on*, vol. 54, pp. 2072–2089, May 2008.
- [35] S. Chaudhari, V. Koivunen, and H. Poor, "Autocorrelation-based decentralized sequential detection of ofdm signals in cognitive radios," *Signal Processing, IEEE Transactions on*, vol. 57, pp. 2690–2700, July 2009.
- [36] A. Hussain, "Multisensor distributed sequential detection," *Aerospace and Electronic Systems, IEEE Transactions on*, vol. 30, pp. 698–708, Jul 1994.

- [37] A. Wald and J. Wolfowitz, "Optimum character of the sequential probability ratio test," *Ann. Math. Stat.*, vol. 19, no. 3, pp. 326–329, 1948.
- [38] D. Warren and P. Willett, "Optimal decentralized detection for conditionally independent sensors," in *American Control Conference, 1989*, pp. 1326–1329, June 1989.
- [39] S. Chaudhari, J. Lunden, V. Koivunen, and H. Poor, "Cooperative sensing with imperfect reporting channels: Hard decisions or soft decisions?," *Signal Processing, IEEE Transactions on*, vol. 60, pp. 18–28, Jan 2012.
- [40] B. Chen, L. Tong, and P. Varshney, "Channel-aware distributed detection in wireless sensor networks," *Signal Processing Magazine, IEEE*, vol. 23, pp. 16–26, July 2006.
- [41] J.-F. Chamberland and V. Veeravalli, "Decentralized detection in sensor networks," *Signal Processing, IEEE Transactions on*, vol. 51, pp. 407–416, Feb 2003.
- [42] B. Liu and B. Chen, "Channel-optimized quantizers for decentralized detection in sensor networks," *Information Theory, IEEE Transactions on*, vol. 52, pp. 3349–3358, July 2006.
- [43] B. Chen, R. Jiang, T. Kasetkasem, and P. Varshney, "Channel aware decision fusion in wireless sensor networks," *Signal Processing, IEEE Transactions on*, vol. 52, pp. 3454–3458, Dec 2004.
- [44] R. Niu, B. Chen, and P. Varshney, "Fusion of decisions transmitted over rayleigh fading channels in wireless sensor networks," *Signal Processing, IEEE Transactions on*, vol. 54, pp. 1018–1027, March 2006.
- [45] I. Bahceci, G. Al-Regib, and Y. Altunbasak, "Serial distributed detection for wireless sensor networks," in *Information Theory, 2005. ISIT 2005. Proceedings. International Symposium on*, pp. 830–834, Sept 2005.
- [46] C. Tepedelenlioglu and S. Dasarathan, "Distributed detection over gaussian multiple access channels with constant modulus signaling," *Signal Processing, IEEE Transactions on*, vol. 59, pp. 2875–2886, June 2011.

- [47] H. Ahmadi and A. Vosoughi, "Distributed detection with adaptive topology and non-ideal communication channels," *Signal Processing, IEEE Transactions on*, vol. 59, pp. 2857–2874, June 2011.
- [48] S. Ross, *Stochastic Processes*. New York, NY: Wiley, 1996.
- [49] T. Yucek and H. Arslan, "A survey of spectrum sensing algorithms for cognitive radio applications," *Communications Surveys Tutorials, IEEE*, vol. 11, pp. 116–130, First 2009.
- [50] J. Ma, G. Li, and B.-H. Juang, "Signal processing in cognitive radio," *Proceedings of the IEEE*, vol. 97, pp. 805–823, May 2009.
- [51] G. Ganesan and Y. Li, "Cooperative spectrum sensing in cognitive radio, part i: Two user networks," *Wireless Communications, IEEE Transactions on*, vol. 6, pp. 2204–2213, June 2007.
- [52] C. Sun, W. Zhang, and K. Letaief, "Cooperative spectrum sensing for cognitive radios under bandwidth constraints," in *Wireless Communications and Networking Conference, 2007. WCNC 2007. IEEE*, pp. 1–5, March 2007.
- [53] J. Unnikrishnan and V. Veeravalli, "Cooperative spectrum sensing and detection for cognitive radio," in *Global Telecommunications Conference, 2007. GLOBECOM '07. IEEE*, pp. 2972–2976, Nov 2007.
- [54] Z. Quan, S. Cui, and A. Sayed, "Optimal linear cooperation for spectrum sensing in cognitive radio networks," *Selected Topics in Signal Processing, IEEE Journal of*, vol. 2, pp. 28–40, Feb 2008.
- [55] J. Ma and Y. Li, "Soft combination and detection for cooperative spectrum sensing in cognitive radio networks," in *Global Telecommunications Conference, 2007. GLOBECOM '07. IEEE*, pp. 3139–3143, Nov 2007.
- [56] A. Wald, *Sequential Analysis*. New York, NY: Wiley, 1947.

- [57] S. Chaudhari, V. Koivunen, and H. Poor, "Autocorrelation-based decentralized sequential detection of ofdm signals in cognitive radios," *Signal Processing, IEEE Transactions on*, vol. 57, pp. 2690–2700, July 2009.
- [58] J. Sreedharan and V. Sharma, "A novel algorithm for cooperative distributed sequential spectrum sensing in cognitive radio," in *Wireless Communications and Networking Conference (WCNC), 2011 IEEE*, pp. 1881–1886, March 2011.
- [59] S.-J. Kim and G. Giannakis, "Sequential and cooperative sensing for multi-channel cognitive radios," *Signal Processing, IEEE Transactions on*, vol. 58, pp. 4239–4253, Aug 2010.
- [60] N. Kundargi and A. Tewfik, "Doubly sequential energy detection for distributed dynamic spectrum access," in *Communications (ICC), 2010 IEEE International Conference on*, pp. 1–5, May 2010.
- [61] Y. Shei and Y.-T. Su, "A sequential test based cooperative spectrum sensing scheme for cognitive radios," in *Personal, Indoor and Mobile Radio Communications, 2008. PIMRC 2008. IEEE 19th International Symposium on*, pp. 1–5, Sept 2008.
- [62] Y. Xin, H. Zhang, and S. Rangarajan, "Ssct: A simple sequential spectrum sensing scheme for cognitive radio," in *Global Telecommunications Conference, 2009. GLOBECOM 2009. IEEE*, pp. 1–6, Nov 2009.
- [63] Z. Quan, W. Zhang, S. Shellhammer, and A. Sayed, "Optimal spectral feature detection for spectrum sensing at very low snr," *Communications, IEEE Transactions on*, vol. 59, pp. 201–212, January 2011.
- [64] J. Font-Segura and X. Wang, "Glrt-based spectrum sensing for cognitive radio with prior information," *Communications, IEEE Transactions on*, vol. 58, pp. 2137–2146, July 2010.
- [65] G. Moustakides, A. Polunchenko, and A. Tartakovsky, "A numerical approach to performance analysis of quickest change-point detection procedures," *Stat. Sinica*, vol. 21, pp. 571–596, April 2011.

- [66] J. Tsitsiklis, "Extremal properties of likelihood-ratio quantizers," *Communications, IEEE Transactions on*, vol. 41, pp. 550–558, Apr 1993.
- [67] D. Siegmund, *Sequential Analysis, Tests and Confidence Intervals*. New York, NY: Springer, 1985.
- [68] B. Ghosh, "On the attainment of the cramer-rao bound in the sequential case," *Sequential Analysis*, vol. 6, no. 3, pp. 267–288, 1987.
- [69] P. Grambsch, "Sequential sampling based on the observed fisher information to guarantee the accuracy of the maximum likelihood estimator," *Ann. Statist.*, vol. 11, no. 1, pp. 68–77, 1983.
- [70] A. Ribeiro and G. Giannakis, "Bandwidth-constrained distributed estimation for wireless sensor networks-part ii: unknown probability density function," *Signal Processing, IEEE Transactions on*, vol. 54, pp. 2784–2796, July 2006.
- [71] E. Msechu and G. Giannakis, "Sensor-centric data reduction for estimation with wsns via censoring and quantization," *Signal Processing, IEEE Transactions on*, vol. 60, pp. 400–414, Jan 2012.
- [72] J.-J. Xiao, A. Ribeiro, Z.-Q. Luo, and G. Giannakis, "Distributed compression-estimation using wireless sensor networks," *Signal Processing Magazine, IEEE*, vol. 23, pp. 27–41, July 2006.
- [73] J.-J. Xiao, S. Cui, Z.-Q. Luo, and A. Goldsmith, "Linear coherent decentralized estimation," *Signal Processing, IEEE Transactions on*, vol. 56, pp. 757–770, Feb 2008.
- [74] Z.-Q. Luo, G. Giannakis, and S. Zhang, "Optimal linear decentralized estimation in a bandwidth constrained sensor network," in *Information Theory, 2005. ISIT 2005. Proceedings. International Symposium on*, pp. 1441–1445, Sept 2005.
- [75] I. Schizas, G. Giannakis, and Z.-Q. Luo, "Distributed estimation using reduced-dimensionality sensor observations," *Signal Processing, IEEE Transactions on*, vol. 55, pp. 4284–4299, Aug 2007.

- [76] I. Schizas, A. Ribeiro, and G. Giannakis, “Consensus in ad hoc wsns with noisy links-part i: Distributed estimation of deterministic signals,” *Signal Processing, IEEE Transactions on*, vol. 56, pp. 350–364, Jan 2008.
- [77] S. Stankovic, M. Stankovic, and D. Stipanovic, “Decentralized parameter estimation by consensus based stochastic approximation,” *Automatic Control, IEEE Transactions on*, vol. 56, pp. 531–543, March 2011.
- [78] V. Borkar and P. Varaiya, “Asymptotic agreement in distributed estimation,” *Automatic Control, IEEE Transactions on*, vol. 27, pp. 650–655, Jun 1982.
- [79] T. Zhao and A. Nehorai, “Distributed sequential bayesian estimation of a diffusive source in wireless sensor networks,” *Signal Processing, IEEE Transactions on*, vol. 55, pp. 1511–1524, April 2007.
- [80] B. Efron and D. Hinkley, “Assessing the accuracy of the maximum likelihood estimator: Observed versus expected fisher information,” *Biometrika*, vol. 65, no. 3, pp. 457–487, 1978.
- [81] A. Shiryaev, *Optimal Stopping Rules*. New York, NY: Springer, 2008.
- [82] T. Vercauteren and X. Wang, “Decentralized sigma-point information filters for target tracking in collaborative sensor networks,” *Signal Processing, IEEE Transactions on*, vol. 53, pp. 2997–3009, Aug 2005.
- [83] J. Chen, Y. Zhao, A. Goldsmith, and H. Poor, “Optimal joint detection and estimation in linear models,” in *Decision and Control (CDC), 2013 IEEE 52nd Annual Conference on*, pp. 4416–4421, Dec 2013.
- [84] B.-N. Vo, B.-T. Vo, N.-T. Pham, and D. Suter, “Joint detection and estimation of multiple objects from image observations,” *Signal Processing, IEEE Transactions on*, vol. 58, pp. 5129–5141, Oct 2010.
- [85] A. Tajar, G. Jajamovich, X. Wang, and G. Moustakides, “Optimal joint target detection and parameter estimation by mimo radar,” *Selected Topics in Signal Processing, IEEE Journal of*, vol. 4, pp. 127–145, Feb 2010.

- [86] G. Jajamovich, A. Tajer, and X. Wang, “Minimax-optimal hypothesis testing with estimation-dependent costs,” *Signal Processing, IEEE Transactions on*, vol. 60, pp. 6151–6165, Dec 2012.
- [87] D. Middleton and R. Esposito, “Simultaneous optimum detection and estimation of signals in noise,” *Information Theory, IEEE Transactions on*, vol. 14, pp. 434–444, May 1968.
- [88] O. Zeitouni, J. Ziv, and N. Merhav, “When is the generalized likelihood ratio test optimal?,” *Information Theory, IEEE Transactions on*, vol. 38, pp. 1597–1602, Sep 1992.
- [89] G. Moustakides, “Optimum joint detection and estimation,” in *Information Theory Proceedings (ISIT), 2011 IEEE International Symposium on*, pp. 2984–2988, July 2011.
- [90] A. Fredriksen, D. Middleton, and V. VandeLinde, “Simultaneous signal detection and estimation under multiple hypotheses,” *Information Theory, IEEE Transactions on*, vol. 18, pp. 607–614, Sep 1972.
- [91] T. Birdsall and J. Gobien, “Sufficient statistics and reproducing densities in simultaneous sequential detection and estimation,” *Information Theory, IEEE Transactions on*, vol. 19, pp. 760–768, Nov 1973.
- [92] B. Baygun and A. Hero, “Optimal simultaneous detection and estimation under a false alarm constraint,” *Information Theory, IEEE Transactions on*, vol. 41, pp. 688–703, May 1995.
- [93] G. Moustakides, G. Jajamovich, A. Tajer, and X. Wang, “Joint detection and estimation: Optimum tests and applications,” *Information Theory, IEEE Transactions on*, vol. 58, pp. 4215–4229, July 2012.
- [94] Z. Govindarajulu, *Sequential Statistics*. Hackensack, NJ: World Scientific Publishing, 2004.

- [95] B. Ghosh and P. Sen, *Handbook of Sequential Analysis*. New York, NY: Marcel Dekker, 1991.
- [96] H. V. Trees and K. Bell, *Detection Estimation and Modulation Theory, Part I (2nd Edition)*. Somerset, NJ: Wiley, 2013.
- [97] Y.-C. Liang, Y. Zeng, E. Peh, and A. T. Hoang, "Sensing-throughput tradeoff for cognitive radio networks," *Wireless Communications, IEEE Transactions on*, vol. 7, pp. 1326–1337, April 2008.
- [98] Y. Chen, Q. Zhao, and A. Swami, "Joint design and separation principle for opportunistic spectrum access in the presence of sensing errors," *Information Theory, IEEE Transactions on*, vol. 54, pp. 2053–2071, May 2008.
- [99] X. Kang, Y.-C. Liang, A. Nallanathan, H. Garg, and R. Zhang, "Optimal power allocation for fading channels in cognitive radio networks: Ergodic capacity and outage capacity," *Wireless Communications, IEEE Transactions on*, vol. 8, pp. 940–950, Feb 2009.
- [100] L. Musavian and S. Aissa, "Capacity and power allocation for spectrum-sharing communications in fading channels," *Wireless Communications, IEEE Transactions on*, vol. 8, pp. 148–156, Jan 2009.
- [101] X. Kang, Y.-C. Liang, H. Garg, and L. Zhang, "Sensing-based spectrum sharing in cognitive radio networks," *Vehicular Technology, IEEE Transactions on*, vol. 58, pp. 4649–4654, Oct 2009.
- [102] Z. Chen, X. Wang, and X. Zhang, "Continuous power allocation strategies for sensing-based multiband spectrum sharing," *Selected Areas in Communications, IEEE Journal on*, vol. 31, pp. 2409–2419, November 2013.
- [103] Y. Li, "Pilot-symbol-aided channel estimation for ofdm in wireless systems," in *Vehicular Technology Conference, 1999 IEEE 49th*, vol. 2, pp. 1131–1135 vol.2, Jul 1999.

- [104] A. Sahai, R. Tandra, S. M. Mishra, and N. Hoven, “Fundamental design tradeoffs in cognitive radio systems,” in *Proc. of Int. Workshop on Technology and Policy for Accessing Spectrum*, Aug 2006.
- [105] Y.-F. Huang, S. Werner, J. Huang, N. Kashyap, and V. Gupta, “State estimation in electric power grids: Meeting new challenges presented by the requirements of the future grid,” *Signal Processing Magazine, IEEE*, vol. 29, pp. 33–43, Sept 2012.
- [106] Y. Huang, H. Li, K. Campbell, and Z. Han, “Defending false data injection attack on smart grid network using adaptive cusum test,” in *Information Sciences and Systems (CISS), 2011 45th Annual Conference on*, pp. 1–6, March 2011.
- [107] Y. Huang, M. Esmalifalak, Y. Cheng, H. Li, K. Campbell, and Z. Han, “Adaptive quickest estimation algorithm for smart grid network topology error,” *Systems Journal, IEEE*, vol. 8, pp. 430–440, June 2014.
- [108] Y. Zhao, A. Goldsmith, and H. Poor, “On pmu location selection for line outage detection in wide-area transmission networks,” in *Power and Energy Society General Meeting, 2012 IEEE*, pp. 1–8, July 2012.
- [109] Y. Zhao, R. Sevlian, R. Rajagopal, A. Goldsmith, and H. Poor, “Outage detection in power distribution networks with optimally-deployed power flow sensors,” in *Power and Energy Society General Meeting (PES), 2013 IEEE*, pp. 1–5, July 2013.

Part VI

Appendices

Appendix A

Proofs in Part I

A.1 Theorem 2

We will prove the first equality in (2.27), and the proof of the second one follows similarly.

Let us first prove the following lemma.

Lemma 5. *As $\alpha, \beta \rightarrow 0$ we have the following KL information at the FC*

$$\hat{I}_1(\mathcal{T}) = |\log \alpha| + O(1), \quad \text{and} \quad \hat{I}_0(\mathcal{T}) = |\log \beta| + O(1). \quad (\text{A.1})$$

Proof. We will show the first equality and the second one follows similarly. We have

$$\begin{aligned} \hat{I}_1(\mathcal{T}) &= \mathbf{P}_1(\hat{L}_{\mathcal{T}} \geq A) \mathbf{E}_1[\hat{L}_{\mathcal{T}} | \hat{L}_{\mathcal{T}} \geq A] + \mathbf{P}_1(\hat{L}_{\mathcal{T}} \leq -B) \mathbf{E}_1[\hat{L}_{\mathcal{T}} | \hat{L}_{\mathcal{T}} \leq -B] \\ &= (1 - \beta)(A + \mathbf{E}_1[\theta_A]) - \beta(B + \mathbf{E}_1[\theta_B]) \end{aligned} \quad (\text{A.2})$$

where θ_A, θ_B are overshoot and undershoot respectively given by $\theta_A \triangleq \hat{L}_{\mathcal{T}} - A$ if $\hat{L}_{\mathcal{T}} \geq A$ and $\theta_B \triangleq -\hat{L}_{\mathcal{T}} - B$ if $\hat{L}_{\mathcal{T}} \leq -B$. From [12, Theorem 2], we have $A \leq |\log \alpha|$ and $B \leq |\log \beta|$, so as $\alpha, \beta \rightarrow 0$ (A.2) becomes $\hat{I}_1(\mathcal{T}) = A + \mathbf{E}_1[\theta_A] + o(1)$. From (2.10) we have $|\hat{\lambda}_n^k| < \infty$ if $0 < \alpha_k, \beta_k < 1$. If we assume $0 < \Delta < \infty$ and $|l_t^k| < \infty, \forall k, t$, then we have $0 < \alpha_k, \beta_k < 1$ and as a result $\hat{I}_i^k(t_1^k) = \mathbf{E}_i[\hat{\lambda}_1^k] < \infty$. Since the overshoot cannot exceed the last received LLR value, we have $\theta_A, \theta_B \leq \Theta = \max_{k,n} |\hat{\lambda}_n^k| < \infty$. Similar to Eq. (73) in [12] we can write $\beta \geq e^{-B-\Theta}$ and $\alpha \geq e^{-A-\Theta}$ where $\Theta = O(1)$ by the above argument, or equivalently, $B \geq |\log \beta| - O(1)$ and $A \geq |\log \alpha| - O(1)$. Hence we have $A = |\log \alpha| + O(1)$ and $B = |\log \beta| + O(1)$. \square

From the assumption of $|l_t^k| < \infty, \forall k, t$, we also have $\hat{I}_i(1) \leq I_i(1) < \infty$. Moreover, we have $E_i[\mathcal{Y}_k] \leq E_i[\tau_1^k] < \infty$ since $E_i[l_1^k] \neq 0$. Note that all the terms on the right-hand side of (2.26) except for $\hat{I}_i(\mathcal{T})$ do not depend on the global error probabilities α, β , so they are $O(1)$ as $\alpha, \beta \rightarrow 0$. Finally, substituting (A.1) into (2.26) we get (2.27).

A.2 Proposition 2

Note that in the noisy channel cases the FC, as discussed in Section 2.3, computes the LLR $\tilde{\lambda}_n^k$ of the signal it receives, and then performs SPRT using the LLR sum \tilde{L}_t . Hence, analogous to Lemma 5 we can show that $\tilde{I}_1(\tilde{\mathcal{T}}) = |\log \alpha| + O(1)$ and $\tilde{I}_0(\tilde{\mathcal{T}}) = |\log \beta| + O(1)$ as $\alpha, \beta \rightarrow 0$. Note also that due to channel uncertainties $|\tilde{\lambda}_n^k| \leq |\hat{\lambda}_n^k|$, so we have $\tilde{I}_i^k(t_1^k) \leq \hat{I}_i^k(t_1^k) < \infty$ and $\tilde{I}_i(1) \leq \hat{I}_i(1) < \infty$. We also have $E_i[\tilde{\mathcal{Y}}_k] \leq E_i[\tau_1^k] < \infty$ as in the ideal channel case. Substituting these asymptotic values in (2.30) we get (2.31).

A.3 Lemma 1

For given q_n^k, \hat{q}_n^k takes the two values defined in (2.66) with probability p and $1 - p$ respectively. Define $\hat{\epsilon} = \frac{\phi}{\hat{r}}$, that is, the common length of the subintervals. Suppose that $(m - 1)\hat{\epsilon} \leq q_n^k < m\hat{\epsilon}$, $m = 1, \dots, \hat{r}$ then \hat{q}_n^k takes the two end values with probabilities $p, (1 - p)$ respectively, but let us consider p unspecified for the moment. We would like to select p so that

$$pe^{\pm b_n^k(\Delta + (m-1)\hat{\epsilon})} + (1 - p)e^{\pm b_n^k(\Delta + m\hat{\epsilon})} \leq e^{\pm b_n^k(\Delta + q_n^k)}. \quad (\text{A.3})$$

Since b_n^k is a sign bit this is equivalent to solving the inequality

$$pe^{\pm(m-1)\hat{\epsilon}} + (1 - p)e^{\pm m\hat{\epsilon}} \leq e^{\pm q_n^k}, \quad (\text{A.4})$$

from which we conclude that

$$p = \min \left\{ \frac{e^{-m\hat{\epsilon}} - e^{-q_n^k}}{e^{-m\hat{\epsilon}} - e^{-(m-1)\hat{\epsilon}}}, \frac{e^{m\hat{\epsilon}} - e^{q_n^k}}{e^{m\hat{\epsilon}} - e^{(m-1)\hat{\epsilon}}} \right\} \quad (\text{A.5})$$

It is straightforward to verify that the second ratio is the smallest of the two, consequently we define p to have this value which is the one depicted in (2.66).

Appendix B

Proofs in Part II

B.1 Lemma 3

In Section 3.2, the LS estimator was shown to be the MVUE under Gaussian noise and the BLUE under non-Gaussian noise. It was also shown that $\text{Cov}(\hat{X}_t|\mathbf{H}_t) = \sigma^2\mathbf{U}_t^{-1}$. Hence, we write

$$\begin{aligned} f\left(\text{Cov}(\hat{X}_{\mathcal{T}}|\mathbf{H}_{\mathcal{T}})\right) &= f\left(\mathbb{E}\left[\sum_{t=1}^{\infty}(\hat{X}_t - X)(\hat{X}_t - X)^T \mathbb{1}_{\{t=\mathcal{T}\}}|\mathbf{H}_t\right]\right) \\ &= f\left(\sum_{t=1}^{\infty}\mathbb{E}\left[(\hat{X}_t - X)(\hat{X}_t - X)^T|\mathbf{H}_t\right] \mathbb{1}_{\{t=\mathcal{T}\}}\right) \end{aligned} \quad (\text{B.1})$$

$$\geq f\left(\sum_{t=1}^{\infty}\sigma^2\mathbf{U}_t^{-1} \mathbb{1}_{\{t=\mathcal{T}\}}\right) \quad (\text{B.2})$$

$$= f\left(\sigma^2\mathbf{U}_{\mathcal{T}}^{-1}\right), \quad (\text{B.3})$$

for all unbiased estimators under Gaussian noise and for all linear unbiased estimators under non-Gaussian noise. The indicator function $\mathbb{1}_{\{A\}} = 1$ if A is true, and 0 otherwise. We used the facts that the event $\{\mathcal{T} = t\}$ is \mathcal{H}_t -measurable and $\mathbb{E}[(\hat{X}_t - X)(\hat{X}_t - X)^T|\mathbf{H}_t] = \text{Cov}(\hat{X}_t|\mathbf{H}_t) \geq \sigma^2\mathbf{U}_t^{-1}$ to write (B.1) and (B.2), respectively.

B.2 Lemma 4

We will first prove that if $\mathcal{V}(z)$ is non-decreasing, concave and bounded, then so is $G(z) = 1 + \mathbb{E} \left[\mathcal{V} \left(\frac{z}{1+zh_1^2} \right) \right]$. That is, assume $\mathcal{V}(z)$ satisfies: (a) $\frac{d}{dz}\mathcal{V}(z) \geq 0$, (b) $\frac{d^2}{dz^2}\mathcal{V}(z) < 0$, (c) $\mathcal{V}(z) < c < \infty, \forall z$. Then by (c) we have

$$1 + \mathcal{V} \left(\frac{z}{1+zh_1^2} \right) < 1 + c, \forall z, \quad (\text{B.4})$$

hence $G(z) < 1 + c$ is bounded. Moreover,

$$\frac{d}{dz}\mathcal{V} \left(\frac{z}{1+zh_1^2} \right) = \frac{\frac{d}{dz}\mathcal{V}(z)}{(1+zh_1^2)^2} > 0, \forall z \quad (\text{B.5})$$

by (a), and thus $G(z)$ is non-decreasing. Furthermore,

$$\frac{d^2}{dz^2}G(z) = \mathbb{E} \left[\frac{d^2}{dz^2}\mathcal{V} \left(\frac{z}{1+zh_1^2} \right) \right] = \mathbb{E} \left[\underbrace{\frac{\frac{d^2}{dz^2}\mathcal{V}(z)}{(1+zh_1^2)^4}}_{<0 \text{ by (b)}} + \underbrace{\frac{\frac{d}{dz}\mathcal{V}(z)}{-(1+zh_1^2)^3/2h_1^2}}_{<0 \text{ by (a) \& } z=\frac{1}{u}>0} \right], \forall z, \quad (\text{B.6})$$

hence $G(z)$ is concave, concluding the first part of the proof.

Now, it is sufficient to show that $\mathcal{V}(z)$ is non-decreasing, concave and bounded. Assume that the limit $\lim_{m \rightarrow \infty} \mathcal{V}_m(z) = \mathcal{V}(z)$ exists. We will prove the existence of the limit later. First, we will show that $\mathcal{V}(z)$ is non-decreasing and concave by iterating the functions $\{\mathcal{V}_m(z)\}$. Start with $\mathcal{V}_0(z) = 0$. Then,

$$\mathcal{V}_1(z) = \min \left\{ \lambda\sigma^2 z, 1 + \mathbb{E} \left[\mathcal{V}_0 \left(\frac{z}{1+zh_1^2} \right) \right] \right\} = \min\{\lambda\sigma^2 z, 1\}, \quad (\text{B.7})$$

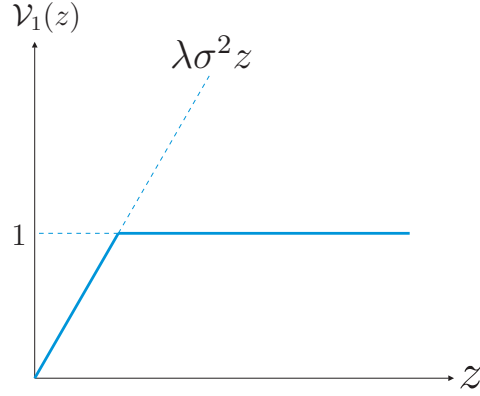
which is non-decreasing and concave as shown in Fig. B.1. Similarly we write

$$\mathcal{V}_2(z) = \min \left\{ \lambda\sigma^2 z, 1 + \mathbb{E} \left[\mathcal{V}_1 \left(\frac{z}{1+zh_1^2} \right) \right] \right\}, \quad (\text{B.8})$$

where $1 + \mathbb{E} \left[\mathcal{V}_1 \left(\frac{z}{1+zh_1^2} \right) \right]$ is non-decreasing and concave since $\mathcal{V}_1(z)$ is non-decreasing and concave. Hence, $\mathcal{V}_2(z)$ is non-decreasing and concave since pointwise minimum of non-decreasing and concave functions is again non-decreasing and concave. We can show in the same way that $\mathcal{V}_m(z)$ is non-decreasing and concave for $m > 2$, i.e., $\mathcal{V}(z) = \mathcal{V}_\infty(z)$ is non-decreasing and concave.

Next, we will show that $\mathcal{V}(z)$ is bounded. Assume that

$$\mathcal{V}(z) < \min\{\lambda\sigma^2 z, c\} = \lambda\sigma^2 z \mathbb{1}_{\{\lambda\sigma^2 z \leq c\}} + c \mathbb{1}_{\{\lambda\sigma^2 z > c\}}. \quad (\text{B.9})$$

Figure B.1: The function $\mathcal{V}_1(z)$ is non-decreasing and concave.

Then, from the definition of $\mathcal{V}(z)$ we have $1 + \mathbb{E} \left[\mathcal{V} \left(\frac{z}{1+zh_1^2} \right) \right] < c$. Since $\mathcal{V}(z)$ is non-decreasing, $\mathbb{E} \left[\mathcal{V} \left(\frac{z}{1+zh_1^2} \right) \right] \leq \mathbb{E} \left[\mathcal{V} \left(\frac{1}{h_1^2} \right) \right]$. From (B.9) we can write

$$1 + \mathbb{E} \left[\mathcal{V} \left(\frac{z}{1+zh_1^2} \right) \right] \leq 1 + \mathbb{E} \left[\mathcal{V} \left(\frac{1}{h_1^2} \right) \right] < 1 + \mathbb{E} \left[\frac{\lambda\sigma^2}{h_1^2} \mathbb{1}_{\{\frac{\lambda\sigma^2}{h_1^2} \leq c\}} \right] + c \mathbb{P} \left(\frac{\lambda\sigma^2}{h_1^2} > c \right), \quad (\text{B.10})$$

Recalling $1 + \mathbb{E} \left[\mathcal{V} \left(\frac{z}{1+zh_1^2} \right) \right] < c$ we want to find a c such that

$$1 + \mathbb{E} \left[\frac{\lambda\sigma^2}{h_1^2} \mathbb{1}_{\{\frac{\lambda\sigma^2}{h_1^2} \leq c\}} \right] + c \mathbb{P} \left(\frac{\lambda\sigma^2}{h_1^2} > c \right) < c. \quad (\text{B.11})$$

For such a c we have

$$\begin{aligned} 1 &< c \mathbb{P} \left(\frac{\lambda\sigma^2}{h_1^2} \leq c \right) - \mathbb{E} \left[\frac{\lambda\sigma^2}{h_1^2} \mathbb{1}_{\{\frac{\lambda\sigma^2}{h_1^2} \leq c\}} \right] \\ &= \mathbb{E} \left[\left(c - \frac{\lambda\sigma^2}{h_1^2} \right) \mathbb{1}_{\{\frac{\lambda\sigma^2}{h_1^2} \leq c\}} \right] = \mathbb{E} \left[\left(c - \frac{\lambda\sigma^2}{h_1^2} \right)^+ \right], \end{aligned} \quad (\text{B.12})$$

where $(\cdot)^+$ is the positive part operator. We need to show that there exists a c satisfying $\mathbb{E} \left[\left(c - \frac{\lambda\sigma^2}{h_1^2} \right)^+ \right] > 1$. Note that we can write

$$\begin{aligned} \mathbb{E} \left[\left(c - \frac{\lambda\sigma^2}{h_1^2} \right)^+ \right] &\geq \mathbb{E} \left[\left(c - \frac{\lambda\sigma^2}{h_1^2} \right)^+ \mathbb{1}_{\{h_1^2 > \epsilon\}} \right] \\ &> \mathbb{E} \left[\left(c - \frac{\lambda\sigma^2}{\epsilon} \right)^+ \mathbb{1}_{\{h_1^2 > \epsilon\}} \right] \\ &= \left(c - \frac{\lambda\sigma^2}{\epsilon} \right)^+ \mathbb{P}(h_1^2 > \epsilon), \end{aligned} \quad (\text{B.13})$$

where $\left(c - \frac{\lambda\sigma^2}{\epsilon}\right)^+ \rightarrow \infty$ as $c \rightarrow \infty$ since λ and ϵ are constants. If $\mathbb{P}(h_1^2 > \epsilon) > 0$, which is always true except the trivial case where $h_1 = 0$ deterministically, then the desired c exists.

Now, what remains is to justify our initial assumption $\mathcal{V}(z) < \min\{\lambda\sigma^2 z, c\}$. We will use induction to show that the assumption holds with the c found above. From (B.7), we have $\mathcal{V}_1(z) = \min\{\lambda\sigma^2 z, 1\} < \min\{\lambda\sigma^2 z, c\}$ since $c > 1$. Then, assume that

$$\mathcal{V}_{m-1}(z) < \min\{\lambda\sigma^2 z, c\} = \lambda\sigma^2 z \mathbb{1}_{\{\lambda\sigma^2 z \leq c\}} + c \mathbb{1}_{\{\lambda\sigma^2 z > c\}}. \quad (\text{B.14})$$

We need to show that $\mathcal{V}_m(z) < \min\{\lambda\sigma^2 z, c\}$, where $\mathcal{V}_m(z) = \min\left\{\lambda\sigma^2 z, 1 + \mathbb{E}\left[\mathcal{V}_{m-1}\left(\frac{z}{1+zh_1^2}\right)\right]\right\}$. Note that $1 + \mathbb{E}\left[\mathcal{V}_{m-1}\left(\frac{z}{1+zh_1^2}\right)\right] \leq 1 + \mathbb{E}\left[\mathcal{V}_{m-1}\left(\frac{1}{h_1^2}\right)\right]$ since $\mathcal{V}_{m-1}(z)$ is non-decreasing. Similar to (B.10), from (B.14) we have

$$1 + \mathbb{E}\left[\mathcal{V}_{m-1}\left(\frac{1}{h_1^2}\right)\right] < 1 + \mathbb{E}\left[\frac{\lambda\sigma^2}{h_1^2} \mathbb{1}_{\{\frac{\lambda\sigma^2}{h_1^2} \leq c\}}\right] + c \mathbb{P}\left(\frac{\lambda\sigma^2}{h_1^2} > c\right) < c, \quad (\text{B.15})$$

where the last inequality follows from (B.11). Hence,

$$\mathcal{V}_m(z) < \min\{\lambda\sigma^2 z, c\}, \quad \forall m, \quad (\text{B.16})$$

showing that $\mathcal{V}(z) < \min\{\lambda\sigma^2 z, c\}$, which is the assumption in (B.9).

We showed that $\mathcal{V}(z)$ is non-decreasing, concave and bounded if it exists, i.e., the limit $\lim_{m \rightarrow \infty} \mathcal{V}_m(z)$ exists. Note that we showed in (B.16) that the sequence $\{\mathcal{V}_m\}$ is bounded. If we also show that $\{\mathcal{V}_m\}$ is monotonic, e.g., non-decreasing, then $\{\mathcal{V}_m\}$ converges to a finite limit $\mathcal{V}(z)$. We will again use induction to show the monotonicity for $\{\mathcal{V}_m\}$. From (B.7) we write $\mathcal{V}_1(z) = \min\{\lambda\sigma^2 z, 1\} \geq \mathcal{V}_0(z) = 0$. Assuming $\mathcal{V}_{m-1}(z) \geq \mathcal{V}_{m-2}(z)$ we need to show that $\mathcal{V}_m(z) \geq \mathcal{V}_{m-1}(z)$. Using their definitions we write $\mathcal{V}_m(z) = \min\left\{\lambda\sigma^2 z, 1 + \mathbb{E}\left[\mathcal{V}_{m-1}\left(\frac{z}{1+zh_1^2}\right)\right]\right\}$ and $\mathcal{V}_{m-1}(z) = \min\left\{\lambda\sigma^2 z, 1 + \mathbb{E}\left[\mathcal{V}_{m-2}\left(\frac{z}{1+zh_1^2}\right)\right]\right\}$. We have $1 + \mathbb{E}\left[\mathcal{V}_{m-1}\left(\frac{z}{1+zh_1^2}\right)\right] \geq 1 + \mathbb{E}\left[\mathcal{V}_{m-2}\left(\frac{z}{1+zh_1^2}\right)\right]$ due to the assumption $\mathcal{V}_{m-1}(z) \geq \mathcal{V}_{m-2}(z)$, hence $\mathcal{V}_m(z) \geq \mathcal{V}_{m-1}(z)$.

To conclude, we proved that $\mathcal{V}_m(z)$ is non-decreasing and bounded in m , thus the limit $\mathcal{V}(z)$ exists, which was also shown to be non-decreasing, concave and bounded. Hence, $G(z)$ is non-decreasing, concave and bounded.

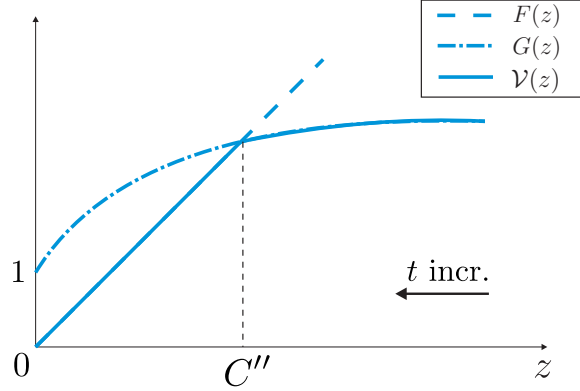


Figure B.2: The structures of the optimal cost function $\mathcal{V}(z)$ and the cost functions $F(z)$ and $G(z)$.

B.3 Theorem 5

The cost functions $F(z)$ and $G(z)$ are continuous functions as F is linear and G is concave. From (3.20) we have $\mathcal{V}(0) = \min\{0, 1 + \mathcal{V}(0)\} = 0$, hence $G(0) = 1 + \mathcal{V}(0) = 1$. Then, using Lemma 4 we illustrate $F(z)$ and $G(z)$ in Fig. B.2. The optimal cost function $\mathcal{V}(z)$, being the minimum of F and G [cf. (3.20)], is also shown in Fig. B.2. Note that as t increases z tends from infinity to zero. Hence, we continue until the stopping cost $F(z_t)$ is lower than the expected sampling cost $G(z_t)$, i.e., until $z_t \leq C''$. The threshold $C''(\lambda) = \{z : F(\lambda, z) = G(z)\}$ is determined by the Lagrange multiplier λ , which is selected to satisfy the constraint $\text{Var}(\hat{x}_{\mathcal{T}}) = \text{E} \left[\frac{\sigma^2}{u_{\mathcal{T}}} \right] = C$ [cf. (3.14)].

B.4 Proposition 3

The simplified distributed scheme that we propose in Section 3.4 is motivated from the special case where $\text{E}[h_{t,i}^k h_{t,j}^k] = 0, \forall k, i, j = 1, \dots, n, i \neq j$. In this case, by the *law of large numbers* for sufficiently large t the off-diagonal elements of $\frac{\bar{\mathbf{U}}_t}{t}$ vanish, and thus we have $\frac{\bar{\mathbf{U}}_t}{t} \cong \frac{\mathbf{D}_t}{t}$ and $\text{Tr}(\bar{\mathbf{U}}_t^{-1}) \cong \text{Tr}(\mathbf{D}_t^{-1})$. For the general case where we might have $\text{E}[h_{t,i}^k h_{t,j}^k] \neq 0$

for some k and $i \neq j$, using the diagonal matrix \mathbf{D}_t we write

$$\mathrm{Tr}(\bar{\mathbf{U}}_t^{-1}) = \mathrm{Tr}\left(\left(\mathbf{D}_t^{1/2} \underbrace{\mathbf{D}_t^{-1/2} \bar{\mathbf{U}}_t \mathbf{D}_t^{-1/2}}_{\mathbf{R}_t} \mathbf{D}_t^{1/2}\right)^{-1}\right) \quad (\text{B.17})$$

$$\begin{aligned} &= \mathrm{Tr}\left(\mathbf{D}_t^{-1/2} \mathbf{R}_t^{-1} \mathbf{D}_t^{-1/2}\right) \\ &= \mathrm{Tr}\left(\mathbf{D}_t^{-1} \mathbf{R}_t^{-1}\right). \end{aligned} \quad (\text{B.18})$$

Note that each entry $r_{t,ij}$ of the newly defined matrix \mathbf{R}_t is a normalized version of the corresponding entry $\bar{u}_{t,ij}$ of $\bar{\mathbf{U}}_t$. Specifically, $r_{t,ij} = \frac{\bar{u}_{t,ij}}{\sqrt{d_{t,i}d_{t,j}}} = \frac{\bar{u}_{t,ij}}{\sqrt{u_{t,ii}u_{t,jj}}}$, $i, j = 1, \dots, n$, where the last equality follows from the definition of $d_{t,i}$ in (3.28). Hence, \mathbf{R}_t has the same structure as in (3.29) with entries

$$r_{t,ij} = \frac{\sum_{k=1}^K \sum_{p=1}^t \frac{h_{p,i}^k h_{p,j}^k}{\sigma_k^2}}{\sqrt{\sum_{k=1}^K \sum_{p=1}^t \frac{(h_{p,i}^k)^2}{\sigma_k^2} \sum_{k=1}^K \sum_{p=1}^t \frac{(h_{p,j}^k)^2}{\sigma_k^2}}}, \quad i, j = 1, \dots, n.$$

For sufficiently large t , by the law of large numbers

$$r_{t,ij} \cong r_{ij} = \frac{\sum_{k=1}^K \frac{\mathbb{E}[h_{t,i}^k h_{t,j}^k]}{\sigma_k^2}}{\sqrt{\sum_{k=1}^K \frac{\mathbb{E}[(h_{t,i}^k)^2]}{\sigma_k^2} \sum_{k=1}^K \frac{\mathbb{E}[(h_{t,j}^k)^2]}{\sigma_k^2}}} \quad (\text{B.19})$$

and $\mathbf{R}_t \cong \mathbf{R}$, where \mathbf{R} is given in (3.29). Hence, for sufficiently large t we can make the approximations in (3.30) using (B.17) and (B.18).

سُبْحَانَكَ لَا عِلْمَ لَنَا إِلَّا مَا عَلَّمْتَنَا إِنَّكَ أَنْتَ الْعَلِيمُ الْحَكِيمُ